

The geomorphology of two hyper-saline springs in the Canadian High Arctic

by
Melissa Karine Ward

Department of Geography
McGill University
Montréal, Québec, Canada

August 2015

A thesis submitted to McGill University in partial fulfillment of the requirements of the
degree of Master of Science

© 2015 Melissa Karine Ward

Abstract

On Axel Heiberg Island in the Canadian High Arctic, low temperature perennial saline springs occur despite cold polar desert conditions marked by a mean annual air temperature close to -20°C . Distinctive landforms are associated with two groups of hyper-saline springs resulting from the winter deposition of salt minerals. These deposits resemble travertine and tufas structurally but unlike true travertine and tufas, which are composed of carbonate minerals, these landforms are composed of salt. Using a variety of field methods (including water and mineral precipitate sampling, stratigraphy, and time lapse photography), laboratory analysis (water chemistry and x-ray diffraction) and computer modelling to simulate mineral precipitation, this research characterizes the geomorphology and geochemistry of two hyper-saline springs on Axel Heiberg Island. The first is located at Stolz Diapir ($79^{\circ}04'30''\text{N}$; $87^{\circ}04'30''\text{W}$); at this site a series of pool and barrage structures staircase down a narrow valley for approximately 800m (several pools are up to 15m wide x 3m deep). The second is located at Wolf Diapir ($79^{\circ}07'23''\text{N}$; $90^{\circ}14'39''\text{W}$), where the deposit forms a large conical mound (2.5m tall x 3m diameter). The travertine/tufa-like appearance of these salt deposits reflects the interaction between changing water temperature, chemistry, flow and local topography. Both sites experience different surface hydrological patterns seasonally. In winter, the extreme cold air temperatures cools water temperatures triggering the rapid precipitation of various salt minerals (mainly hydrohalite, $\text{NaCl}\cdot 2\text{H}_2\text{O}$ and mirabilite, $\text{Na}_2\text{SO}_4\cdot 10\text{H}_2\text{O}$) generating the deposits. Warming air temperature in summer produces halite from the incongruent melting of hydrohalite. Parts of the deposits dissolve and mechanically erode due to spring flow, and snowmelt. These salt deposits are one of few large scale salt deposits resembling travertines and tufas and may be the largest surface deposits of hydrohalite in the world. The salt deposits further the science of travertine and tufa formation, not only providing an example of morphology similarities with different mineralogy, but also for furthering the understanding of abiotic processes generating these morphologies.

Résumé

De nombreuses sources d'eaux salées se situent sur l'île Axel Heiberg (Haut-arctique canadien), malgré un climat désertique polaire et une température annuelle moyenne de -20°C . Des dépôts de sel sont associés à deux sources d'eaux hyper salées résultant de la déposition durant l'hiver de sels minéraux. Ces dépôts ressemblent aux travertins et tufs structurellement, mais contrairement aux vrai travertins et tufs, qui sont composés de minéraux carbonatés, ces dépôts sont formés par le sel. En utilisant une variété de méthodes de terrain (y compris l'échantillonnage d'eaux et minéraux, la stratigraphie et la chronophotographie, « timelapse »), des analyses de laboratoire (chimie de l'eau et de diffractométrie de rayons X) et un modèle informatique pour simuler la précipitation minérale, cette recherche caractérise la géomorphologie et géochimie de deux sources hyper salées sur l'île Axel Heiberg. Le premier site est situé à Stolz Diapir ($79^{\circ}04'30''\text{N}$; $87^{\circ}04'30''\text{W}$). À ce site, une série de structures de barrages et bassins en forme d'escalier descend dans une vallée étroite sur environ 800m (plusieurs bassins mesurent jusqu'à 15m de large et 3m de profond. Le deuxième site se situe à Wolf Diapir ($79^{\circ}07'23''\text{N}$; $90^{\circ}14'39''\text{O}$) le dépôt de sel de ce site ressemble à un grand monticule conique (2,5m de haut et 3m de diamètre). L'apparence de ces dépôts de sel qui ressemblent aux travertins/tufs reflète l'interaction entre les changements de température de l'eau, la chimie, l'écoulement et de la topographie locale. Les deux sites éprouvent des conditions saisonnières de l'hydrologie de surface des sources d'eaux. En hiver, les températures extrêmes froides de l'air refroidissent les températures de l'eau et cela déclenche la précipitation rapide de divers minéraux de sels (principalement hydrohalite, $\text{NaCl}\cdot 2\text{H}_2\text{O}$ et mirabilite, $\text{Na}_2\text{SO}_4\cdot 10\text{H}_2\text{O}$) qui génèrent les dépôts. Pendant l'été, le réchauffement des températures de l'air dissout certaines parties des dépôts en raison du débit de la source, de la fonte des neiges et de la fonte de l'hydrohalite. Ces dépôts de sel sont l'un des rares dépôts de sel à grande échelle qui ressemblent aux travertins et tufs et pourraient de plus être un des plus grands dépôts de surface d'hydrohalite dans le monde. Les dépôts de sel approfondissent la science de la formation des travertins et tufs non seulement en fournissant un exemple de similarités morphologiques avec une minéralogie différente, mais aussi en favorisant la compréhension des processus abiotiques générant ces morphologies.

Acknowledgements

The completion of this thesis would not have been possible without the support from many people and to whom I am entirely grateful. I owe you so much more than a shout out within my acknowledgements but at least it's a start.

First and foremost I would like to thank my supervisor, Wayne Pollard, for whom none of this would have been possible. Thank you for taking a chance on an enthusiastic individual with an imperfect undergraduate academic record (on a side note thank you to my Faculty of Science advisor Zelda Ghan for helping me get through undergrad!). I fully realize the opportunity I was given and how it has changed my life in unexpected and better ways. Thank you for your support, encouragement, and knowledge both in the field and in Burnside. I only hope that my work and this thesis has met (and maybe even exceeded?) your expectations. Prof. Pollard is an amazing supervisor who deeply cares for his students. He will give you any and every opportunity possible. He prepares you for your career (whether in being academia or not) from day one. He teaches you to be an independent thinker, researcher and gives you a freedom with your project that is unmatched by other supervisors. I thank you for everything you have done for me. Everything I will achieve within my career will have begun when you agreed to let me be your graduate student and I will never be able to express how thankful I am for this.

I would like to thank Dale Andersen and Jared Simpson for their help in the field; and particularly to Dale for passing on various tricks of the trade for fieldwork in polar environments. You gave me knowledge and an awareness, particularly for safety measures, that I will use for all my future field seasons.

Thank you to Monique Riendeau in the Department of Materials Engineering at McGill for your work to analyse my water chemistry and for helping me with my x-ray diffraction work. Thank you to Christopher Omelon for your help, for allowing me to borrow your Dewar for transporting frozen samples and for taking the time to host me in Austin to do some SEM work with you. Thank you to Benoit Carrier for picking me up at

the airport in Ottawa for my first three field seasons. Thank you to Nigel Roulet for being my Department of Geography internal thesis reader and to Denis Lacelle for being my external thesis examiner.

Furthermore I would like to thank my friends and family for your love, support and for doing your best to understand what it is I do (particularly my parents)! Thank you to Michael Angelopoulos, Heather Cray and Michael Becker for helping me figure out graduate school, for reading and editing various abstracts and for exchanging ideas with me. A special thank you to my best friend and boyfriend, Michael Angelopoulos, for being my biggest fan from day one. It was always a pleasure to talk about my project and science with you and thank you for always being there for me, I never would have been able to do it without you. Thank you to my parents and brother (Kevin Ward), for taking care of my guinea pigs while I was in the field (also thank you to my pets for being great creatures of comfort during times of stress). Finally, a special thank you to my wonderful parents, Danny and Lise Ward for all your love, support, and for never questioning why their only daughter would ever not only want to go to the Arctic but also go to the Arctic and sleep in a heatless tent in -35°C . You are both inspiring individuals, I love you with all my heart and would not of gotten to where I am today without you.

Logistical support for this research was provided by the Canadian Polar Continental Shelf Project (PSCP), and the McGill Arctic Research Station (MARS). Funding was provided by the Natural Sciences and Engineering Research Council (NSERC) and ArcticNet (both awarded to W. Pollard). Additional student support was provided by the Northern Scientific Research Training program (NSTP), the Canadian Astrobiology Training Program (CATP) NSERC CREATE M.Sc Fellowship and National Geographic Society's Young Explorer Award.

Table of Contents

Abstract	ii
Résumé	iii
Acknowledgements	iv
List of Figures	ix
List of Tables	xii
Chapter 1: Introduction	1
1.1 Scientific Rationale	1
1.2 Research Objectives	3
1.2.1 Hypotheses	4
1.2.2 Specific Objectives	4
Chapter 2: Background Literature	6
2.1 Permafrost, Permafrost Hydrology and Icings	6
2.2 Brines	10
2.3 Cold Temperature Hydrated Evaporative Minerals	13
2.3.1 Mirabilite	13
2.3.2 Hydrohalite	14
2.4 Travertine and Tufa Deposits	16
2.4.1 Travertine/Tufa Morphological Terminology	19
Chapter 3: Study Area	21
3.1 Regional Setting	21
3.2 Climate	22
3.3 Regional Geology	23
3.4 Permafrost Conditions	24
3.5 Spring Activity on Axel Heiberg Island	24
3.6 Microbiology	27
3.7 Study Sites	28
3.7.1 Stolz Diapir	28
3.7.2 Wolf Diapir	29
Chapter 4: Methodology	30

4.1 Introduction	30
4.2 Site Selection and Field Methods	30
4.2.1 Differential GPS Survey	32
4.2.2 Abney Survey	32
4.2.3 Mineral Samples	33
4.2.4 Water Sampling	33
4.2.5 Field Instrumentation: Temperature Loggers and Time Lapse Cameras	35
4.3 Laboratory analyses	36
4.4 Chemical Modelling	37
Chapter 5: Results	39
5.1 Field results	39
5.1.1 Morphology of Mineral Precipitates (Travertine/Tufa)	39
5.1.1.1 Stolz Diapir	39
5.1.1.1.1 Barrage structures	40
5.1.1.1.2 Pools	44
5.1.1.2 Wolf Diapir	46
5.1.2 Stratigraphy (Stolz Diapir)	49
5.1.3 Topographic Surveys (Stolz Diapir)	51
5.1.4 Spring Discharge	53
5.1.5 Field Instrumentation	54
5.1.5.1 Hobo Temperature Data Logger (Stolz Diapir)	54
5.1.5.2 Time Lapse Cameras (Stolz Diapir)	58
5.1.5.2.1 Outlet Time Lapse Camera	58
5.1.5.2.2 Lower Valley Time Lapse Camera	69
5.2 Laboratory Results	76
5.2.1 Water Chemistry	76
5.2.1.1 Stolz Diapir	76
5.2.1.2 Wolf Diapir	79
5.2.2 Mineralogy Results	80
5.2.2.1 Stolz Diapir	80
5.2.2.2 Wolf Diapir	82
5.3 Computer Simulations using Frezchem v. 5.2	83

Chapter 6: Discussion	85
6.1 Winter versus summer processes	85
6.1.1 Winter Processes	86
6.1.1.1 Temperature Regime and Mineral Precipitation	86
6.1.1.2 Mineral Deposit Textures and Crusts	91
6.1.1.3 Travertine/Tufa Morphology	94
6.1.1.3.1 Barrages	96
6.1.1.3.2 Mounds	99
6.1.2 Summer Processes	100
6.1.2.1 Stolz diapir	100
6.1.2.2 Wolf diapir	102
6.1.2.3 Legacy features	103
6.2 Conceptual Model	107
6.2.1 Stolz Diapir	107
6.2.2 Wolf Diapir	111
Chapter 7: Conclusions	115
7.1 Significance of this research	116
Chapter 8: References	119
Chapter 9: Appendices	126
Appendix A	127
Appendix B	129
Appendix C	131
Appendix D	133

List of Figures

Chapters 1 and 2

Figure 1.1: The Pamukkale Travertine Terraces in Turkey have been visited by tourists for decades and is an important source of revenue for the country (Source: Nomadic Vision Photography/Flickr; http://www.rumblerum.com/wp-content/uploads/2014/12/Pamukkale-Travertine-Terraces-Turkey-4.jpg).....	1
Figure 2.1: The distribution of groundwater, occurring in unfrozen areas (taliks) within permafrost. Suprapermafrost occurs above the permafrost table, intrapermafrost occurs within permafrost and subpermafrost occurs below the permafrost table. Figure also shows seasonal frost within the active layer; icings and frost mounds are associated with groundwater within permafrost environments (Woo, 2012).....	7
Figure 2.2: Talik formation and spring occurrence in areas of continuous permafrost; Mineralized springs have a high total dissolved solids (TDS) concentration above 1000 mg/L; whereas freshwater springs have a TDS below 100 mg/L. (simplified from Van Everdingen 1991, Woo, 2012).....	8
Figure 2.3: Mineral precipitation sequences by concentration mechanism (evaporation or freeze-drying; Herrero <i>et al.</i> , 2015).....	13
Figure 2.4: Phase diagram of the NaCl-H ₂ O system. Hydrohalite being forming in solution below 0.12°C until it reaches a eutectic point at -21.1°, after only ice and hydrohalite is present below this temperature (Marion and Grant, 1994; Light <i>et al.</i> , 2009).....	15
Figure 2.5: Diagram of an icing mound as observed by Dzents-Litovskiy (1966) in the Kempendyay springs in Eastern Siberia (from Fomenko, 1976).....	18
Figure 2.6: (A) Terraces composed of mirabilite (Na ₂ SO ₄ *10H ₂ O) in Burgos, Spain (Herrero <i>et al.</i> , 2015); (B) Halite terrace-like features in Iran (Filippi <i>et al.</i> , 2011).....	19
Figure 2.7: Travertine morphology as described in (and figure modified from) Pentecost and Viles (1994); (A) barrage morphology, “(a) large lake barrages, (b) barrage system on travertine slope” (Pentecost and Viles, 1994, p. 309); and (B) mound morphology, “(a) low mound, (b) steep mound or fissure ridge, (c) mound with central pool, (d) tall submerged lake mound” (Pentecost and Viles, 1994, p. 309).....	20

Chapter 3

Figure 3.1: A false colour Landsat mosaic of Axel Heiberg Island showing ice caps, glaciers and fiords with map insert modified from Grasby <i>et al.</i> , 2003). Purple circles indicate the location of the following: (1) McGill Arctic Research Station (M.A.R.S); (2) Eureka Weather Station on Ellesmere Island; (3) Stolz Diapir study site and (4) Wolf Diapir study site (also known as Lost Hammer).....	21
Figure 3.2: Springs identified on Axel Heiberg Island, (1) Gypsum Hill, (2) Colour Peak, (3) Whitsunday Bay, (4) Middle Fiord, (5) Bunde Fiord, (6) Skaere Fiord and (7) Strand Fiord (Pollard <i>et al.</i> , 2009).....	26
Figure 3.3: Results from a two year monitoring of the Colour Peak Springs for discharge (flow rate), water temperature at the spring outlet and air temperature (Andersen <i>et al.</i> , 2002).....	27

Chapter 4

Figure 4.1: Water samples (WS), time lapse cameras (TLC) and Hobo data logger (HDL) locations at Stolz Diapir site. WS1 represents the winter outlet, WS2 is the summer outlet, WS3/HDL is the halfway point of the deposit for water sampling and the location of the hobo data logger, WS4 is the valley opening and WS5 is the salt pan within the floodplain. Lines at TLC locations shows approximate field of view of the cameras.....	34
Figure 4.2: Water sample locations at Wolf Diapir site. WS1 (Water Sample 1) represents the outlet, and WS2 is the spring channel located 5m away from the outlet.....	35

Chapter 5

Figure 5.1: Aerial view of the Stolz site (image taken in helicopter in July 2014).....	40
Figure 5.2: Seasonal difference of the deposit at Stolz Diapir, both images were taken at approximately the same location with a similar orientation; (A) taken in April 2012 by Prof. Pollard and (B) taken in July 2013.....	41
Figure 5.3: Large barrage structures with emptied pool. Dimensions of terrace in image A are 26m in length and 1.6m in height.....	42
Figure 5.4: Various textures along the bottom surface of the spring channels and pools. (A) Shows a cauliflower-like texture located in the pool the hobo temperature data logger was collected; and (B) shows a smooth spherical texture at a smaller pool just downstream from the time lapse camera located at the valley opening.....	43

Figure 5.5: Location of pools identified in April 2014. Pool measurements are: (pool 1) 41.21m by 24.52m; (pool 2) 25.70m by 11.52m; (pool 3) 27.80m by 12.25m; and (pool 4) 53.60m by 23.80m. Each pool is a few meters deep.....	44
Figure 5.6: (A) Image taken in April, 2012. During winter barrage structures fill up with water creating pools that staircase down the valley (image taken by W. Pollard). (B) Examples of inundated barrages in smaller in size located at the valley opening in April 2014.....	45
Figure 5.7: (A) Pool inflow type (upwelling pipe) identified for the first time with halolites upwelling in pulses as seen in (B); (C) halolite diameter was approximately a centimeter.....	46
Figure 5.8: Wolf Diapir spring in winter, the mound fills up with water and it overflows it sides. Image taken in 2008 by Prof. Pollard.....	46
Figure 5.9: (A) Wolf Diapir spring deposit in summer; (B) mound/dome part of the deposit; (C) smooth and compact texture; (D) terraces, approximately 2cm cascading down the mound only at this location and (E) large terrace/platform feature.....	47
Figure 5.10: Measured dimensions (using measuring tape) of the cone and platform of the salt deposit at Wolf diapir.....	49
Figure 5.11: Stratigraphic columns analysed located where the hobo temperature data logger was set up; (A) shows layering of a barrage structure, and (B) shows layering with respect to a pool floor.....	50
Figure 5.12: Examples of degrees of amount of sediments transported to the salt deposit during summer to produce the dark brown to lighter brown layers seen in the stratigraphy; (A) shows mud transported by the spring snowmelt to produce the dark brown layers, and (B) shows the transportation of sediments (most likely by wind) producing the lighter brown layers.....	50
Figure 5.13: (A) Frozen layer identified during stratigraphic analysis, (B) Sample of frozen layer immediately after collection (C) After being exposed to an elevated air temperature, the mineral dissolved. After sample was dried, halite was identified.....	52
Figure 5.14: DEM results of salt deposit at Stolz Diapir. Orange line in both images highlights valley wall.....	53
Figure 5.15: Abney profile of valley. Slope gradually decrease down the valley and average slopes ranged between 9% and 14%.....	51
Figure 5.16: (A) The hobo temperature data logger when put in place on July 10 th , 2013 and (B) when collected on April 15 th , 2014; note the minerals that precipitated and deposited on the sensor cables, as well as the floating raft crust identified.....	54
Figure 5.17: Temperature results collected from the hobo temperature data logger put in place in a pool at the center of the deposit. Note readings by the logger within the black box to be faulty and should not be used. Mean air temperature measurements from the Eureka Weather Station included for comparison. The Eureka Weather Station recorded a record low temperature measurement during this time so it is possible the calibration of the data loggers to be inaccurate.....	56
Figure 5.18: Temperature results collected from the hobo temperature data logger set up on ridge above the deposit. This logger recorded air temperature and soil temperatures at various depths (0-2cm; 10cm; and 30cm from surface). Mean air temperature measurements from the Eureka Weather Station included for comparison.....	57
Figure 5.19: Time lapse camera located at the outlet the day it was set up (A) in July 2013 and when it was collected (B) in April, 2014.....	59
Figure 5.20: Deposit immediately before and after time lapse camera set up (A) in July 2013 and when it was collected (B) in April, 2014. Exact camera location is shown by blue circle.....	59
Figure 5.21: First image taken by time lapse camera after put in place. Author for scale.....	61
Figure 5.22: First snowfall of the season. The snow remained on the ground throughout the rest of the study period.....	62
Figure 5.23: Red box indicating area where change occurs in figure 5.24.....	62
Figure 5.24: Sign of erosion indicated by red arrow or water level that is rising. This would be produce by water channeling within tunnels through the deposit that are carved during the summer months.....	63
Figure 5.25: First pools fill up on October 13 th , 2013. Image taken during the April 2014 field season inserted to show the differences between the pools between both time periods. The pool depicted by the red arrow was measured (27.80m by 12.25m). The purple line highlights the barrage in common within both images and the green arrow shows the location of a pool in April that resembled a tunnel in the time lapse images.....	63
Figure 5.26: One of the two pools drains but the other remains filled. This could indicate that multiple tunnels carved by water within the summer runs through the deposit and that these two pools are not directly connected.....	64
Figure 5.27: Removal of surface snow, but what triggered this is not clear (shown by red arrows).....	64
Figure 5.28: Pool furthest away fills up again after draining on October 14 th , 2013. More snow has fallen on the deposit.....	65

Figure 5.29: Within a day a large amount of water all over the deposit within view of the time lapse camera. This is the first image showing active terracing capture by the time lapse cameras and is highlighted by the dark purple square. An image taken from other terraces near the valley opening is included to give an idea of what the smaller terraces look like.....	65
Figure 5.30: After a snowstorm that lasted 8 days (the images taken on those days had no visibility) with temperatures varying between -22.60°C and -30.69°C the upper terraces now appear to be active with many small terraces forming during this time. The very large pool that was in the previous images has emptied, what appears to be a tunnel may be the source the water drained from and the large emptied tunnel has filled with water to create another pool.....	66
Figure 5.31: Some of the upper terraces have drained and it is unclear how.....	67
Figure 5.32: Upper pools that previously drained have filled up again.....	67
Figure 5.33: Final image that is clear, all images after this date are black (snow covered the lenses) until mid-April.....	68
Figure 5.34: First completely clear image after snow blew off the camera lens. One pool (the furthest away) has remained filled since October 13 th , 2013 and the other pool (closest) since November 7 th , 2013. The upper terraces are no longer active and snow depth on the deposit has increased.....	68
Figure 5.35: Time lapse camera located just upstream of the valley opening the day it was set up (A) in July 2013 and when it was collected (B) in April, 2014 and, (C) it's location in July, 2014 to show the morphology of the deposit where the camera was.....	69
Figure 5.36: Picture 1 from the lower valley time lapse camera. Field Assistant for scale.....	71
Figure 5.37: Clear image taken on August 5 th provides the best detail for comparison.....	71
Figure 5.38: Part of the deposit begins to collapse (indicated by red arrow). The spring water was not visible at this location during field work.....	72
Figure 5.39: Further collapse. The deposit where the spring water flows gets completely dissolved and the stream bed becomes visible (as shown by the pebbles that became visible).....	72
Figure 5.40: Stream bed pebbles are no longer visible and bed appears white from precipitating salt minerals.....	73
Figure 5.41: This picture clearly shows the accumulation of recently deposited salt and preliminary pooling.....	73
Figure 5.42: Water level continues to rise.....	74
Figure 5.43: Water level continues to rise.....	74
Figure 5.44: First clear image taken after a snowstorm (figure 5.30 shows an image taken on the same day by the other time lapse camera where most of the terraces are actively growing can be seen for the first time). This picture includes the first indication of overflow activity further upstream shown by the purple arrow.....	75
Figure 5.45: Last visible image taken by the lower valley time lapse camera (corresponds to the disappearance of twilight like the other camera). A malfunction stopped the camera at the end of December, 2013. This image show widespread changes in the hydrology and a definite shift to overflow processes.....	76
Figure 5.46: Piper diagram of water samples collected at the inflow waters and at various point within the deposit (outflow, stratigraphy site, valley opening and Whitsunday Floodplain).....	77
Figure 5.47: Piper diagram of Wolf Diapir spring water chemistry at the outlet and in the channel 5m away from outlet. Both samples were collected in June 2013.....	80
Figure 5.48: X-ray Diffraction peaks for thernadite (Na ₂ SO ₄) and halite (NaCl).....	81
Figure 5.49: X-ray Diffraction patterns for selected samples from the Stolz Diapir site, the primary peaks correspond with halite and thernadite.....	81
Figure 5.50: X-ray Diffraction patterns from selected samples from the Wolf Diapir site, the primary peaks correspond with halite and thernadite.....	82

Chapter 6

Figure 6.1: Image taken from helicopter that shows the inflow stream flowing into the diapir and the outlet on the other side that is driving the salt deposit. The water of the inflow is fresh whereas the water in the outlet is highly mineralized (dominated by sodium and chloride ions) indicating contact with the evaporates within the diapir (circled in black).....	87
Figure 6.2: Example of meniscus caused by surface tensions of flow over small barrages (a few centimeters in height) at Stolz. Image taken by Prof. Pollard in 2008.....	98
Figure 6.3: (A) a barrage wall broke, unleashing the water within its pool was destroyed parts of the deposit downstream, known as a washout event; (B) pool drained an emptied from a specific location.....	101

Figure 6.4: Image taken from helicopter at the end of June, 2014 at Stolz. Blue arrows point to entry points of freshwater from snowmelt.....102

Figure 6.5: (A) and (C) are images from Harrison and Jackson (2008). Higher river flows carved part of the deposit in 2004 and these dissolved parts of the deposit are still easily seen in 2013 (B and D are comparable angles of the images by Harrison and Jackson (2008) of the deposit and images were taken in June 2013).....105

Figure 6.6: Images showing the evolution of the Stolz deposit over time between 2005 and 2013. The year the image was taken is shown on the image itself. A legacy feature identified as a barrage wall can be recognized within each image and has been traced with a dashed dark blue line. Note that this feature does change slightly over time. The image taken in 2005 was taken by Dale Andersen, the images between 2006 and 2012 were taken by Wayne Pollard. The image from 2013 was taken by the author.....106

Figure 6.7: (A) Spring outlet of Stolz Diapir. The red arrows point to some of the salt located on the upper reaches of the valley. Blue arrows show flow direction of annual snow melt streams that may have carved the valley over time. (B) Cobbles within the valley mouth, adjacent to the deposit, suggesting they were placed by stream activity at an earlier time when discharge was greater108

Figure 6.8: (A) example of snowmelt only dissolving part of the deposit, image taken in July 2014; (B) example of new terrace formation on the side that was dissolved and larger terraces on the side that remained intact (highlighted within box), image taken in April 2012 by Prof. Pollard109

Figure 6.9: Sketch of various points in the formation of the Wolf deposit. (A) the deposit would have initially formed by an icing-like process; (B) side view of the deposit, the terrace and saltpan would likely have been a continuous deposit before large scale disturbances from dissolution by other fresh water springs; and (C) aerial view of the deposit before large scale disturbances.....113

Figure 6.10: Image of Wolf deposit highlighting the section of the mound that has rebuilt after it was dissolved in 2004. (A) the section as it is being rebuilt. Image taken in 2008 by Prof. Pollard; and (B) the section is done being rebuilt as the rim of the whole mound is at the same height.....114

Chapter 7

Figure 7.1: Comparison of a features identified on Mars (A and C; Allen and Oehler, 2008) to the deposits on Axel Heiberg Island (B and D). (A) A feature with a central like depression (10m diameter) looks similar to the mound at Wolf Diapir (B) and (C) features (>100m) thought to be terraces would form similarly to the terraces at Stolz Diapir (D).....118

List of Tables

Chapters 2 and 4

Table 2.1: Compiled using Sonnenfeld and Perthuisot (1989). Certain geochemical indicators are used to classify brines and determine their source waters.....11

Table 2.2: Main distinguishing characteristics between travertines and tufas. Taken from Capezuoli *et al.* (2013).....17

Table 4.1: Minerals (solid species) in Frezchem Model, version 5.2 (source: http://www.dri.edu/images/stories/research/projects/FrezChem/Release_Notes_5.2.pdf).....38

Chapter 5

Table 5.1: Major ion concentrations of water samples taken both in summer (July 2013) and winter (April 2014). Due to the high concentration of ions, results are presented in g/L rather than mg/L.....78

Table 5.2: Water chemistry data for Wolf Diapir Spring. Samples collected in June 2013. Due to the high concentration of ions, results are presented in g/L rather than mg/L.*Data from Niederberger *et al.*, 2010.....79

Table 5.3: Concentrations of mineral precipitates determined by Frezchem v.5.2. Water chemistry shown in table 5.1 was used to obtain results below for Stolz and table 5.2 for Wolf. *Simulations where eutectic point was reached at 228.15K (no liquid remaining so all possible minerals had precipitated. **Simulation where eutectic point was reached at 248.25K.....84

Chapter 1: Introduction

“Science is about more than finding general laws that can be immediately put to use in other scientific disciplines or technology. Science is also about observing beautiful, intriguing natural processes, and having the curiosity to want to find out how they work” (Hammer, 2008, p.265).

1.1 Scientific Rationale

Travertine and tufa deposits occur around the world and produce some of Earth’s most unique landscapes, for example, the Pamukkale Travertine Terraces in Turkey, (figure 1.1); the Mammoth Hot Springs travertine terraces, Yellowstone National Park; and the tufa towers at Mono Lake, California. These landforms are generated by precipitating carbonate minerals that drive active surface growth (as opposed to dissolution and erosion) within flowing water environments (Hammer, 2008) and can take on a variety of morphologies (e.g. conical mounds, stalactites, stalagmites, spheres, terraces and steps).



Figure 1.1: The Pamukkale Travertine Terraces in Turkey have been visited by tourists for decades and is an important source of revenue for the country (Source: Nomadic Vision Photography/Flickr; <http://www.rumblorum.com/wp-content/uploads/2014/12/Pamukkale-Travertine-Terraces-Turkey-4.jpg>).

Several, less well known, deposits are associated with hydrothermal springs in Canada including some in the Mackenzie Mountains of the Northwest Territories (e.g. the Rabbit Kettle hot springs). Most of these are classic travertine deposits associated with hydrothermal groundwater discharge. One notable exception are the small-scale travertine deposits associated with cold groundwater discharge at Colour Peak on Axel Heiberg Island in Nunavut (Omelon *et al.*, 2006). The latter are distinctive because of their geothermal nature and permafrost setting (Pollard *et al.*, 1999).

Within the Canadian High Arctic are also a series of salt formations that morphologically resemble travertines and tufas but do not contain carbonates in their mineralogy. These deposits are composed of predominantly salt minerals (NaCl and NaSO₄) and therefore cannot be considered travertines or tufas, but rather as travertine and tufa analogues. As part of an ongoing research program on High Arctic perennial springs by McGill researchers, two sites characterized by salt deposition (at Wolf and Stolz Diapirs, respectively) have been identified on Axel Heiberg Island (Pollard, 2005).

This research represents the first comprehensive study of the geomorphology and geochemistry of spring deposit at the Stolz Diapir site. Previous studies at this site are limited to geologic characterization of the diapir structure (Schwerdtner and Van Kranendonk, 1984) and icings processes (Pollard, 2005). This study provides new and valuable observations on saline groundwater processes in permafrost environments, it serves as a baseline for future studies at these sites and as an analogue for potential groundwater on Mars. This site is dramatically different from previously studied perennial springs on Axel Heiberg (Colour Peak, Gypsum Hill and Wolf Diapir; Pollard *et al.*, 1999)

and Ellesmere Islands (Ice river, Obalyaa Bay; Grasby *et al.*, 2014), and is the only spring with a known groundwater source.

1.2 Research Objectives

The primary aim of the proposed research is to characterise and explain the geomorphic and geochemical characteristics of two hyper-saline springs on Axel Heiberg Island. Cold perennial springs located at Stolz Diapir (Whitsunday Bay) and Wolf Diapir (Strand Fiord) exhibit unusual travertine/tufa-like structures related to the precipitation of dissolved salts under cold arctic winter conditions. The questions driving this study pertain mainly to the hypothesized seasonal role of hydrohalite ($\text{NaCl} \cdot 2\text{H}_2\text{O}$) precipitation at both springs as a geomorphic process. Some of the questions this study addresses include: (1) how do these travertine/tufa-like structures form?; (2) does the combination of extremely cold winter temperatures and freezing depression of saline groundwater play a role in the formation of these landforms?; (3) do cold winter temperatures lead to eutectic freezing conditions of saline groundwaters and the formation of hydrohalite?; and (4) what are the geomorphic implications of this type of system? Although widely reported as part of sea ice formation and laboratory experiments, the depositional process, patterns and impacts of hydrohalite at the landscape scale have not been previously reported in the literature. We believe that these unique landforms could be the largest surface deposits of hydrohalite on Earth. What differentiates the Wolf Diapir and Stolz Diapir springs from other springs on Axel Heiberg and Ellesmere Islands is the singular importance of sodium chloride (NaCl) minerals precipitating rather than carbonate or calcium sulfate minerals.

1.2.1 Hypotheses

To address these questions the following hypotheses will be tested:

(1) The hyper-saline nature of groundwater discharge linked to salt diapirs (geologic structures) on Axel Heiberg Island causes depressed freezing conditions leading eutectic freezing conditions.

(2) Hydrohalite is the primary mineral precipitating at both springs during the winter.

(3) Salt minerals (primarily hydrohalite) create travertine/tufa-like structures when precipitation occurs under extreme cold conditions.

(4) Because hydrohalite is hypothesized to be the dominant mineral precipitating during winter, it is a hydrated mineral and incorporates water within its crystal lattice. Hydrohalite, together with ice crystals, form an impermeable layer changing the local flow patterns and surface hydrology (mostly flow patterns of the springs) and therefore will change seasonally with the precipitation and dissolution of hydrohalite.

1.2.2 Specific Objectives

To test these hypotheses, the following research objectives will be met through a combination of field investigation, laboratory analyses and chemical modelling.

(1) Determine the topographic and geomorphic characteristics of hyper-saline perennial spring systems located at Wolf and Stolz diapirs on Axel Heiberg Island in the Canadian High Arctic.

(2) Characterize surface and downstream hydrology of these springs and assess how they change seasonally.

(3) Characterize the chemistry of hyper-saline discharge.

(4) Characterize the mineralogy of precipitates forming travertine/tufa-like structures.

(5) Use Frezchem (version 5.2), an equilibrium chemical thermodynamic computer model that simulates and predicts the behaviour of concentrated electrolyte solutions at extremely cold temperatures, to simulate mineral precipitation.

(6) Develop a conceptual physical model to explain of how both spring deposits formed.

Chapter 2: Background Literature

2.1 Permafrost, Permafrost Hydrology and Icings

The physical properties of ground material (size, and composition of soil particles; subsurface structures and rock type distribution) affect groundwater movement and storage (Freeze and Cherry, 1979; Woo, 2012). Permafrost, defined as ground material that has remained frozen for at least two consecutive years (van Everdingen, 1998), further impacts the occurrence, movement and quality of groundwater in Polar Regions (Prowse & Ommanney, 1990). The freezing of ground material decreases its hydraulic conductivity by several orders of magnitude, thus the presence of permafrost acts as an aquiclude limiting groundwater infiltration and movement (Woo 2012; van Everdingen, 1990). Frozen ground also affects water properties and chemistry. According to van Everdingen (1990), changes in physical properties include: a decrease (by several orders of magnitude) of hydraulic and electrical conductivity; a decrease in specific heat capacity; an increase in thermal conductivity and viscosity if waters are liquid but below 0°C (are hydrochemical). Permafrost tends to increase the residence time of groundwater by reducing rates of recharge, movement and discharge. Generally an increase in residence time will increase the mineralization of groundwater due to a longer contact time with rock material, however low temperature conditions tend to reduce reaction and dissolution rates (van Everdingen, 1990). At lower temperatures the solubility of CO₂ decreases, thus calcite and dolomite precipitation are more likely to increase; gypsum also has an increased solubility at lower temperatures.

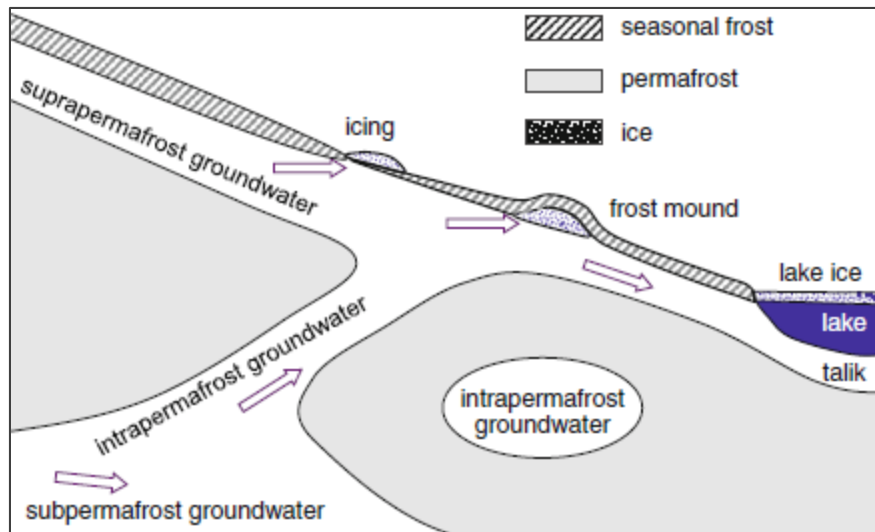


Figure 2.1: The distribution of groundwater, occurring in unfrozen areas (taliks) within permafrost. Suprapermfrost occurs above the permafrost table, intrapermafrost occurs within permafrost and subpermafrost occurs below the permafrost table. Figure also shows seasonal frost within the active layer; icings and frost mounds are associated with groundwater within permafrost environments (Woo, 2012).

Groundwater in permafrost regions is divided into separate zones with varying degrees of connectivity depending on the nature (i.e. continuous vs discontinuous) and depth of permafrost (figure 2.1). These unfrozen zones, known as taliks, partition groundwater into hydrologic systems that occur either above the permafrost table (suprapermfrost), within the permafrost (intra-permafrost) or below permafrost (sub-permafrost; van Everdingen, 1990). “Springs are points of natural, concentrated discharge of groundwater, at a rate high enough to maintain flow on the surface” (van Everdingen, 1991, p. 8). The rate of discharge of spring waters reflects the flow rate of groundwater. The chemistry of the water discharging reflects the composition of the rock material the groundwater flows through as well as its residence time (van Everdingen, 1991). Perennial springs are distinguished by continuous flow year round as opposed to seasonal springs and seeps where discharge is intermittent and often reflect a seasonal control on the hydrologic system. Perennial springs can occur in areas of continuous permafrost if

supplied by waters that reach the surface through various types of taliks. These taliks include: hydrothermal, where water is maintained by groundwater above 0°C; or hydrochemical, where mineralized water depresses the freezing temperature so that the groundwater is unfrozen but is maintained below 0°C (figure 2.2; van Everdingen, 1990). Springs supplied only by supra- or intrapermafrost groundwater from snowmelt, glacial meltwater or active layer thaw will become dormant during cold winter months as the ground refreezes or source waters are depleted. For obvious reasons perennial springs occurring in areas of thick continuous permafrost are extremely rare (Pollard and van Everdingen, 1992). Conditions required for perennial discharge include: a subpermafrost groundwater source (aquifer), a supply that must be high enough to generate year round flow and a mechanism or structure that connects the subpermafrost aquifer to the ground surface. Perennial springs occur on Axel Heiberg and Ellesmere Island, in the Canadian High Arctic despite highly variable air temperatures with minimums frequently reaching -55°C (Pollard *et al.*, 1999; Grasby *et al.*, 2014).

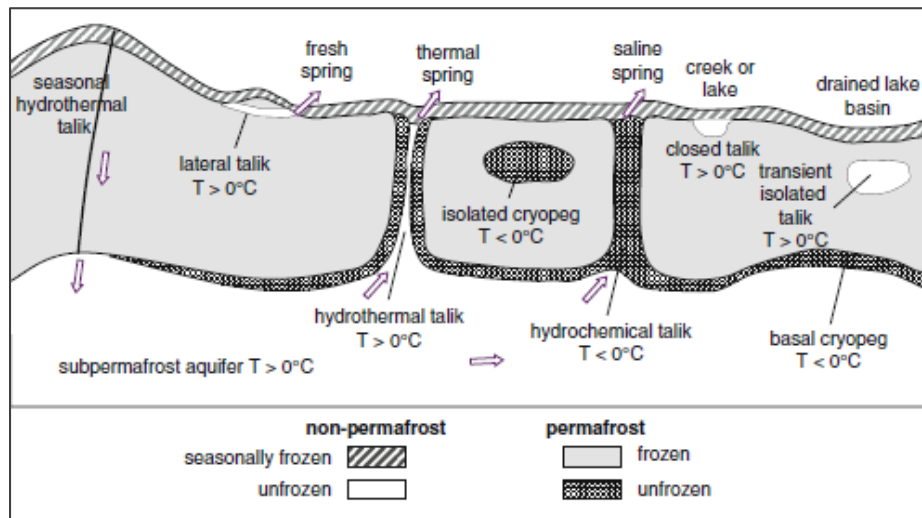


Figure 2.2: Talik formation and spring occurrence in areas of continuous permafrost; Mineralized springs have a high total dissolved solids (TDS) concentration above 1000 mg/L; whereas freshwater springs have a TDS below 100 mg/L. (simplified from Van Everdingen 1991, Woo, 2012).

During winter, groundwater that reaches the surface freezes, and forms successive sheets of ice called icings. Icings are also referred to *aufeis* and *naleds* (German and Russian terms). Icings are “sheet-like masses of layered ice that form on either the ground surface or on river or lake ice” (Pollard, 2005 p. 52; Pollard and van Everdingen 1992). Generally three types of icings are recognized based on the water source: ground icings (water seeps from ground), spring icings (water seeps from spring outlets), and river icings (water from below river ice reaches the surface by fractures in the ice). Hu and Pollard (1997) showed that the process of icing accumulation usually occurs sporadically (in space not time) over a limited distance depending on discharge and is not dependent on past ice accumulations. This produces an icing growth that is discontinuous spatially but generally self leveling. The level of activity and size of the icing is determined by the groundwater source and discharge. Suprapermafrost water in areas of continuous permafrost will either freeze *in situ* or become exhausted, causing the icing to go dormant before winter ends. The formation of these types of icings tends to be localized and limited to the discharge outlet. Icings formed by intrapermafrost or subpermafrost waters will remain active and continue to grow at points far from discharge points as long as mean daily air temperature remains below 0°C; because discharge rates and temperatures are generally higher (Pollard, 2005). Mean spreading length of an icing is depended on the following factors: air temperature and wind speed, water discharge and slope of the icing surface (Hu and Pollard, 1997). Heldmann *et al.*, (2005) studied the icings produced at the Colour Peak and Gypsum Hill Springs and found that the bulk ice produced contained 30-285 ppt of salt. Although hydrohalite is not mentioned specifically in this study, the environmental conditions and high salinity of spring waters are suitable for hydrohalite to occur.

2.2 Brines

Saline waters are made up of ions in solution that can precipitate to form evaporative minerals. The presence and concentration of six main cations/anions (Na^+ , Mg^{2+} , Ca^{2+} , K^+ , Cl^- and SO_4^{2-}) within a solution determines which brine category the solution falls into (Braitsch, 1971). Table 1, compiled using Sonnenfeld and Perthuisot (1989), shows that brines can be broken down into their source fluids (first 3 rows) and their classification (last 4 rows). Natural brines are a mixture of several basic types of solutions. According to Sonnenfeld (1984), saline waters can pick up their solutes from various sources: (1) sea water concentration; (2) leaching of older non-evaporitic rocks (chemical weathering); (3) leaching of older evaporative rocks (redissolution); (4) products of volcanic emanations; (5) sea spray and (6) formation waters altered by rock-water interactions in the bedrock

When a solution is supersaturated with a specific salt mineral, salt precipitation occurs by brine fractionation from the removal of water as a solvent. Salt precipitation occurs by two mechanisms depending on temperature: either solar driven evaporation (evaporative fractionation) at temperatures above -5°C or freezing fractionation (at temperatures below -5°C ; Sonnenfeld and Perthuisot, 1989; Herrero *et al.*, 2015). Freezing fractionation is only important in cold environments. Deposits are usually small scale and are either groundwater or lacustrine derived. Freezing fractionation occurs when freezing concentrates brines enough for precipitation to be achieved by removing water as ice and tends to produce a high concentration of hydrated evaporative minerals that have very low solubility in water (Sonnenfeld, 1984; Marion and Kargel, 2008).

Table 2.1: Compiled using Sonnenfeld and Perthuisot (1989). Certain geochemical indicators are used to classify brines and determine their source waters.

	Name	Source	Cation Weight Ratio			Principal Anion	Specific Gravity
			$\frac{Na_2}{Ca}$	$\frac{K_2}{Ca}$	$\frac{Mg}{Ca}$		
Source Fluids	Marine Brine	Concentrated sea water	13.2	0.475	3.18	----	----
	Continental Brine	Concentrated from groundwater	0.25± 0.087	0.06± 0.012	0.29± 0.12	---	---
	Formation Waters	Water circulating in deeper bedrock horizons	Negligible			---	---
Undersaturated Brine Classification	Hypohaline waters (low salinity)	----	---	---	---	CO ₂ ²⁻ or HCO ₃ ⁻	Less than 1.08
	Mesohaline waters (medium salinity)	----	---	---	---	SO ₄ ²⁻	1.08-1.18
	Hyper-saline waters (high salinity)	----	---	---	---	Cl ⁻	Above 1.18
	bitterns	---	---	---	---	Cl ⁻	1.3 (on account of higher Mg content)

Figure 2.3 outlines the mineral precipitation sequences of evaporative minerals based on solution concentration mechanism (evaporation or freezing fractionation). Assuming the seawater solute composition is similar, one can see that mineral precipitates differ between precipitation by evaporation and by freezing fractionation. The main difference between the two is that calcium carbonate (CaCO₃) and gypsum (CaSO₄*2H₂O) will precipitate first by evaporation but mirabilite (Na₂SO₄.10H₂O) precipitates (after ice) when freezing fractionation is the mechanism. As shown in figure 2.3, when freezing fractionation is the mechanism of salt precipitation, the following mineral sequence occurs with corresponding eutectic temperatures (of final mineral solidification): ice (-1.9°C), mirabilite (Na₂SO₄.10H₂O; -8.2°C), hydrohalite (NaCl*2H₂O; -22.9°C), sylvite (KCl),

magnesium chloride dodecahydrate ($\text{MgCl}_2 \cdot 12\text{H}_2\text{O}$; -36°C) and finally antarcticite ($\text{CaCl}_2 \cdot 6\text{H}_2\text{O}$; -54°C ; Sonnenfeld, 1984; Marion *et al.*, 1999; Marion and Kargel, 2008). This freezing fractionation mineral sequence (known as the Ringer-Nelson-Thompson pathway) is widely used and is supported by experimental and theoretical work. Another mineral sequence suggested by experimental work done by Glitterman (1937) offers a different pathway (Marion *et al.*, 1999; Marion and Kargel, 2008).

The Glitterman pathway has gypsum precipitating at -22.2°C alongside hydrohalite (which begins at -22.9°C) and the last salt of the sequence to precipitate is $\text{MgCl}_2 \cdot 12\text{H}_2\text{O}$ at -36°C . Precipitating hydrohalite ($\text{NaCl} \cdot 2\text{H}_2\text{O}$) lowers the concentration of sodium ions causing mirabilite ($\text{NaSO}_4 \cdot 10\text{H}_2\text{O}$) to go back into solution. This increase of sulfate ions allows gypsum to precipitate. The contrasting mineral sequences reflects different experimental methodologies between studies. Glitterman (1937) used a static approach when freezing seawater to allow precipitating minerals to fully equilibrate (at times up to four weeks), while experiments of the Ringer-Nelson-Thompson pathway (Ringer, 1906; Nelson and Thompson, 1954; Richardson, 1976 and Herut *et al.*, 1990) used a dynamic approach and allowed minerals to equilibrate for only a few hours. Both pathways likely occur in nature. A second difference in the methodology used to determine precipitate pathways is the initial solution used. Ringer-Nelson-Thompson pathway experiments (Ringer, 1906; Nelson and Thompson, 1954; Richardson, 1976 and Herut *et al.*, 1990) used seawater as the initial solution for freezing. In order for gypsum to precipitate at low temperatures, a sufficient amount of mirabilite needs to be present to insure an adequate supply of sulfate ions. Theory suggests that at -20°C precipitated mirabilite holds 90% of the available sulfate ions (Marion *et al.*, 1999). The Glitterman experiment as well as

experimental work done by Marion *et al.*, (1999) added mirabilite crystals to the solution to ensure a sufficient supply of sulfate for the precipitation of gypsum.

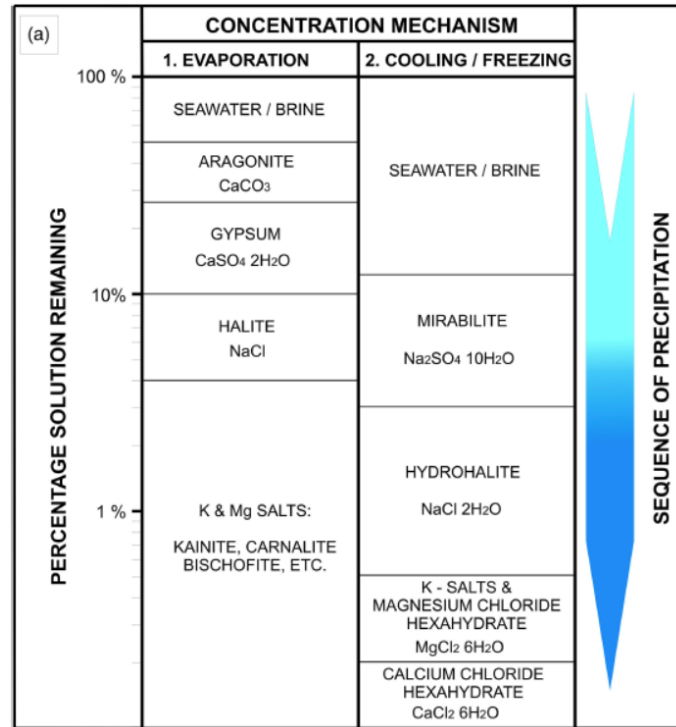


Figure 2.3: Mineral precipitation sequences by concentration mechanism (evaporation or freeze-drying; Herrero *et al.*, 2015).

2.3 Cold Temperature Hydrated Evaporative Minerals

2.3.1 Mirabilite

Mirabilite ($\text{NaSO}_4 \cdot 10\text{H}_2\text{O}$), also known as Glauber's salt, occurs in sulfate rich brines of saline lakes and springs; and is one of the most common evaporitic minerals precipitating in cool environments (Herrero *et al.*, 2015). The mineral is highly reactive due to its high solubility and low melting point; however the actual precipitation of sulfate minerals are generally 'sluggish' (Garrett, 2001; Marion and Kargel, 2008). In environments where the mean annual temperature is lower than -3°C , mirabilite can form thick deposits that can persist year round (Herrero *et al.*, 2015). When air temperatures are

above zero for a few months of the year, mirabilite deposits become unstable and dissolve. Various experimental studies reference different eutectic temperatures for mirabilite precipitation with values ranging between -6.3°C and -8.2°C (Marion *et al.*, 1999; Sonnenfeld, 1984). Mirabilite crystals are colourless, transparent, and vitreous and form a monoclinic prism (Braitsch, 1971). Relatively pure and massive mirabilite deposits occur when concentrations of other salts in solutions are low (Garrett, 2001). Examples of these deposits are known to occur in Great Salt Lake (Utah, USA), Gulf of Kara Bogaz (Turkmenistan) and the Canadian-Montana-South Dakota prairies. If environmental conditions are right and a mirabilite deposit survives, it can form a permanent deposit that grows year after year (Garrett, 2001). The mineral can crystallize in a number of places: from lake and playas bottoms to surface waters and near surface sediments.

Mirabilite's dehydrated form is thenardite (NaSO_4) and forms mainly from metamorphosed mirabilite (Braitsch, 1971). This occurs either when temperatures increase above 32.4°C or from a salting out effect when present in a sodium chloride rich brine (Sonnenfeld, 1984; Garrett, 2001). It commonly occurs as a fine white powder.

2.3.2 Hydrohalite

Hydrohalite ($\text{NaCl}\cdot 2\text{H}_2\text{O}$) is a stable phase of the $\text{NaCl}\text{-H}_2\text{O}$ system (figure 2.4) that begins to precipitate by freezing fractionation at temperatures below 0.12°C , forming hydrohalite and a brine solution until it reaches the eutectic point at -21.1°C where the remaining solution freezes. Above 0.12°C hydrohalite melts incongruently to NaCl (halite) and a NaCl saturated solution, losing 54.3% of its volume (Craig *et al.*, 1974; Craig *et al.*,

1975; Light *et al.*, 2009; Sonnenfeld, 1984). The environmental conditions required for hydrohalite to form make it one of the rarest stable minerals on Earth and forms within sea ice and in hyper-saline lakes (Matsubaya *et al.*, 1978; Sonnenfeld, 1984). The mineral's crystal form has been described as a non-cubic morphology (unlike halite) that is clear and colourless commonly taking on a monoclinic prism similar to gypsum ($\text{CaSO}_4 \cdot 2\text{H}_2\text{O}$; Craig & Light, 1975).

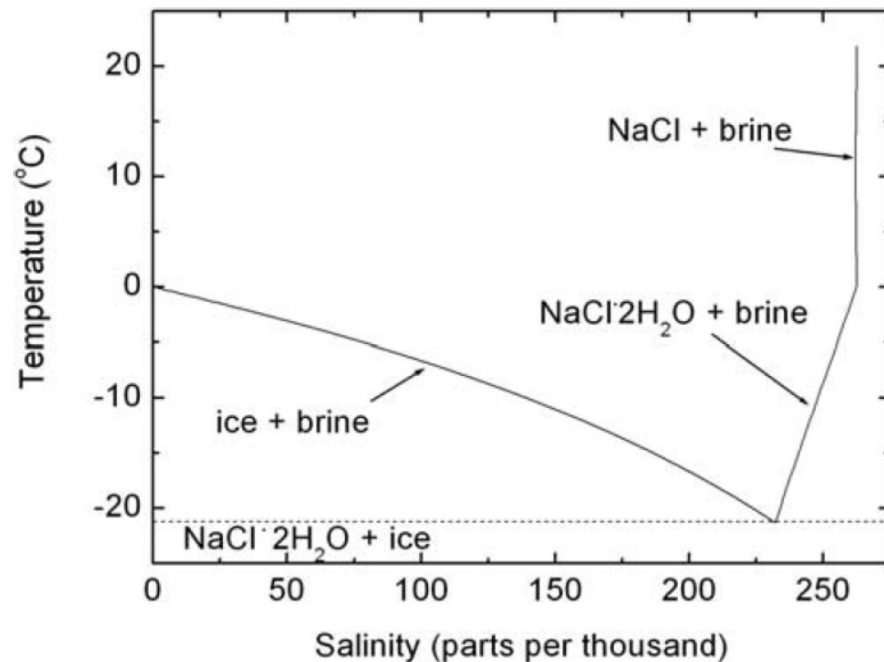


Figure 2.4: Phase diagram of the NaCl-H₂O system. Hydrohalite begins precipitating in solution below 0.12°C until it reaches a eutectic point at -21.1°, after only ice and hydrohalite is present below this temperature (Marion and Grant, 1994; Light *et al.*, 2009).

Hydrohalite has been observed in nature in only a few locations: the saline Lakes of Siberia during winter, playas in the Great Plains of North America and in Lake Bonney, Antarctica. Craig *et al.*, (1974) described the hydrohalite deposit in Lake Bonney as occurring on the bottom of the lake below a depth of 28m where denser brines sank coating a 10cm thick halite deposit. Last (1984) mentions hydrohalite precipitates from the chloride rich brine of Patience Lake, Saskatchewan during the winter. In Siberia, according to

Sonnenfeld (1984); Dzens-Liovskiy (1968) observed that hydrohalite precipitates and is maintained in the bottom of a deep saline lake (Lake Razval) in Siberia. At these depths the brines remain perennially cold as a result of the steep shores and stratified waters because solar energy only heats up the surface waters. However, in these cases the description of hydrohalite is anecdotal and in none of these studies has analytical empirical evidence provided for its occurrence. In 2005, Pollard described a pool and barrage structure occurring at the Stolz Diapir spring at Whitsunday Bay on Axel Heiberg Island during the winter was composed of hydrohalite, determined by mass analysis of decomposed crystalline samples.

2.4 Travertine and Tufa Deposits

The most common types of mineralized spring deposits are tufas and travertines (van Everdingen, 1991). These deposits are made up of calcium carbonate (CaCO_3) and take on a wide range of structures and morphologies (Ford and Pedley, 1996). These spring deposits occur by the precipitation of carbonate minerals at specific points of CO_2 degassing within supersaturated waters (with respect to CaCO_3). This supersaturation may be achieved by evaporation, biological activity, aeration, subsequent cooling and loss of dissolved gases and so the formations of minerals occur (van Everdingen, 1991).

The boundary between tufa and travertine forms is unclear. Pentecost and Viles (1994) distinguish the two based on degree of lithification, while Ford and Pedley (1996) differentiate tufas based on low Mg-content and temperature of the water it precipitates in regardless of the degree of cementation. The tufa and travertine classification debate still continues. Table 2.1 from Capezzuoli *et al.*, (2013) offers a summary of main

distinguishing characteristics between travertines and tufas. Because of the nature of the mineralogy observed in the Axel Heiberg springs this study does not attempt to classify these deposits as either tufas or travertines but rather consider the deposits as tufa and travertine analogues.

Table 2.2: Main distinguishing characteristics between travertines and tufas. Taken from Capezzuoli *et al.* (2013).

	Travertine	Tufa
Depositional processes	Dominantly abiotic	Dominantly biotic
HCO ₃ ⁻ content (mmol/l)	>7	<6
δ ¹³ C (PDB‰)	-1 to +10	<0
DIC (mmol/l)	>10	<8
Water temperature	Thermal, generally higher than 30°C	Ambient, generally lower than 20°C
Mineralogy	Calcite, aragonite	Calcite
Depositional rate	Higher (cm to m/year)	Lower (mm to cm/year)
Fabric	Mainly regularly bedded to fine laminated	Mainly poorly bedded
Crystal calcite size	Macro (dendritic, bladed or acicular) to micritic crystals	Dominantly micritic to microsparitic crystals
Primary porosity	Generally low (less than 30%)	Generally high (over 40%)
Biological content	Low (bacteria and cyanophytes)	Very high (micro to macrophytes)
Depositional morphologies	Multi-symmetrical bodies (mounds, ridges and slopes)	Axial-symmetrical bodies (cascade, dams and barrages)
Distinctive lithofacies	Coated bubbles, shrubs	Phytoherms
Hydrological setting	Regular, generally permanent flow	Variable, rainfall-dependent flow
Climatic control on deposition	Less dependent	Strictly dependent
Anthropogenic influence on deposition	Scarcely influenced	Deeply influenced
Tectonic relation	Always present	Often absent

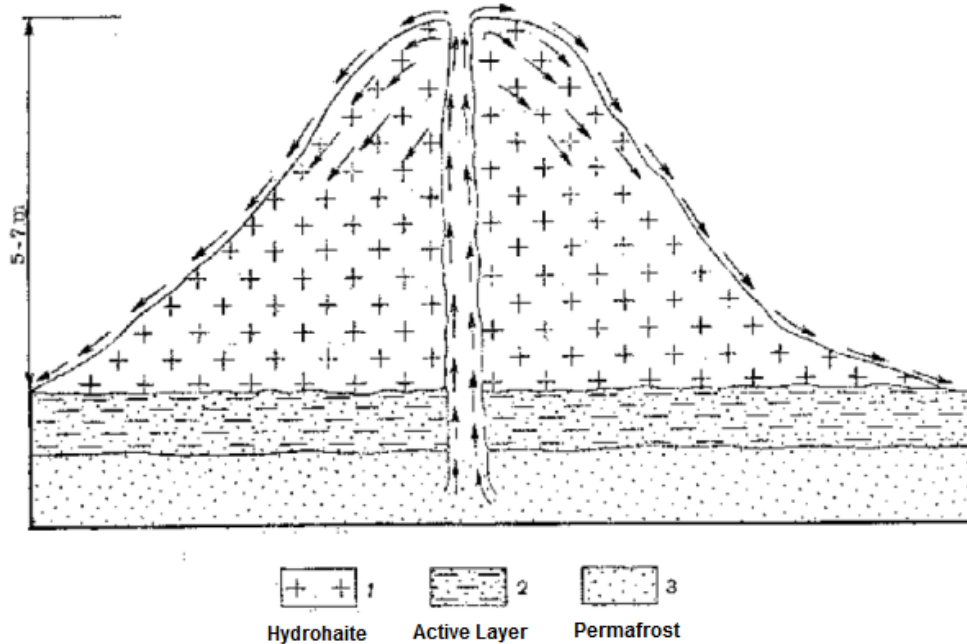


Figure 2.5: Diagram of an icing mound as observed by Dzents-Litovskiy (1966) in the Kempendyay springs in Eastern Siberia (from Fomenko, 1976).

Few examples of travertine/tufa analogues made from salt exist in the literature. Last (1989) described tufa-shaped deposits composed largely of Na and Mg salts occurring in saline lakes within the Great Plains of North America. Last (1989) noted saline springs building large cones shaped structures (up to 3m high) and ‘sinter-like ridges’ as a result of temperature differences between the lake brine and the discharging groundwater. During the winter if the springs remain active, Last (1989) mentions that hydrohalite precipitates, however his descriptions lack detail and it is not clear if these mounds contain only hydrohalite, only ice or both. Dzents-Litovskiy (1966) describes a similar process in the Kempendyay springs in Eastern Siberia (figure 2.5). Large icing mounds composed of hydrohalite can accumulate between 3-7m after a single winter season. These mounds accumulate due to difference in temperature between the air and the brine reaching the ground surface, leading to rapid precipitation of hydrohalite, however it is unclear if

hydrohalite was actually identified scientifically or if its presence is speculative. Pollard's (2005) observations of hydrohalite forming as part of the icings at Stolz Diapir on Axel Heiberg Island led to the proposal of a new type of 'brine icing' as this went against the traditional view of the formation of ice as a purifying process rather than being made up of low temperature hydrated minerals. Herrero *et al.*, (2015) provides an image of terrace like structures formed from a Na_2SO_4 rich spring in Burgos, Spain (figure 2.6A). Small halite structures resembling barrages were recorded by Filippi *et al.*, (2011) in Iran (figure 2.6B). Both Herrero *et al.*, (2015) and Filippi *et al.*, (2011) do not offer an explanation behind the formation of these barrage systems.

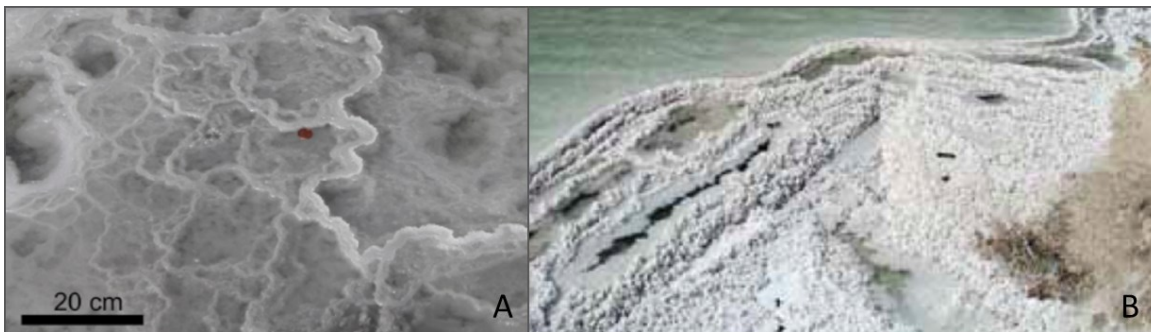


Figure 2.6: (A) Terraces composed of mirabilite ($\text{Na}_2\text{SO}_4 \cdot 10\text{H}_2\text{O}$) in Burgos, Spain (Herrero *et al.*, 2015); (B) Halite terrace-like features in Iran (Filippi *et al.*, 2011).

2.4.1 Travertine/Tufa Morphological Terminology

The lack of consensus on travertine and tufa classification has led to confusing terminology to describe their morphology. This section will outline specific terminology used in this study.

This study uses the term 'barrage' to describe the morphology of the deposit at Stolz as defined by Pentecost and Viles (1994) as "vertical accretions leading to water impoundment as pools, pounds and lakes" (p.309, figure 2.7A). Note that other studies use

the term ‘dam’ rather than ‘barrage’, but both terms refer to the same morphology (e.g. Wooding, 1991; Pentecost, 2005). Furthermore, many in the travertine (less so in the tufa) literature uses the word ‘terrace’ and ‘barrage’ interchangeably (Hammer *et al.*, 2010 (p. 345) defines “‘barrages’ as terraces that are filled with water, forming pools and lakes”) which may not be correct as when travertine ‘terraces’ are emptied they specifically display a barrage morphology. The term ‘terrace’ will only be used in this study to describe other studies that specifically use this word. In addition, this study uses the term ‘barrage’ regardless of size and ‘pool’ will be used to denote any body of water stored by a barrage (Hammer *et al.*, 2010).

The term ‘mound’ will be used to describe the deposit at Wolf (figure 2.7B). Note other studies use the term ‘dome’ to describe similar morphological deposits (e.g. Pentecost and Viles, 1994; Kerr and Turner, 1996).

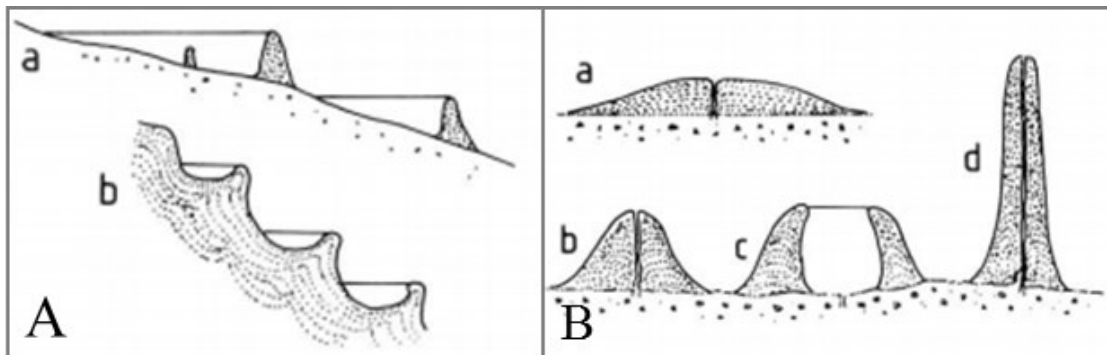


Figure 2.7: Travertine morphology as described in (and figure modified from) Pentecost and Viles (1994); (A) barrage morphology: “(a) large lake barrages, (b) barrage system on travertine slope” (Pentecost and Viles, 1994, p. 309); and (B) mound morphology: “(a) low mound, (b) steep mound or fissure ridge, (c) mound with central pool, (d) tall submerged lake mound” (Pentecost and Viles, 1994, p. 309).

Chapter 3: Study Area

3.1 Regional Setting

This is primarily a field study concerned with the geomorphic investigation of unique hyper-saline spring systems linked to two evaporate diapirs (Stolz and Wolf) on Axel Heiberg Island in Nunavut (figure 3.1).

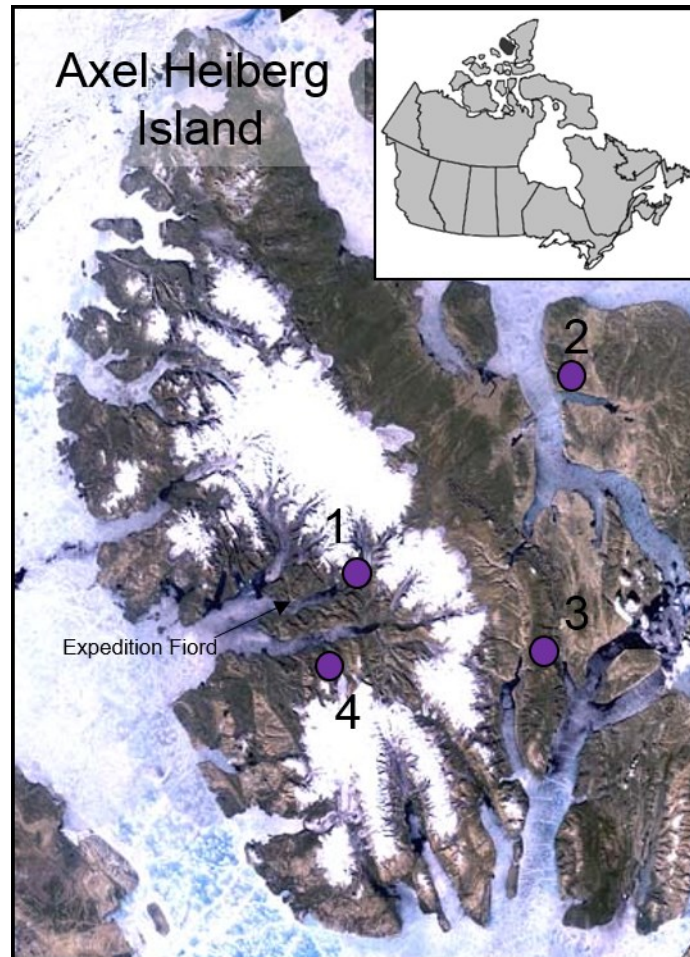


Figure 3.1: A false colour Landsat mosaic of Axel Heiberg Island showing ice caps, glaciers and fiords with map insert modified from Grasby *et al.*, 2003). Purple circles indicate the location of the following: (1) McGill Arctic Research Station (M.A.R.S); (2) Eureka Weather Station on Ellesmere Island; (3) Stolz Diapir study site and (4) Wolf Diapir study site (also known as Lost Hammer).

Axel Heiberg is a 370 km long island located along the eastern margin of the Sverdrup sedimentary basin in the Canadian High Arctic, extending 78°08'N to 81°21'N and from 85°00'W to 96°00'W. It is the second most Northerly Island (after Ellesmere Island) within the Canadian Arctic Archipelago and is situated approximately 1,200km south of the geographic North Pole (Pollard, 2005b; Jackson & Harrison, 2006). Ice covers 31.5% or approximately 11,734Km² of the island's surface and is made up of large ice caps (the Muller and Stacie Ice caps) overlaying the interior in addition to various glaciers types (e.g. valley) and smaller ice caps (Pollard, 2005b). The Princess Margaret Mountain Range dominates the island's topography, providing an alpine topography that characterizes the island. Along the perimeter of Axel Heiberg Island are three bays (Whitsunday, Sand and Good Friday) and multiple fiords (Expedition, Strand, Li, Middle, Skaere, Wolf and Glacier fiords). Finally, the island is inhabited (the closest community is Grise Fiord located on Ellesmere Island) and houses two research centers: the McGill Arctic Research Station (MARS) and the CSA (Canadian Space Agency) station run by the CARN program (Canadian Analogue Research Network; Pollard, 2005b; Pollard *et al.*, 2009).

3.2 Climate

The climate of Axel Heiberg Island is polar desert with dry, cold winters and cool summers. Historical meteorological data from Eureka Weather Station (located on Ellesmere Island at 79°59'00"N; 85°56'00"W; the closest weather station to Axel Heiberg Island) provides a mean annual, January and July temperatures of -19.7°C, -36.1°C and +5.4°C with minimum air temperatures frequently reach -55°C (Pollard *et al.*, 2009). Long term measurements at Colour Lake at the McGill Arctic Research Station (MARS) offer a

mean annual air temperature of -15.5°C (Andersen *et al.*, 2008). Annual precipitation recorded at the Eureka Weather Station is roughly 64mm with over half of the precipitation amount as snow (Pollard and Bell, 1998).

3.3 Regional Geology

The Eureka Sound fold belt on Axel Heiberg Island contains the thickest Mesozoic sequence of the Sverdrup basin. The Sverdrup Basin is a 12-15km thick sedimentary basin composed of varying marine lutaceous and non-marine arenaceous deposits ranging from early Pennsylvanian to early Tertiary in age (Pollard, 2005; Jackson & Harrison, 2006). Orogenic activity during the Tertiary produced the mountainous topography as well as widespread diapirism around the basin.

Diapirs are “masses of salt that have flowed ductilely and appear to have discordantly pierced or intruded” the overlying sedimentary-clastic rocks (Hudec & Jackson, 2012, p. 24; Jackson and Talbot, 1991). At least 100 diapirs have been identified within the Sverdrup basin, of these about 60 are exposed including 46 on Axel Heiberg Island (Thorsteinsson, 1974; Jackson & Harrison, 2006). The Island has the second greatest concentration of exposed diapirs in the world, second to Iran (Harrison and Jackson, 2014). Stolz diapir, located close to Whitsunday Bay, is the only diapir on the island with an exposed halite (NaCl) core (Hugon & Schwerdtner, 1982). The source material for the diapirs within the Sverdrup Basin is the Otto Fiord Formation, an evaporative belt 800 km long and 240 km wide where evaporites accumulated during Carboniferous rifting (Thorsteinsson, 1974; Davies & Nassichuk, 1975; Jackson & Harrison, 2006).

3.4 Permafrost Conditions

Axel Heiberg Island lies within the continuous permafrost zone; permafrost depth has been measured to between 400-600m from oil and gas exploration wells (Pollard *et al.*, 2009). The thickness of the active layer is between 40-60cm. Numerous permafrost landforms are present around the island including ice wedge and polygonal terrains, icings and frost mounds. Several pingos have been documented; most occur in glacier floodplains and are probably hydraulic systems in nature, for example two small pingos at Middle Fiord lie less than 100m from glacier termini (Pollard *et al.*, 2009). Ice wedge polygons 8m-14m in diameter are common on most tundra surfaces. Patterned ground, mainly poorly sorted and non-sorted circles and stripes occur on sparsely vegetated surfaces. Ground ice is a common constituent of permafrost made up of pore ice, segregated ice lenses, injection, vein and massive ice. Massive ice may be either buried glacier ice or intrasedimental in origin. Permafrost features associated with the perennial springs include icings, icing mounds, icing blisters and frost blisters. Small palsa mounds occur in organic-rich wetlands. Despite the very cold climate of the region it seems that many of the largest glaciers are wet-based and do not have well developed permafrost beneath them. This has significant implications for subglacial erosional and hydrologic regimes.

3.5 Spring Activity on Axel Heiberg Island

Seven springs (figure 3.2) have been identified on Axel Heiberg Island, four of which have been confirmed to flow year round (Pollard, personal communication). These four springs include: (1) Gypsum Hill, located at 79°24'30"N, 90°43'05"W; (2) Colour Peak, located at 79°22'48"N, 91°16'24"W; (3) Whitsunday Bay (Stolz Diapir), located at

79°04'30"N; 87°04'30"W; and (4) Strand Fiord (Wolf Diapir), located at 79°07'23"N; 90°14'39"W. These springs are not associated with any volcanic (geothermal) heat source and, along with recently identified springs on Ellesmere Island (Grasby *et al.*, 2014), are among the only known examples of cold perennial springs occurring in thick cold permafrost on Earth (Andersen *et al.*, 2002). The waters of all four springs are characterized by hyper-saline waters (brines; Pollard *et al.*, 1999). The spring chemistry reflects a long period of contact with evaporate deposits that are part of the geology of the Sverdrup Basin (Pollard, 2005). The groundwater source has been studied but remains uncertain, however recent meteoric water and surface water have been excluded (Pollard *et al.*, 1999). It has been proposed that the groundwater source for most of the springs may come from (1) an ancient formational subpermafrost source (perhaps relict seawater), (2) deep-circulation of warm based glacial melt-water, or (3) complex geological processes associated with decaying hydrous minerals (Pollard *et al.*, 1999; Pollard, personal communication). Andersen *et al.*, (2002) proposed that the water source for the Gypsum Hill and Colour Peak springs could come from Phantom Lake, a very deep ice domed lake adjacent to the Thompson Glacier. Anderson's model suggests the water enters the subpermafrost hydrological system via a through talik and connects to the springs by flowing through the evaporate layers. Furthermore, Grasby *et al.* (2012) suggests that formation waters in the Sverdrup Basin have a seawater origin with local anomalies of highly saline waters associated with diapirs.

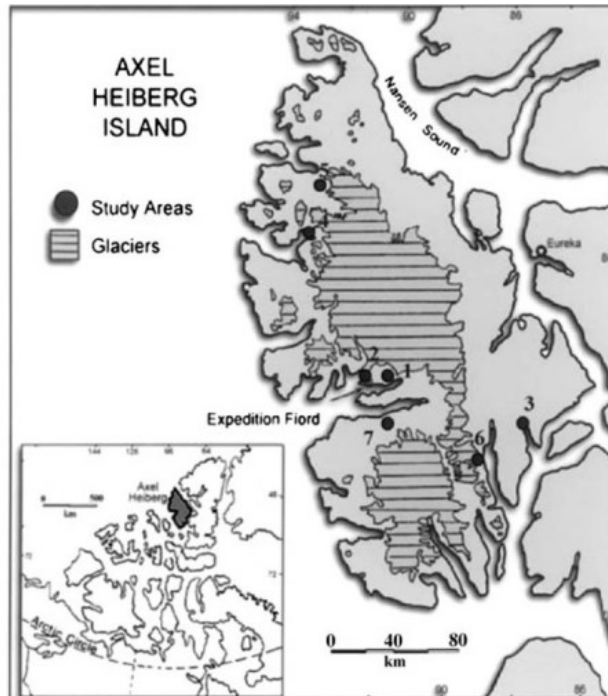


Figure 3.2: Springs identified on Axel Heiberg Island, (1) Gypsum Hill, (2) Colour Peak, (3) Whitsunday Bay, (4) Middle Fiord, (5) Bunde Fiord, (6) Skaere Fiord and (7) Strand Fiord (Pollard *et al.*, 2009).

The springs at Gypsum Hill and Colour Peak have been extensively studied for their water chemistry, mineral precipitates, hydrology and microbiology. The Colour Peak spring system is made up of 20 outlets covering an area of 900m² (Omelson *et al.*, 2001, 2006). Various small scale travertine deposits were recorded and the precipitation of calcite is thought to be a result of CO₂ outgassing based on saturation index calculations. The Gypsum Hills springs covers a 2000-2500m² area and is made of 40 outlets (Pollard *et al.*, 2009). Mineral precipitates are largely made up of a gypsum crust resulting from the lower water alkalinity and a higher concentration of SO₄²⁻ (Omelson *et al.*, 2006). The spring outlet temperatures and discharges were monitored continuously for five years (Pollard *et al.*, 1999). Results showed that the Gypsum Hill springs varied between -3.5 and +6.6°C and Colour Peak varied between -4.0 and +5.6°C despite large fluctuations in air temperature

throughout the year (Pollard *et al.*, 1999). Discharge rates remained consistent throughout the year as well. Discharge rates at Colour Peak vary between 1.3-1.8L/s with an estimated total discharge of 20-25L/s; at Gypsum hill discharge rates at various outlets are highly variable but flow at constant rates, the largest outlet measured had a 0.9-1.0L/s discharge rate, while the total estimated is between 10-15L/s (Pollard *et al.*, 1999).

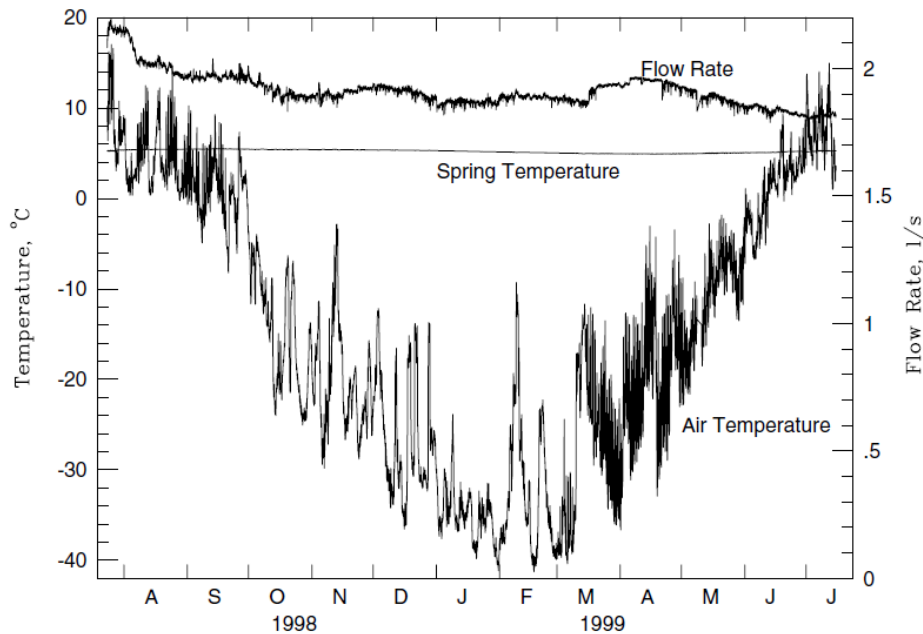


Figure 3.3: Results from a two year monitoring of the Colour Peak Springs for discharge (flow rate), water temperature at the spring outlet and air temperature (Andersen *et al.*, 2002).

3.6 Microbiology

The microbial ecology of springs at Gypsum Hill, Colour Peak, and Wolf Diapir have also been investigated (Perreault *et al.*, 2007, 2008; Niederberger *et al.*, 2010; Lay *et al.*, 2012). These studies show that life can occur despite their harsh sub-zero environment, prolonged periods of darkness and sunlight during the year, and can tolerate high amounts of salinity. Communities at each of the springs are composed mostly of bacteria and a smaller portion of archaea. Microbial life in the Gypsum Hill and Colour Peak springs

appears to depend on sulfur-based chemolithoautotrophy (Perreault *et al.*, 2007, 2008); while microbial life at the Wolf Diapir springs depend on methane. Methane gas seeps from the source waters are thought to provide “an energy and carbon source for sustaining anaerobic oxidation of methane-based microbial metabolism” (Niederberger *et al.*, 2010, p. 1327). Channel waters supported more of an oxidizing, less reducing environment for microbial communities.

3.7 Study Sites

This thesis focuses on two hyper-saline spring systems on Axel Heiberg Island: Wolf Diapir near Strand Fiord at 79°07'23"N; 90°14'39"W and Stolz Diapir near the head of Whitsunday Bay at 79°04'30"N; 87°04'30"W (figure 3.1).

3.7.1 Stolz Diapir

The Stolz Diapir spring has remained largely unstudied, although has been mentioned in a few publications. Hugon and Schwerdtner (1982) briefly mention the spring within their study of the geologic structure of Stolz Diapir. They describe the spring as “a white deposit of crumbly polycrystalline halite with average thickness of 1.5m, which resembles a large snowdrift” (p. 303). The spring is again referenced in Schwerdtner and Van Kranendonk (1984). The only paper to describe the deposit in more detail and the pool and barrage structures is by Pollard (2005). Based on several years of observation, Pollard (2005) describes a series of pools (up to 3 m deep and 10 m wide) and barrage structures formed by precipitating hydrohalite that staircase down the valley. It then merges with a fan-shaped icing that is 100-150m in length, 25m wide (100m wide at its widest point) and 3.5m thick spread out on the Whitsunday river floodplain. A salt travertine/tufa deposit up

to 5m thick located at the spring outlet and 1m thick at the valley mouth was also reported (Pollard, 2005).

3.7.2 Wolf Diapir

The spring at Wolf Diapir was discovered by W. Pollard in 2004 during an aerial survey in the Strand Fiord area and visited first in 2005 and first reported in the literature in 2010 by Niederberger *et al.* The salt deposit at this site resembles a large hollow cone-shaped mound (2.5m tall and 3m in diameter; Battler *et al.*, 2013) at the outlet and a large 100m by 15m salt pan down slope whose size varies each year (Pollard, personal communication). During the summer, the mound is empty and the spring discharge dissolves one side of the mound to create one continuous stream; during the winter this summer outflow is blocked off and the mound fills with water and overflows the sides (Niederberger, *et al.*, 2010). Previous studies at this site have focused on the microbiology (Niederberger *et al.*, 2010; Lay *et al.*, 2012) and the mineralogy (Battler *et al.*, 2013). Battler *et al.* (2013, p.371) determined the most abundant minerals “are, in decreasing order, halite, thenardite, gypsum, mirabilite, other Na-bearing sulphates, and presumed detrital minerals (quartz, plagioclase, clays). Very few samples contain carbonate minerals; one sample contained magnesite, and one contains calcite.” Although Niederberger *et al.* (2010) mention the metastable nature of some samples, since samples tended to liquefy when warmed, W. Pollard (one of the co-authors) suggested the potential occurrence of hydrohalite, although its presence at this site has remained unconfirmed until this research. All previous studies of the Wolf Diapir spring fail to fully characterize the geomorphic nature of the unusual salt deposit.

Chapter 4: Methodology

4.1 Introduction

This thesis is the product of a geomorphology study that has as its primary objective the explanation of unique salt (travertine/tufa-like) structures at two hyper-saline spring sites on Axel Heiberg Island. Since geomorphology is concerned with the investigation of landforms, landscape processes, and their environmental significance, fieldwork remains an important component of most geomorphic research. Remote Arctic fieldwork is physically difficult and inherently risky both from a scientific point of view and logistical perspective. Most geomorphic studies include supporting laboratory research and/or numerical simulation as part of their analytical framework. Accordingly, the research design for this study has three parts, including: (1) a field program comprised of four periods of fieldwork between April 2013 and July 2014 involving field measurements and sampling followed by (2) laboratory based geochemical analyses, and (3) the application of an equilibrium chemical thermodynamic model to test hypothesized mineralogical processes.

The following methods discussion adopts the same framework and is therefore divided into 3 parts; first, a detailed breakdown of field activities followed by (2) a description of laboratory analyses and (3) a description of modelling approaches.

4.2 Site Selection and Field Methods

Of the four spring systems on Axel Heiberg Island that are confirmed to be active year round, the Wolf Diapir and Stolz Diapir sites were chosen because of the significant

presence of sodium chloride minerals precipitating rather than carbonate or calcium sulfate minerals, as well as the lack of previous research on their geomorphology and geochemistry. Fieldwork was done over a period of two years with two field trips per year (April and July) to encompass both summer and winter processes (fieldwork done in April allowed measurement and sampling under extreme cold conditions with temperatures $<-30^{\circ}\text{C}$ but with 20+ hours of daylight).

The Stolz Diapir site was particularly exciting because this research represents the first comprehensive study on this spring deposit. Previous work at the site has focused on diapir geology (Schwerdtner and Van Kranendonk, 1984) or icing activity during the winter (Pollard, 2005). Annual observations of the spring deposit have been done (in April and again in summer) by Prof. Wayne Pollard, but mainly as part of the larger program of spring research. The four periods of field work include: a short reconnaissance visit in April 2013 which involved collection of water and precipitate samples and an extended visit in April 2014 when additional sampling, flow observations and the bulk of winter fieldwork was done. Field work in July 2013 included detailed mapping, stratigraphic observations, discharge measurements, inflow and outflow sampling as well as the installation of temperature loggers and time lapse cameras and in June 2014 which focused on repetitive observations and sampling but no new work.

Since previous work at Wolf Diapir focused on microbiology and mineralogy, this research focused specifically on the geomorphology and geochemistry with the aim of complementing previous work. Although dramatically different this study site was considered secondary to Stolz Diapir for the following reasons: firstly because of time constraints, secondly because winter access was problematic and thirdly because of

previous studies. Work done at the Wolf Diapir site was limited to visits in June 2013 (reconnaissance) and July 2014. As a result the data and analysis for this site is limited but sufficient to make general geomorphic comparisons with the Stolz Diapir study site.

4.2.1 Differential GPS Survey

GPS points were collected using a Trimble 5700 differential GPS at the Stolz Diapir site. The purpose of this data collection was to create a baseline to monitor changes in the deposit over time, to create a Digital Elevation Model (DEM) of the salt deposit and to record specific structural features. These features include the largest barrage structures (tape measurements were also done to validate GPS points), water sample locations, and the location of stratigraphy work.

4.2.2 Abney Survey

A slope survey of the valley and the travertine/tufa deposit at the Stolz Diapir site was done using an Abney clinometer and tape measure. Because the deposit is very thick and the valley floor is rarely exposed, the slope survey was conducted on the surface of the deposit to capture as much of the valley as possible, and involved surveying long distances and did not include specific structures. A generalized valley slope profile was created by calculating elevation changes over horizontal distances using basic trigonometry.

4.2.3 Mineral Samples

Mineral (precipitate) samples were collected to represent the full range of precipitate locations, structures and settings within the spring systems. Samples were aseptically placed in sterilized Whirl-Pak® sample bags. July sampling included a combination of surface and subsurface materials including from a 2m section excavated through the floor of one of the larger pools. July samples were transported and stored at 5°C-10°C in a cooler. Samples collected in April included crystal clusters from the travertine/tufa surface as well as the submerged floor of several of the larger pools. Excess water was drained from the submerged mineral samples before bagging. April mineral samples were transported and stored at -21°C to -25°C. In previous experiments, Pollard found that samples collected under cold conditions from active and pool structures tended to be unstable at temperatures >0°C freely melting (dissociating) into a mixture of NaCl brine and salt crystals.

4.2.4 Water Sampling

Water samples were collected in the field using 250mL acid washed polyethylene bottles. Samples locations were chosen to represent changes at regular intervals along the spring outflow. At the Stolz Site this included the inflow stream and snow deposits, the spring outlet, the halfway point of the deposit, the valley mouth and the salt pan on the Whitsunday floodplain (figure 4.1). Samples for the Wolf Diapir site (figure 4.2) included the outlet and the spring channel 5m away from the outlet. Water samples were collected at the same locations for each field season wherever possible. The location of the main spring outlet migrated between seasons and from one summer to the next. In July 2014, the

outlet at the Stolz site was covered by a recent debris slide so a water sample was taken at the first point outflow down valley (and thus is the sample considered to be from the summer outlet position).

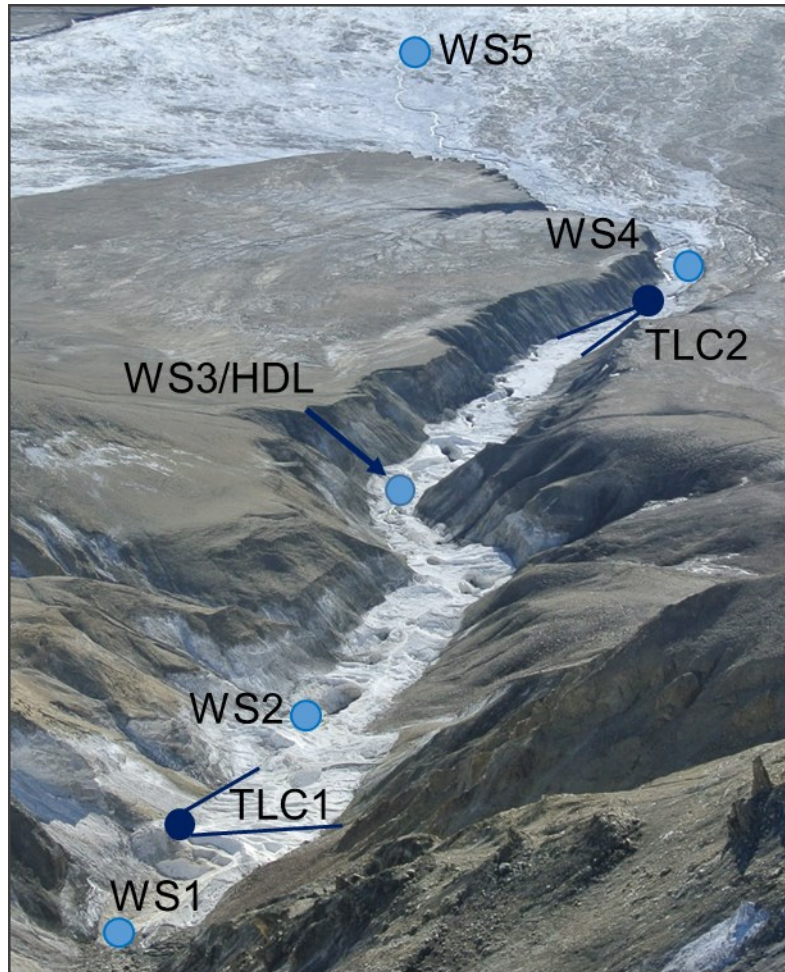


Figure 4.1: Water samples (WS), time lapse cameras (TLC) and Hobo data logger (HDL) locations at Stolz Diapir site. WS1 represents the winter outlet, WS2 is the summer outlet, WS3/HDL is the halfway point of the deposit for water sampling and the location of the hobo data logger, WS4 is the valley opening and WS5 is the salt pan within the floodplain. Lines at TLC locations shows approximate field of view of the cameras.



Figure 4.2: Water sample locations at Wolf Diapir site. WS1 (Water Sample 1) represents the outlet, and WS2 is the spring channel located 5m away from the outlet.

4.2.5 Field Instrumentation: Temperature Loggers and Time Lapse Cameras

The saline nature of these sites proved to be extremely problematic for instrumentation installed in and around the springs. For example, 4-channel and 2-channel Hobo® data loggers that were set up (June 27th, 2013) inside the mound at the spring outlet at Wolf Diapir (designed to collect temperatures in a vertical profile with each sensor spaced 65cm) failed because brine readily penetrated the housing of both loggers. At Stolz Diapir, 4-channel Hobo® data logger was suspended over a series of lower pool and barrage structures (Figure 4.1) with three sensors cables suspended from the logger into a pool and one sensor suspended above the anticipated full pool water depth to record air temperatures. Initially all four sensors recorded ambient air temperatures but as the pool filled during winter the three suspended sensors sequentially deviated from the air temperature providing a time series record of water level change. A second 4-channel Hobo® data logger and a 2-channel (temperature, relative humidity) Hobo® data logger were installed above the outflow valley to record air temperature (x2), relative humidity and soil temperatures at 0cm, 10cm and 15 cm depths. These loggers were installed on

June 27th, 2013 and successfully collected until April 2014 when they were retrieved. A third 4-channel Hobo® data logger was installed in the inflow stream at Stolz Diapir with three sensors at different depths in the stream and one sensor to collect air temperature. The data from this logger provided mixed results.

At Stolz Diapir, two time lapse cameras (Bushnell Trophy Cam XLT) were installed on July 10th, 2013 to collect daily (1X at solar noon) images of surface hydrologic processes. These cameras were downloaded on April 18th, 2014. These cameras were chosen specifically for their reliability and because they had a one year battery life (lithium batteries were used to ensure functionality in cold temperatures); were able to withstand cold temperatures and had night time photography capabilities. Cameras motion sensors were disabled to conserve battery life. One camera was installed at the spring outlet and oriented downstream and the second lower in the travertine/tufa structure just before the valley opening was oriented upstream (figure 4.1).

4.3 Laboratory Analyses

Bulk analysis of mineral precipitates was determined by x-ray diffraction using a Bruker D8 Discovery X-ray Diffractometer in the Department of Materials Engineering at McGill University. Mineral samples were oven dried for two days and grinded into a fine powder using a mortar and pestle before x-ray diffraction took place.

Water samples were analyzed for major ion concentrations (Na^+ , Ca^{2+} , Mg^{2+} , K^+ , Cl^- , SO_4^{2-} , NO_3^- , and PO_4^{3-}) by Ion Chromatography using a Dionex DX-00 Ion Chromatography in the Department of Materials Engineering at McGill University. Hyper-

saline samples had to be diluted by 100x for Ca^{2+} , Mg^{2+} , K^{+} ions to be within the detectable range of the instrument and by 1000x to detect Na^{+} and Cl^{-} ions. Neither NO_3^{-} nor PO_4^{3-} were detected in any of the water samples analyzed. The water fraction of thawed dissociated mineral samples were also analysed for the same ions as the water samples.

4.4 Chemical Modelling

This study used Frezchem, a FORTRAN version of the Spencer-Møller-Weare model, to calculate the composition of solids and liquids and sequence of precipitation for solutions under freezing conditions. Other water chemistry models generally only have capabilities to calculate compositions above 0°C . The model uses chemical thermodynamic principles over a -60°C to $+25^{\circ}\text{C}$ temperature range and uses the Pitzer equations (specific ion interaction equations) to calculate activity coefficients for water and ions in complex solutions and at high ionic strengths (Marion, 1997).

Currently there are 16 versions of the model available (at <http://www.dri.edu/frezchem>) with different features and environmental parameters available within each version. The model's author (Giles Marion) recommends using earlier versions of the model if features added in later versions are not required because he feels the earlier versions are more robust. In this study version 5.2 was employed (this version is parameterized for the Na-K-Mg-Ca-Cl-SO₄-H₂O system) as it has all the capabilities needed for this study. A list of minerals calculated by the Frezchem model are found in table 4.1.

This study used water chemistry data for samples collected directly in the field to determine the sequence of mineral precipitates for both the Wolf Diapir and Stolz Diapir

spring systems. Each sample chemistry was run in the model twice first using the evaporation precipitation mechanism at +7°C (the average summer temperature recorded by the hobo data logger) and then using the freezing fractionation precipitation mechanism over a temperature range of +15°C to -45°C (temperature range recorded by hobo data logger). Results from both runs were added and are presented in table 5.3. To ensure the functionality of the model, input water chemistry had to be charge balanced. The author specifies to adjust the charge balance using chloride ions. To do so this study had to add chloride ions to each sample.

Table 4.1: Minerals (solid species) in Frezchem Model, version 5.2 (source: http://www.dri.edu/images/stories/research/projects/FrezChem/Release_Notes_5.2.pdf)

#	Species	#	Species	#	Species
31	H ₂ O(cr,l)	46	MgSO ₄ •K ₂ SO ₄ •6H ₂ O(cr)	61	CaMg(CO ₃) ₂ (cr)
32	NaCl•2H ₂ O(cr)	47	Na ₂ SO ₄ •MgSO ₄ •4H ₂ O(cr)	62	Na ₂ CO ₃ •7H ₂ O(cr)
33	NaCl(cr)	48	CaSO ₄ •2H ₂ O(cr)	63	KHCO ₃ (cr)
34	KCl(cr)	49	CaSO ₄ (cr)	64	CaCO ₃ (cr,aragonite)
35	CaCl ₂ •6H ₂ O(cr)	50	MgSO ₄ •12H ₂ O(cr)	65	CaCO ₃ (cr,vaterite)
36	MgCl ₂ •6H ₂ O(cr)	51	Na ₂ SO ₄ •3K ₂ SO ₄ (cr)		
37	MgCl ₂ •8H ₂ O(cr)	52	CaCO ₃ (cr,calcite)		
38	MgCl ₂ •12H ₂ O(cr)	53	MgCO ₃ (cr)		
39	KMgCl ₃ •6H ₂ O(cr)	54	MgCO ₃ •3H ₂ O(cr)		
40	CaCl ₂ •2MgCl ₂ •12H ₂ O(cr)	55	MgCO ₃ •5H ₂ O(cr)		
41	Na ₂ SO ₄ •10H ₂ O(cr)	56	CaCO ₃ •6H ₂ O(cr)		
42	Na ₂ SO ₄ (cr)	57	NaHCO ₃ (cr)		
43	MgSO ₄ •6H ₂ O(cr)	58	Na ₂ CO ₃ •10H ₂ O(cr)		
44	MgSO ₄ •7H ₂ O(cr)	59	NaHCO ₃ •Na ₂ CO ₃ •2H ₂ O(cr)		
45	K ₂ SO ₄ (cr)	60	3MgCO ₃ •Mg(OH) ₂ •3H ₂ O(cr)		

Chapter 5: Results

Chapter 5 follows the same structure as in chapter 4 and is divided into three sections: (1) field, (2) laboratory and (3) modelling results. Each section covers findings from both study sites, although in some cases the Stolz Diapir site includes additional material (e.g. time lapse cameras). Section 5.1 is sub-divided into (a) morphology; (b) stratigraphy; (c) spring discharge; and (d) automated systems (Hobo temperature logger and time lapse camera). Section 5.2 comprises the laboratory results and is separated into (a) water chemistry (including major ion identification) and (b) mineralogy. Section 5.3 contains results Frezchem version 5.2 using input data from section 5.2.

5.1 Field results

5.1.1 Morphology of Mineral Precipitates (Travertine/Tufa)

5.1.1.1 Stolz Diapir

The salt deposit investigated at Stolz Diapir occurs autochthonously in a narrow, steep-sided tributary valley carved by a small stream fed by meteorogenic perennial groundwater discharge emanating from the base of the diapir. The valley begins abruptly at the spring outlet and has down cut through surficial colluvial and glacial sediments into steeply dipping bedrock (shale). The morphology of the salt (travertine/tufa-like) precipitates exhibit a distinct down valley progression of structures that begin at the spring outlet and continue downstream to the Whitsunday River floodplain (figure 5.1).

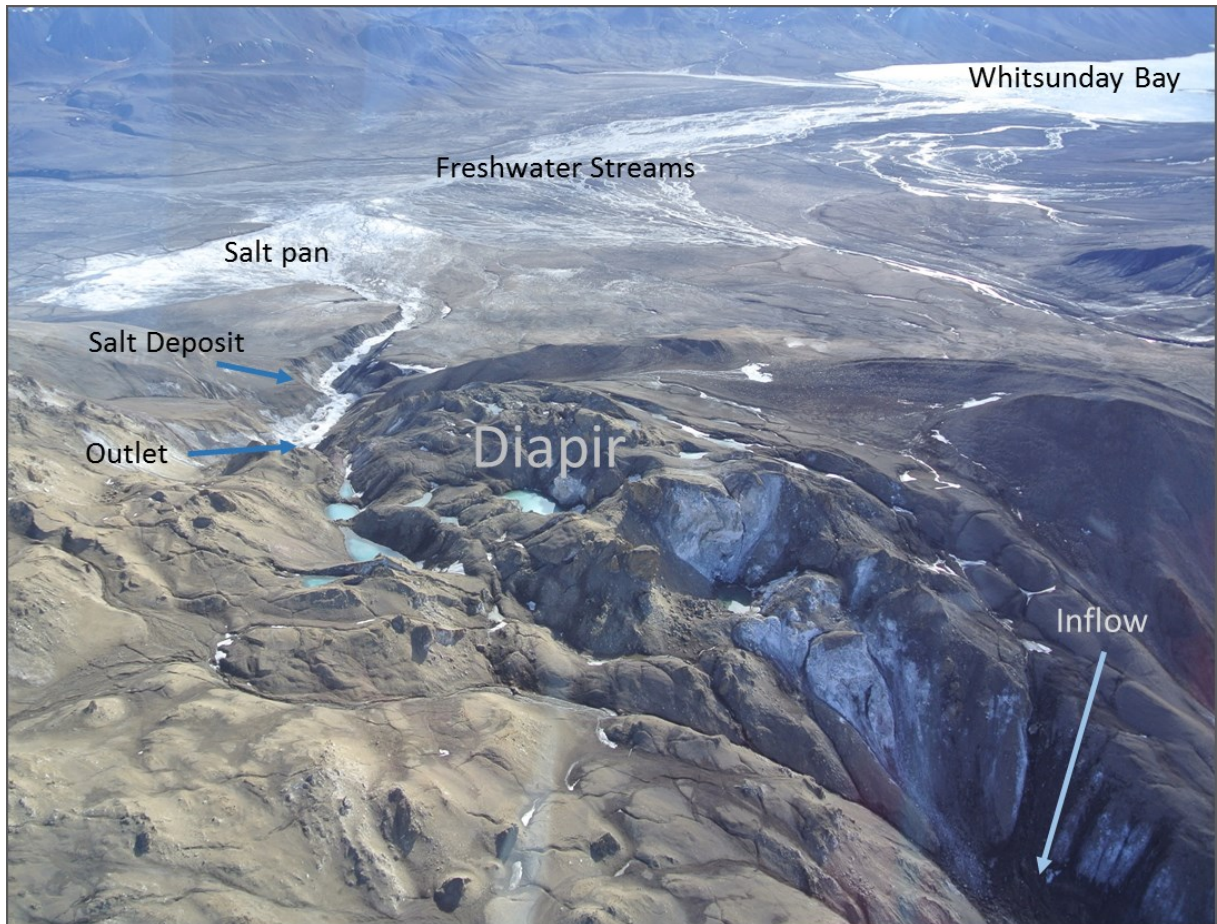


Figure 5.1: Aerial view of the Stolz site (image taken in helicopter in July 2014)

5.1.1.1.1 Barrage structures

These structures consist of a series of barrages that dam stream flow producing elongated pools that stair case down the narrow valley for approximately 800m. At the mouth of the valley, the salt spreads out and forms a large salt pan that extends 300m into the Whitsunday River floodplain where it is truncated by a large freshwater river that flows into the Arctic Ocean via Whitsunday Bay (figure 5.1).



Figure 5.2: Seasonal difference of the deposit at Stolz Diapir, both images were taken at approximately the same location with a similar orientation; (A) taken in April 2012 by Prof. Pollard and (B) taken in July 2013.

The barrage features vary greatly in size and shape, ranging 30m wide and 2-3m high to only a few centimeters in width and height. The size, shape and spacing of the barrage structures and the pools they create are closely linked to their position in the valley, the valley width and slope. Generally the thickest salt accumulation (~ 4m) and the larger barrages occur in the upper part of the valley while the barrages in the lower half of the valley are smaller and salt accumulation is much thinner. The barrages are typical fluvial travertines or tufas that are mainly curvilinear with a downstream convexity, particularly the larger dams in the upper valley. The downstream side of larger barrages have small micro-barrages created when the pools overflow and a thin layer of water flows down the barrage face. It is important to note that the pool-barrage system with flow topping the barrage is only active during cold winter months, the pools drain in the spring and the spring fed stream flow occurs along the streambed under the salt deposit (figure 5.2). Detailed measurement of barrage size and shape was possible only during the summer.

The upper barrage structures near the outlet are characterized by loosely packed cubic crystals and hexagonal pseudomorphs in the summer. From the halfway point downstream, a fine white powder forms a light dusting on the surface of the deposit and is present all the way into the Whitsunday River floodplain. The deposit becomes progressively more compact with increasing distance away from the outlet. Smaller barrage structures (a few meters in length and approximately 30cm in height) occur in this part of the valley. Toward the valley opening, a distinct hard crustal layer develops (<1cm thick), with a mixture of white precipitates and mineral sediments mixed in. In addition, the deposit itself is thicker (approximately 2.5m and is 3-4m thick at the outlet) in the upper reaches of the deposit and gradually thins out until the plain is reached. Density measurements of the deposit show below 1m from the deposit surface the deposit reaches a maximum density of 1.42 gm/cm³.

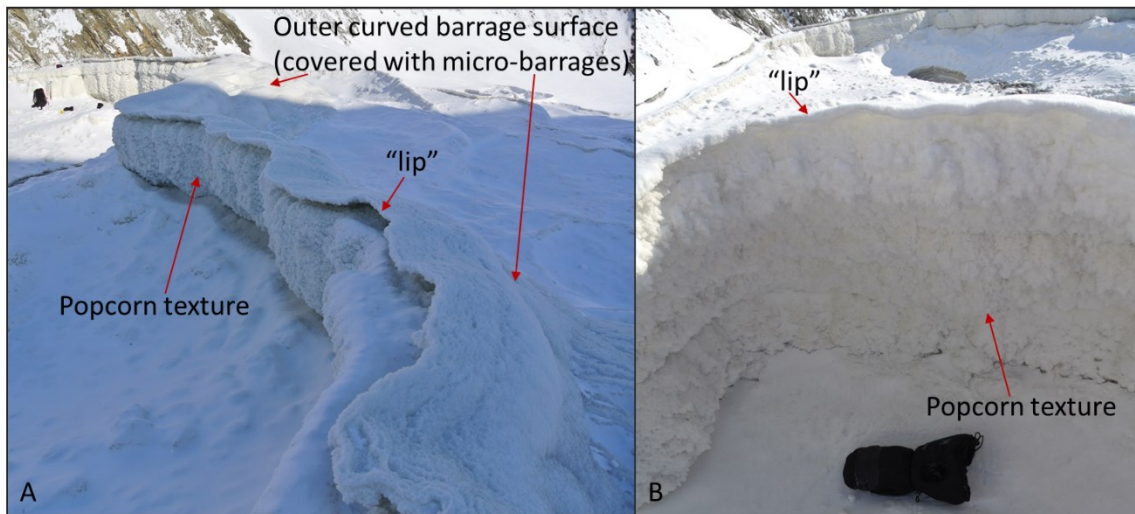


Figure 5.3: Large barrage structures with emptied pool. Dimensions of terrace in image A are 26m in length and 1.6m in height.

Figure 5.3 shows a typical salt barrage structure that forms at Stolz Diapir. Figure 5.3A is one of the larger barrages (length is 26m and 1.6m high) and displays an interesting

morphology: the inside of the barrages is near vertical and has a ‘popcorn-like’ texture formed by precipitating minerals. The outside of the structure is curved and is covered with a series of micro-barrages. The top of the barrage forms a ‘lip’ that is thin and curves upstream. The lip is a continuous surface that follows the overall down valley curvature. The lip is a continuous surface that follows the overall down valley curvature. The upstream side is much thinner than the main barrage wall and creates a hollow space between the top of the thicker barrage wall and the lip. Figure 5.3B shows a slightly different barrage structure that formed on an angle inclined upstream. The formation of the lip in figure 5.3B differs from figure 5.3A in that it is formed as a gradual continuation of the barrage structure (with the same thickness of the barrage wall).

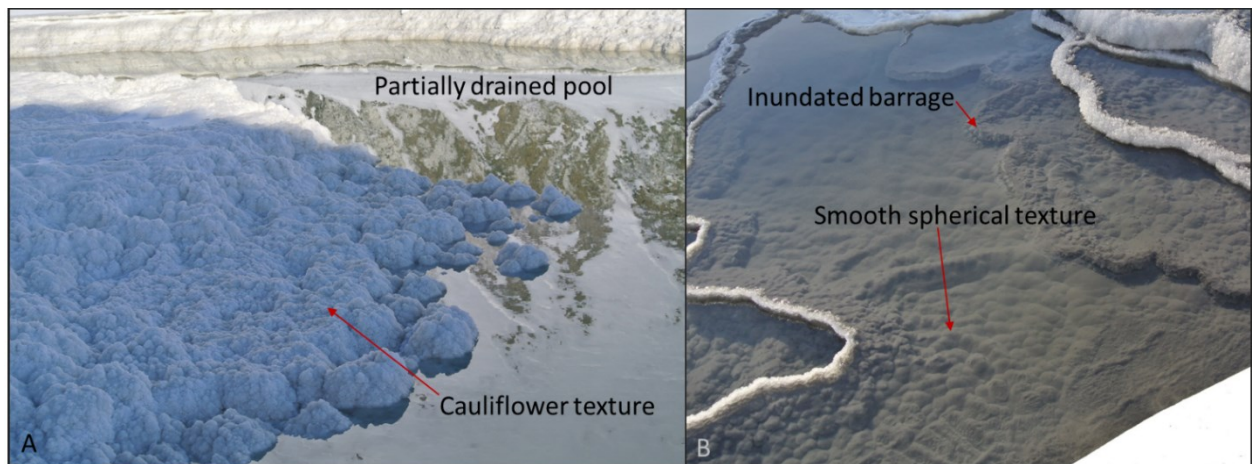


Figure 5.4: Various textures along the bottom surface of the spring channels and pools. (A) Shows a cauliflower-like texture located in the pool the hobo temperature data logger was collected; and (B) shows a smooth spherical texture at a smaller pool just downstream from the time lapse camera located at the valley opening.

Figures 5.3 and 5.4 show various surface textures that form on the deposit. Figure 5.3 shows the ‘popcorn’ texture that is common inside the pool of larger barrage walls. The partially drained pool (where the hobo data logger was installed) in figure 5.4A illustrates the ‘cauliflower’ texture that coats the pool sides. Figure 5.4B shows the smooth ‘ball’

texture that coats the pool bottoms. The size of the spheres varies such that smaller sizes occur near the valley mouth within smaller pools and larger spheres occurring upstream in larger pools. Another morphologic feature was observed in the pool containing the hobo data logger (Figure 5.16B) is a thin sinter crust called a “floating raft” (Filippi *et al.*, 2011, p. 146).

5.1.1.1.2 Pools

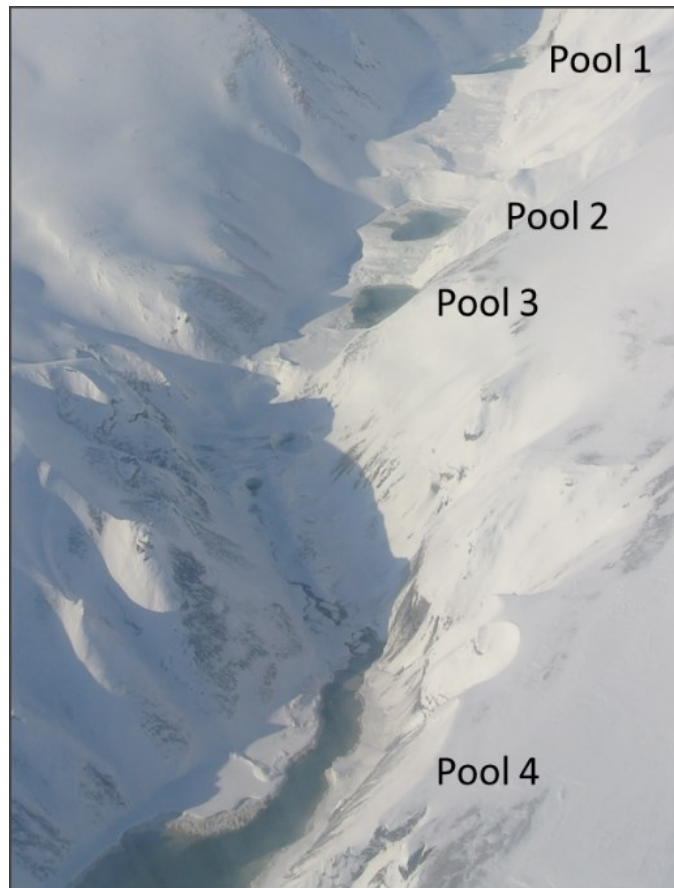


Figure 5.5: Location of pools identified in April 2014. Pool measurements are: (pool 1) 41.21m by 24.52m; (pool 2) 25.70m by 11.52m; (pool 3) 27.80m by 12.25m; and (pool 4) 53.60m by 23.80m. Each pool is a few meters deep.

The pools that form during the winter vary in size from year to year. Four large pools were still active in April 2014 (Figure 5.5); pool dimensions were: (pool 1) 41.21m by 24.52m; (pool 2) 25.70m by 11.52m; (pool 3) 27.80m by 12.25m; and (pool 4) 53.60m by 23.80m and pool depth was between 2-3m. It is common for larger pools to inundate two or more smaller pools to form a single large pool (figure 5.6).

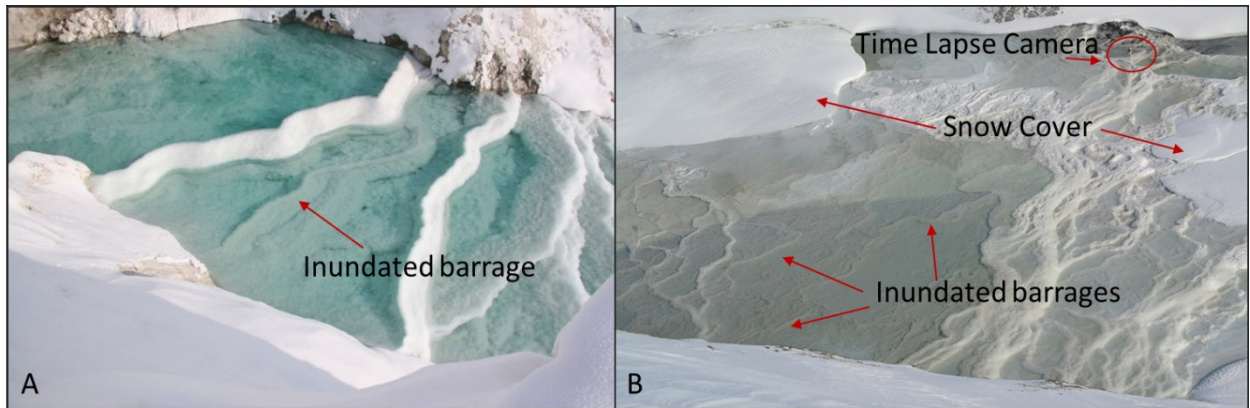


Figure 5.6: (A) Image taken in April, 2012. During winter barrage structures fill up with water creating pools that staircase down the valley (image taken by W. Pollard). (B) Examples of inundated barrages in smaller in size located at the valley opening in April 2014.

A phenomenon not seen during previous winter field programs are regions of upwelling within pools (figure 5.7A). This was observed in pools 2 and 3 where subsurface flow (piping) between pools fed upwelling sustained the water level of the pool. A curious feature of one upwelling was the suspended transport of clear salt ‘pellets’ (see B and C in figure 5.7). These pellets were approximately a centimeter in diameter and tended to occur in pulses; x-ray diffraction confirmed the pellets were composed of halite (after being dried), and are thus identified as halite oolites or “halolites” (Weiler *et al.*, 1974, p.626).

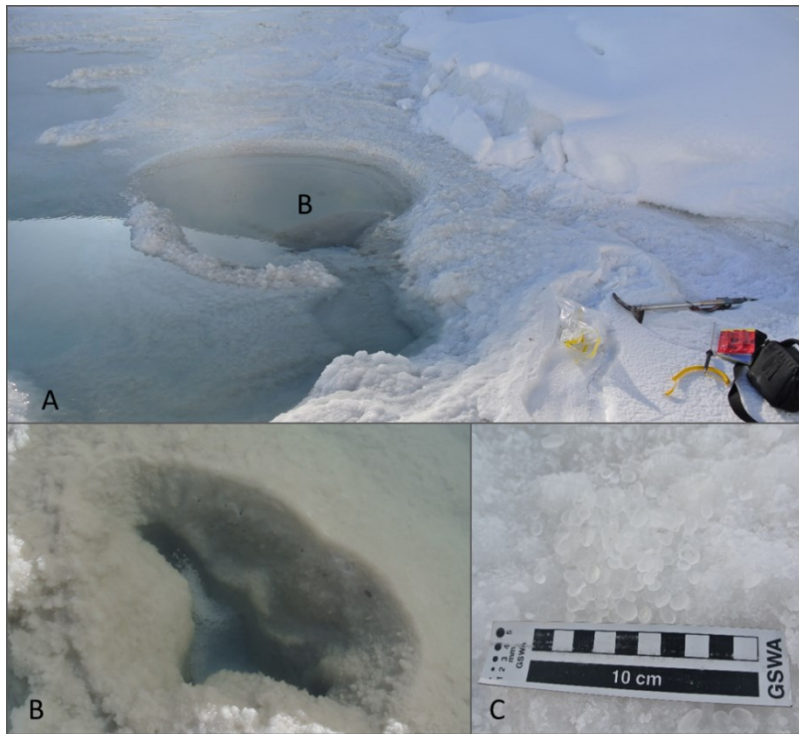


Figure 5.7: (A) Pool inflow type (upwelling pipe) identified for the first time with halolites upwelling in pulses as seen in (B); (C) halolite diameter was approximately a centimeter.

5.1.1.2 Wolf Diapir



Figure 5.8: Wolf Diapir spring in winter, the mound fills up with water and it overflows it sides. Image taken in 2008 by Prof. Pollard.

The salt deposit at Wolf Diapir (erroneously referred to as Lost Hammer Diapir in other publications e.g. Battler *et al.*, 2013 and Neiderberger *et al.*, 2010) forms a cone shaped deposit (figure 5.9A and B) similar to a tufa mound (Ford and Pedley, 1996) with a thin salt platform structure extending downslope from the mound (figure 5.9A and E).

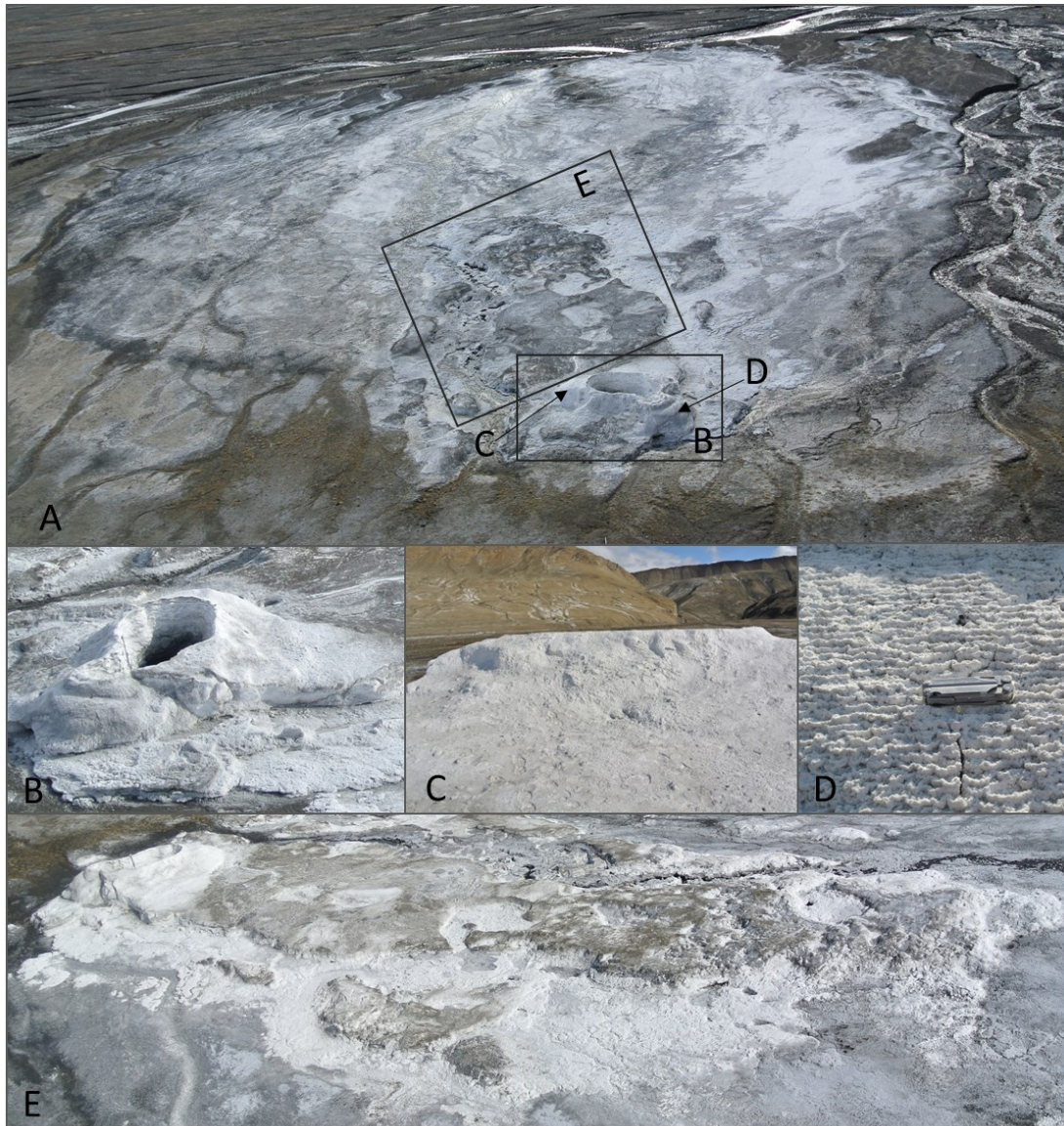


Figure 5.9: (A) Wolf Diapir spring deposit in summer; (B) mound part of the deposit; (C) smooth and compact texture; (D) micro-barrages, approximately 2cm cascading down the mound only at this location and (E) large terrace/platform feature.

Like Stolz Diapir this is an autochthonous deposit formed by a meteogenic spring system during winter. It is a relatively low flow system ($\sim 1\text{-}2\text{L/s}$), forms over a single outlet and forms as precipitated salts accumulate around the outflow. During winter, cold saline water collects inside the mound with the overflow forming a salt platform down slope (figure 5.8). Each summer flow from the spring generates a small stream that dissolves part of the mound and flows downslope into a river fed by glacial meltwater. In July 2013, the flow path was on the left hand side (of the mound, facing the salt platform) and in July 2014, the flow path was to the right hand side.

The overall size and shape of the mound did not vary between field seasons (June/July 2013 and 2014). The inner mound length was 5.50m; inner width was 3.30m and mound height was 2.20m. The basal mound length was 11.20m and basal width was 8.30m. The total length of the salt deposit (including mound) was 61.0m and the maximum width of the terrace was 22.0m (Figure 5.10). The mound displays two different surface textures: the first (figure 5.9C) is a smooth and compact texture covered in a fine white powder that covers the majority of the mound; the second (figure 5.9D) is made up of micro-barrages (barrage height approximately 2 cm) that is located in a small section at the side facing away from the salt platform.

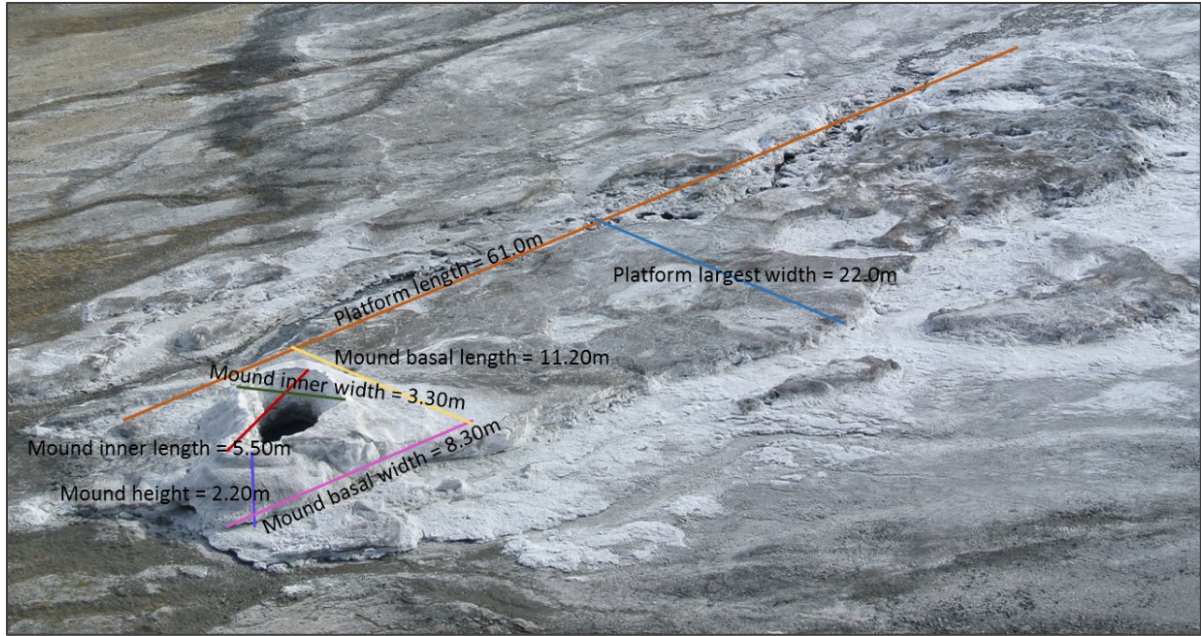


Figure 5.10: Measured dimensions (using measuring tape) of the cone and platform of the salt deposit at Wolf diapiir.

5.1.2 Stratigraphy (Stolz Diapiir)

Figure 5.11 shows two stratigraphic sections excavated in the floor of a drained pool that is approximately the halfway point of the Stolz Diapiir salt deposit. Figure 5.11B shows layering related to small barrage structures whereas figure 5.11A reflects repeated periods of accumulation within a pool floor. The white layers correspond to the winter salt precipitation and accumulation of hydrated salt minerals. The brown to dark brown layers reflect the short summer season while the pool is empty and is the result of sediments being transported into the deposit by wind, rain and runoff (during the spring snowmelt; see figure 5.12 for examples). It is not possible at this stage to comment on whether the layers can be used to date the deposit or be used to calculate accumulation rates. Since pools do not fill every year and due to widespread erosion of the salt surface, a count of the layers (summer bands) might only provide an indication of the number of cycles of filling and

drainage, for example the 16-17 sediment rich bands probably reflect at least the same number of cycles.

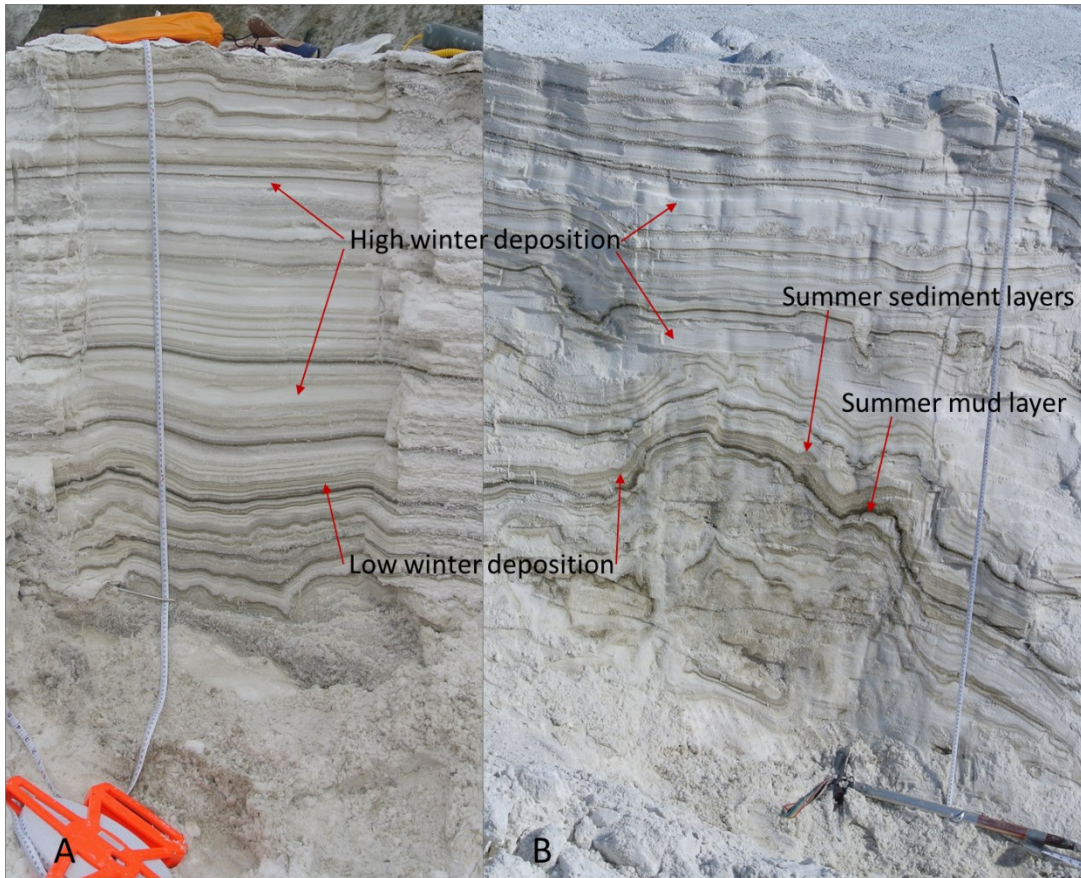


Figure 5.11: Stratigraphic sections located where the hobo temperature logger was installed; (A) shows layering of a barrage structure, and (B) shows layering with respect to a pool floor.

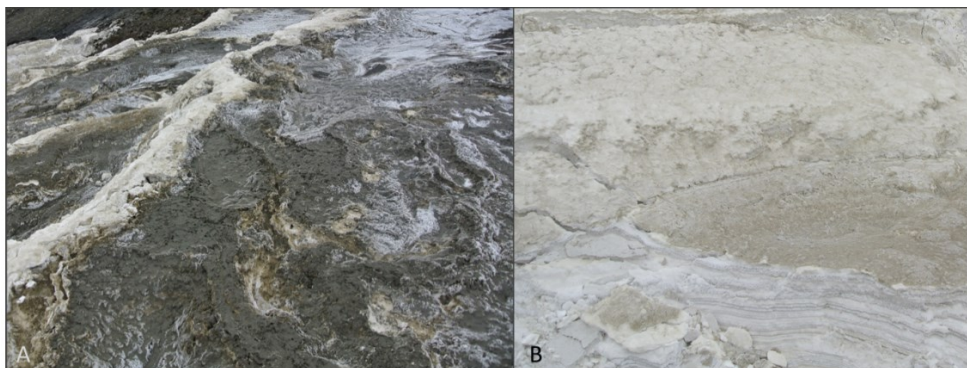


Figure 5.12: Examples of sediments transported onto the salt deposit during summer to produce the dark to lighter brown layers seen in the stratigraphy; (A) shows mud transported by snowmelt to produce the dark brown layers, and (B) shows the transportation of sediments (most likely by wind) producing the lighter brown layers.

Stratigraphic analysis during the summer led to the discovery of thick frozen layers within the deposit (figure 5.13A). These layers began ~47cm below the surface. The temperature of this layer was 0.5°C (the digital thermometer used to measure salt and water temperatures has a resolution of $\pm 0.2^\circ\text{C}$, also note this measurement probably reflects minor warming due to exposure to the 10.0°C air temperature). Samples that were collected from this layer and exposed to ambient temperatures reverted to a mixture of brine and salt grains (figure 5.13B shows the layer when collected and in figure 5.13C shows the same sample after 2 hours). X-ray diffraction analysis of the residual salt materials indicate it is almost pure NaCl (halite).

Similar stratigraphic analysis was not conducted on the salt mound at Wolf Diapir because it would have destroyed the mound.

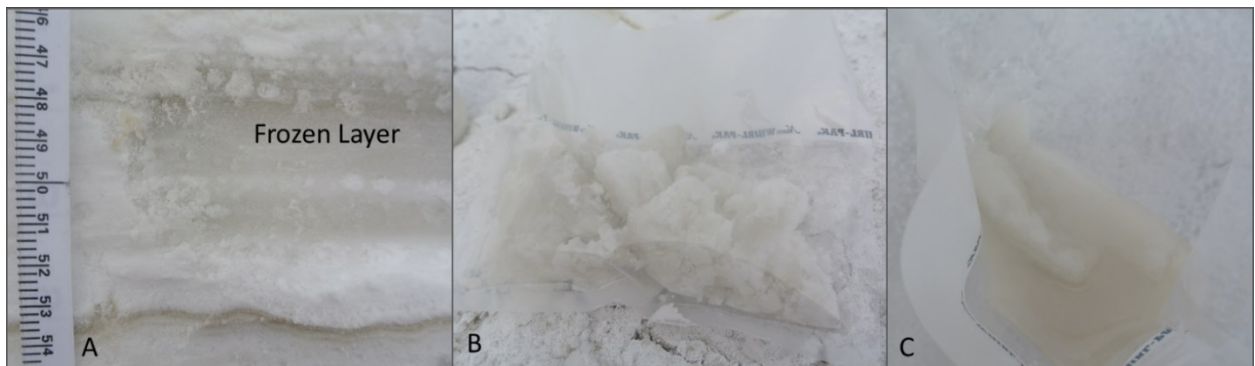


Figure 5.13: (A) Frozen layer identified during stratigraphic analysis, (B) Sample of frozen layer immediately after collection (C) After being exposed to an elevated air temperature, the mineral dissolved. After sample was dried, halite was identified.

5.1.3 Topographic surveys (Stolz Diapir)

Topographic and elevation data were collected to help characterize the gross morphology of salt deposit at Stolz Diapir. Figure 5.14 shows the DEM created by dGPS

points collected in the field. The elevations of the salt deposit (including the salt pan) vary between 20.0m and 120.0m above sea level. Slopes of the deposit were determined using an Abney profile and results are presented in figure 5.15. The slope of the salt surface generally varied between 9% and 14%.

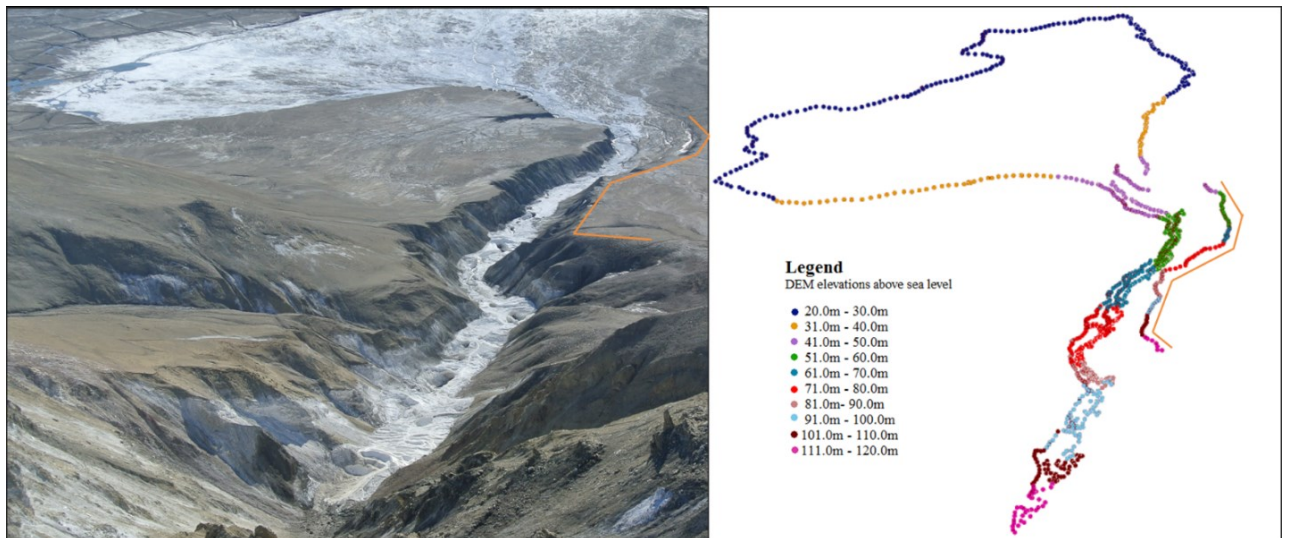


Figure 5.14: DEM results of salt deposit at Stolz Diapir. Orange line in both images highlights valley wall.

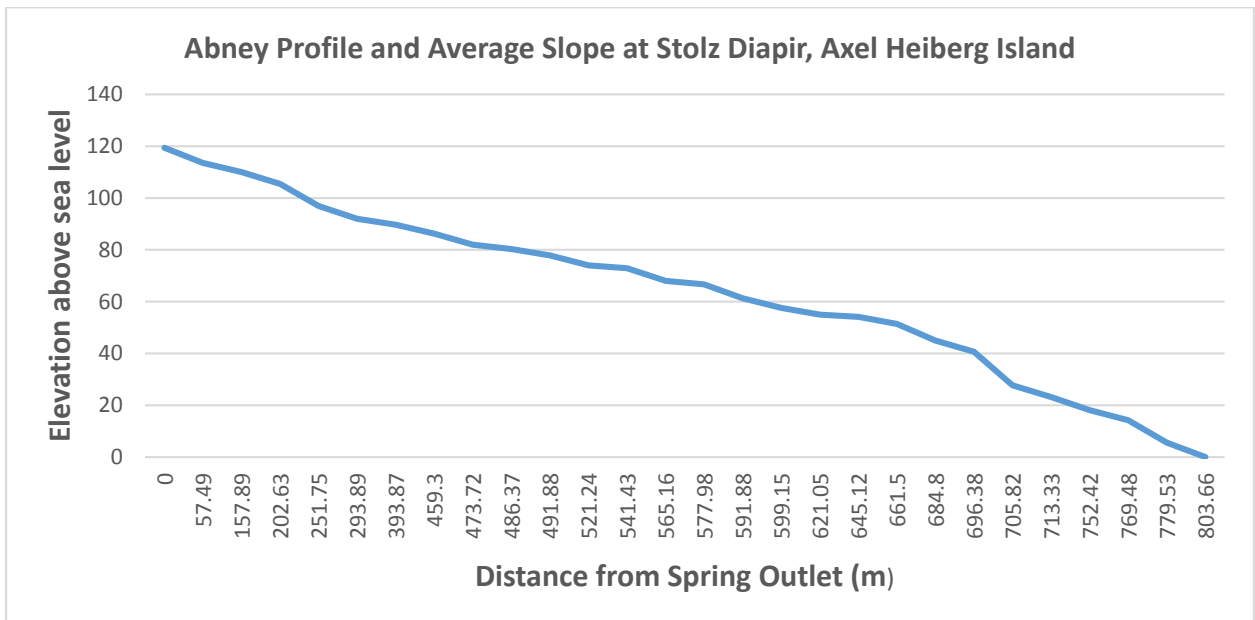


Figure 5.15: Abney profile of valley. Slope gradually decrease down the valley and average slopes ranged between 9% and 14%.

5.1.4 Spring Discharge

Discharge measured at Stolz Diapir is quite variable ranging from 11.33L/s in July 2014 to as high as 30.5L/s in June 2008. Discharge at Wolf Diapir forms a small pool (1m in diameter) hidden within the mound and could not be measured directly. Based on the amount of flow in seeps from the side of the mound within the salt deposit downstream it is estimated to be only a few (1 to 2) litres per second. Battler *et al.* (2013) reports a discharge of 4-5L/s however based on annual observations by Prof. Pollard (since 2011) this seems to be an overestimation.

Observed water temperatures at spring outlets are constant at -1.9°C at Stolz and approximately -4.3°C at Wolf regardless of air temperature. Spring temperatures downstream reflect either warming or cooling by ambient conditions. During the April 2014 field season, liquid water temperature within the salt pan in the Whitsunday floodplain was -21.4°C.

Spring water chemistry for both sites is presented in section 5.2. The discharge at both sites is classified as hyper-saline. The Total Dissolved Solids (TDS) within the water exceeded the range of the YSI 63 field conductivity meter (>999 ppm) and pH values ranged 6.70-8.16 at Stolz Diapir and 6.87-7.18 at Wolf Diapir.

5.1.5 Field Instrumentation

5.1.5.1 Hobo Temperature Data Logger (Stolz Diapir)

The 4-channel Hobo temperature logger that was installed at the halfway point in the Stolz Diapir deposit (figure 5.16) collected air and water temperatures from July 2013 until April 2014. Despite the three water sensors becoming encrusted with salt (figure 5.16B), the timing and temperature of the pool infill process was successfully recorded (figure 5.16A). Figure 5.16 includes three plots; unshielded air temperature, Eureka air temperature and water temperature. Only one of the three water temperature sensors is plotted.

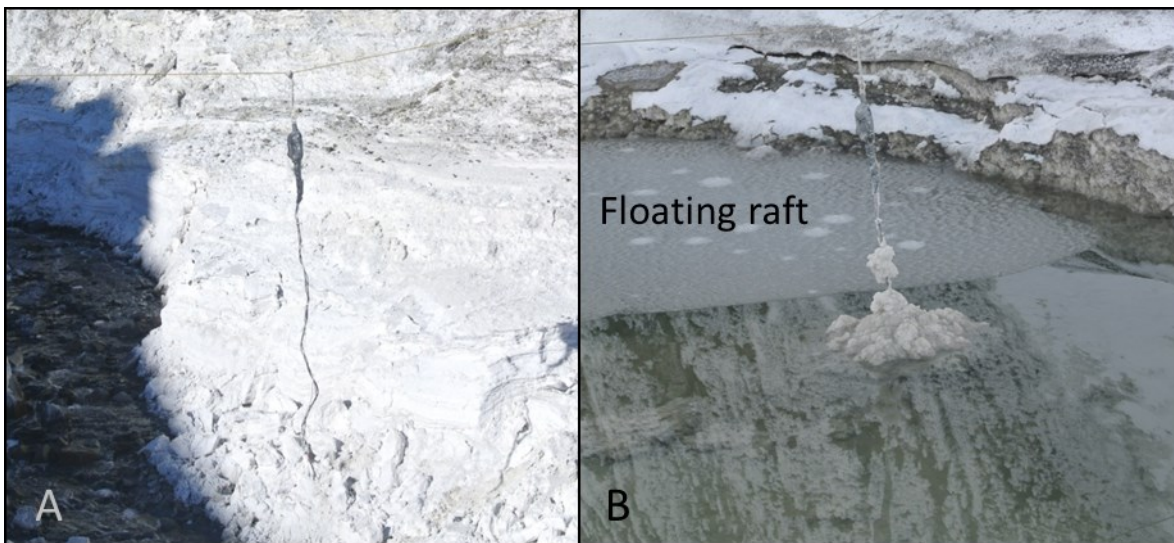


Figure 5.16: (A) The hobo temperature data logger when put in place on July 10th, 2013 and (B) when collected on April 15th, 2014; note the minerals that precipitated and deposited on the sensor cables, as well as the floating raft crust identified.

Mean daily air temperatures recorded at the Eureka Weather Station are included to validate the readings collected by the temperature logger. The Eureka Weather Station measured record low temperatures in late February 2014 and temperatures recorded by the

logger drop to almost -70°C (see the black square in figure 5.17). Temperatures were so cold that they were outside the operational range for the hobo data logger, resulting in an erroneous series of values.

On November 26th, 2014 the logger successfully detected when the pool filled with water by recording a dramatic (15°C) divergence (warming) in temperature by the sensors suspended within the basin. This logger recorded a drainage event on December 20th, 2014 and its subsequent refilling on December 21st. Despite varying air temperatures, water temperatures remain stable throughout the study period.

Figure 5.18 shows results from the hobo logger set up on the ridge overlooking the deposit and collected temperature measurements for almost one year (July 10th, 2013 to June 27th, 2014). The air temperature measurements from both loggers were compared and found to match very well (except for the erroneous readings of the other logger in mid-February). Soil temperatures at depths of 0-2cm; 10cm and 30cm from are shown. Results from the third hobo logger set up (figure 5.18, collected data during the same time period as the second logger) at the inflow stream indicate that recharge stopped on August 21st, 2013 and returned on May 26th, 2014.

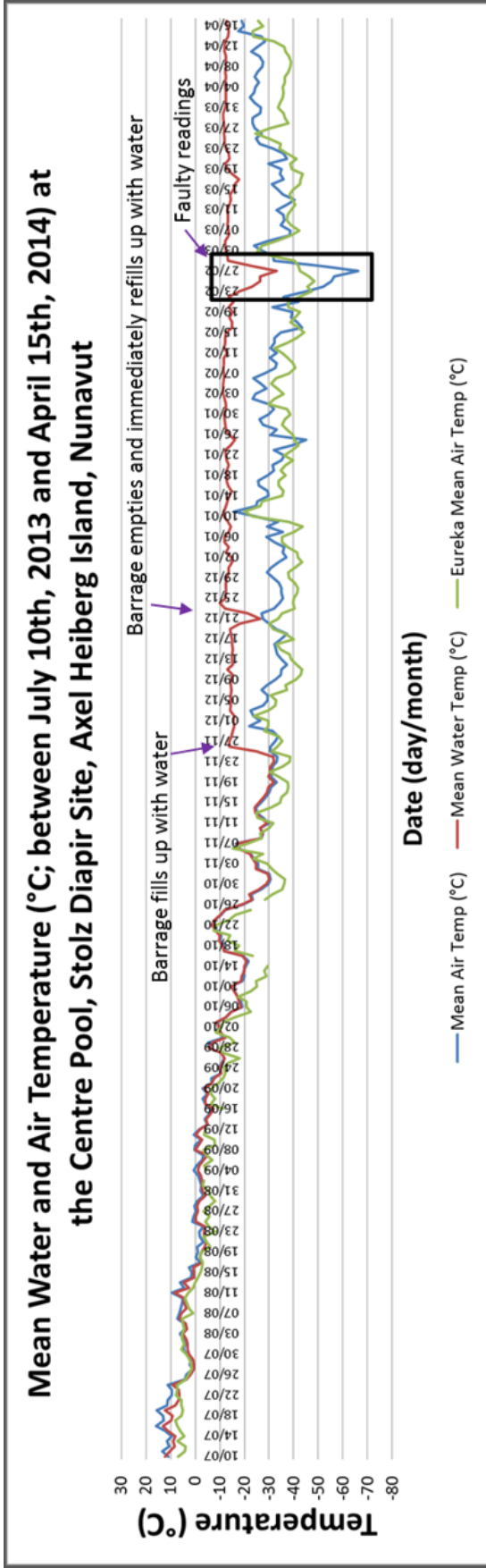


Figure 5.17: Temperature results collected from the hobo temperature data logger put in place in a pool at the center of the deposit. Note readings by the logger within the black box are erroneous and should not be used. Mean air temperature measurements from the Eureka Weather Station included for comparison. The Eureka Weather Station recorded a record low temperature measurement during this time so it is likely that temperatures were so cold that they fell outside the operational range of the hobo logger resulting in erroneous measurements.

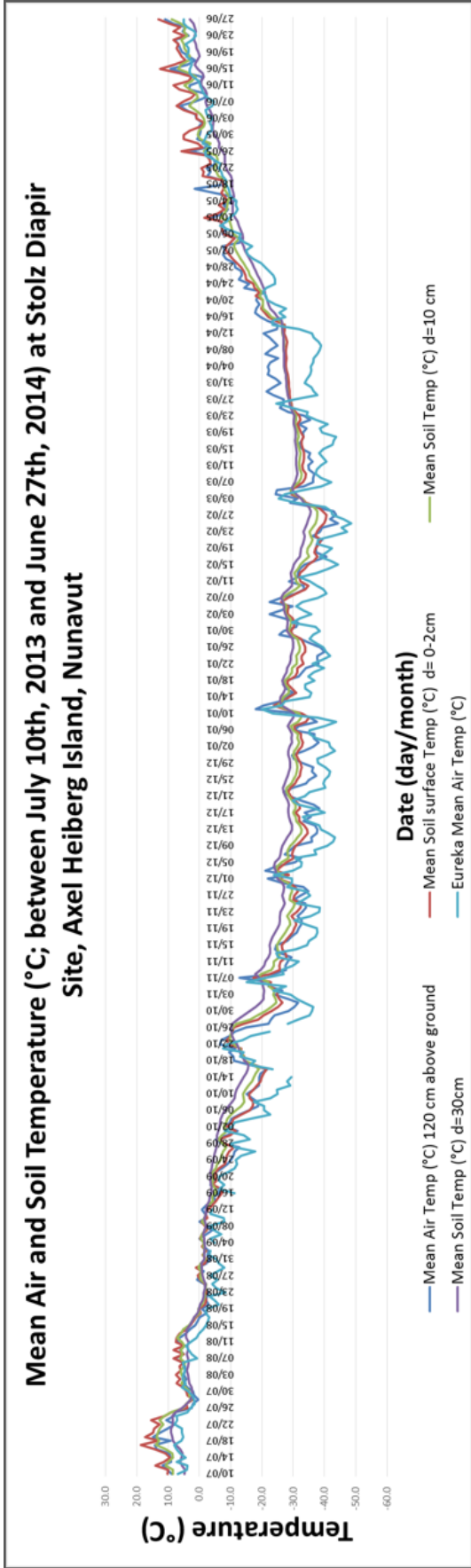


Figure 5.18: Temperature results collected from the hobo temperature data logger set up on ridge above the deposit. This logger recorded air temperature and soil temperatures at various depths (0-2cm; 10cm; and 30cm from surface). Mean air temperature measurements from the Eureka Weather Station included for comparison.

5.1.5.2 Time Lapse Cameras (Stolz Diapir)

Time lapse cameras provide complementary observations that help characterize the hydrology and salt dissolution/precipitation at the Stolz Diapir deposit and spring. The time lapse record provided a clear picture of the timing of the transition from summer to winter regimes. Selected images presented from the time lapse cameras located at the spring outlet (figures 5.21-5.34) and at the valley opening (figures 5.36-5.45) capture the key winter transition to the overflow regime that drives the pool and barrage system. Air temperatures from the hobo temperature logger are included on each image because travertine/tufa formation occurs when rapid precipitation of hydrohalite occurs below the eutectic point (-21.1°C) at the water surface from the rapid cooling by air temperatures to deposit and build up the barrage structures. Hydrohalite is able to precipitate within solution at temperatures between 0.12°C and -21°C to coat the sides of the pools and streambeds but the hydrohalite precipitated would have a slushy texture and likely would not be solid enough to maintain barrage structures.

5.1.5.2.1 Outlet Time Lapse Camera

Figure 5.19 shows the initial camera set up (July 9th, 2013) and when the images were collected (April 8th, 2014). The camera was located on the upper edge of the salt deposit at the valley wall immediately above the top of the highest barrage (figure 5.20). Surprisingly by April 2014 the barrage wall had accreted almost to the base of the time lapse camera.

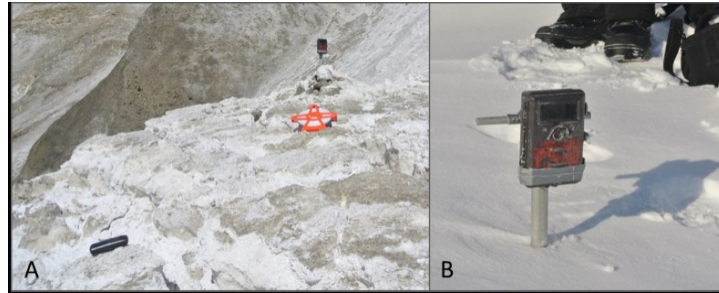


Figure 5.19: Time lapse camera located at the outlet the day it was set up (A) in July 2013 and when it was collected (B) in April, 2014.



Figure 5.20: Deposit immediately before and after time lapse camera set up (A) in July 2013 and when it was collected (B) in April, 2014. Exact camera location is shown by blue circle.

Figure 5.21 is from Day 1 (July 10th, 2013) and includes the author for scale. The first snowfall was on August 18th and marks the beginning of continuous snow cover for

the season (Figure 5.22). The first observable changes to the salt deposit occur on October 12th (figure 5.24, figure 5.23 is included to serve as a comparison), part of the deposit that has either collapsed or been eroded, marking the beginning of a transition from the subsurface dominated flow (piping) to surface flow, or increased wetness that marks a rise of water level. The following day two pools fill up, one of which is located where the previous collapse occurred (Figure 5.25). During fieldwork in April 2014, two pools near the outlet were still full, one of which is one of the first pool to fill up, shown in figure 5.25. Images from the time lapse camera suggest this pool remained full for the entire winter season. A photo taken by the author on April 18th is included to highlight the similarity with late season features. The next day, one of the two pools drains (Figure 5.26) while the other pool remains full indicating that even though a single spring forms the entire deposit, a complex hydrology involving multiple pathways may exist within the deposit allowing for selective hydrological activity. It is also possible that part of an old barrage collapsed, allowing the pool to drain, indicating that pools stay full only once the barrages are strong enough to retain the water. On October 15th, (figure 5.27) the ‘darkening’ around the pool is most likely a result of the removal of surface snow, however, it is not clear what triggered it. It looks similar to figure 5.24, so may reflect dissolution erosion by the spring water. The pool that drained on October 14th filled up again on October 23rd (figure 5.28).

Several dramatic changes occur on October 29th, when during a single 24 hour period most of the deposit within the field of view of the time lapse camera is filled with water (figure 5.29). The upper pools appear to be filled sequentially by overflow from the first (upper most) pool situated at the spring outlet. This picture also provides the first

image capturing active barrage construction (highlighted by the purple box in figure 5.29). These barrages appear to be relatively small, the inserted photo taken near the valley opening is to provide a clearer example of their appearance.

A snow storm, between October 30th and November 7th, 2013, obscured the camera lens resulting in several lost frames. Temperatures during this time ranged from -22.6°C to -30.7°C. The image taken on November 7th (figure 5.30) shows the upper barrages still full with several new pools that have formed since October 29th, 2014.

Another pool empties on November 8th (figure 5.31) but also refills the next day (figure 5.32). The image taken on November 10th, 2013 (figure 5.33) is the last clear picture and corresponds to when twilight ends (following the polar sunset on Oct. 21st) until April 15th, (figure 5.34). Images from March suggest the lens had frosted over (part of the image becomes visible but then gets covered up again a few days later).



Figure 5.21: First image taken by time lapse camera after put in place. Author for scale.



Figure 5.22: First snowfall of the season. The snow remained on the ground throughout the rest of the study period.

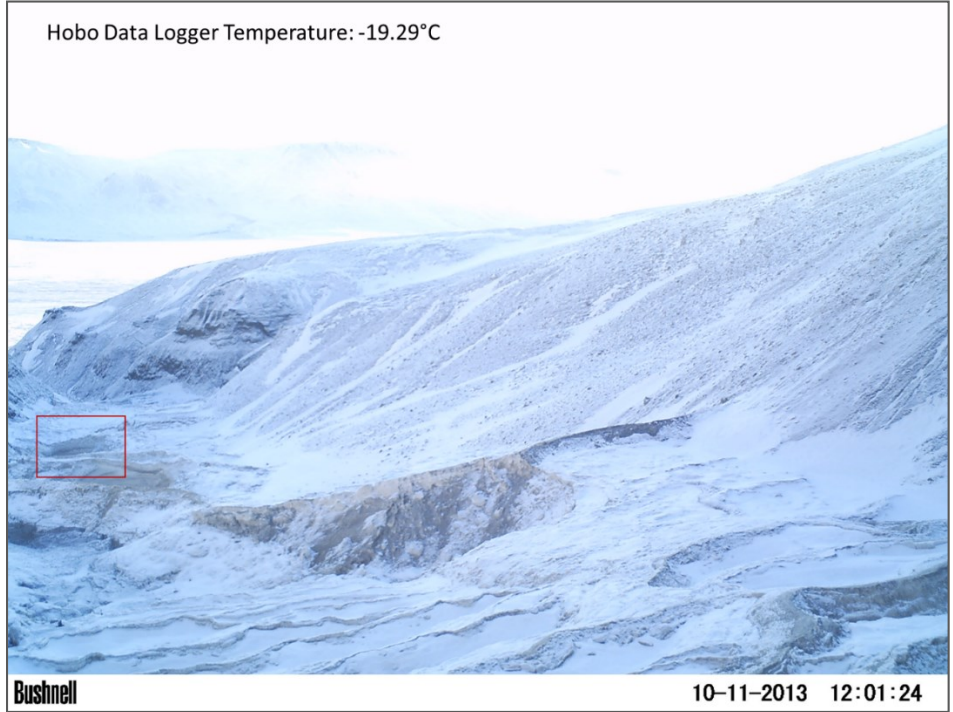


Figure 5.23: Red box indicating area where change occurs in figure 5.24.



Figure 5.24: Sign of erosion indicated by red arrow or water level that is rising. This would be produce by water channeling within tunnels through the deposit that are carved during the summer months.



Figure 5.25: First pools fill up on October 13th, 2013. Image taken during the April 2014 field season inserted to show the differences between the pools between both time periods. The pool depicted by the red arrow was measured (27.80m by 12.25m). The purple line highlights the barrage in common within both images and the green arrow shows the location of a pool in April that resembled a tunnel in the time lapse images.

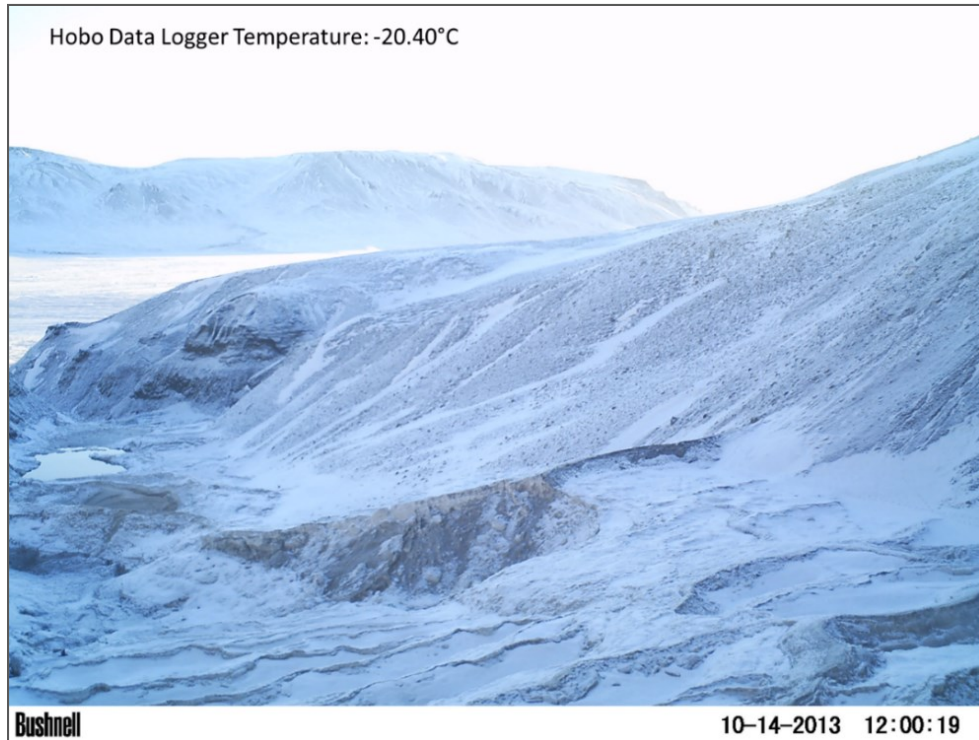


Figure 5.26: One of the two pools drains but the other remains filled. This could indicate that multiple tunnels carved by water within the summer runs through the deposit and that these two pools are not directly connected.

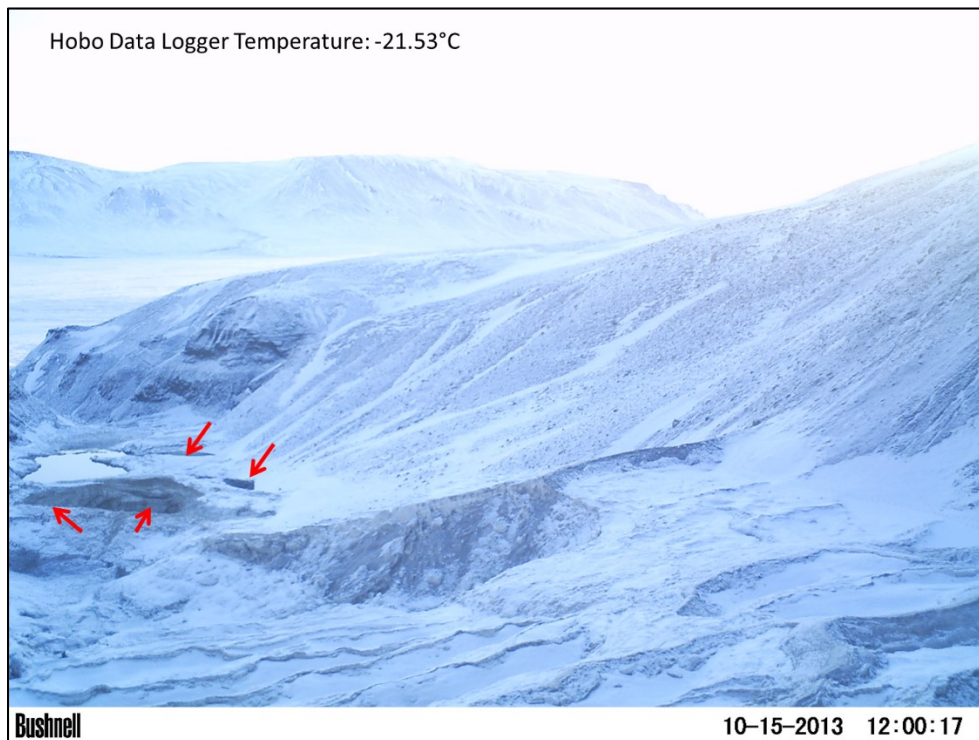


Figure 5.27: Removal of surface snow, but what triggered this is not clear (shown by red arrows)



Figure 5.28: Pool furthest away fills up again after draining on October 14th, 2013. More snow has fallen on the deposit.

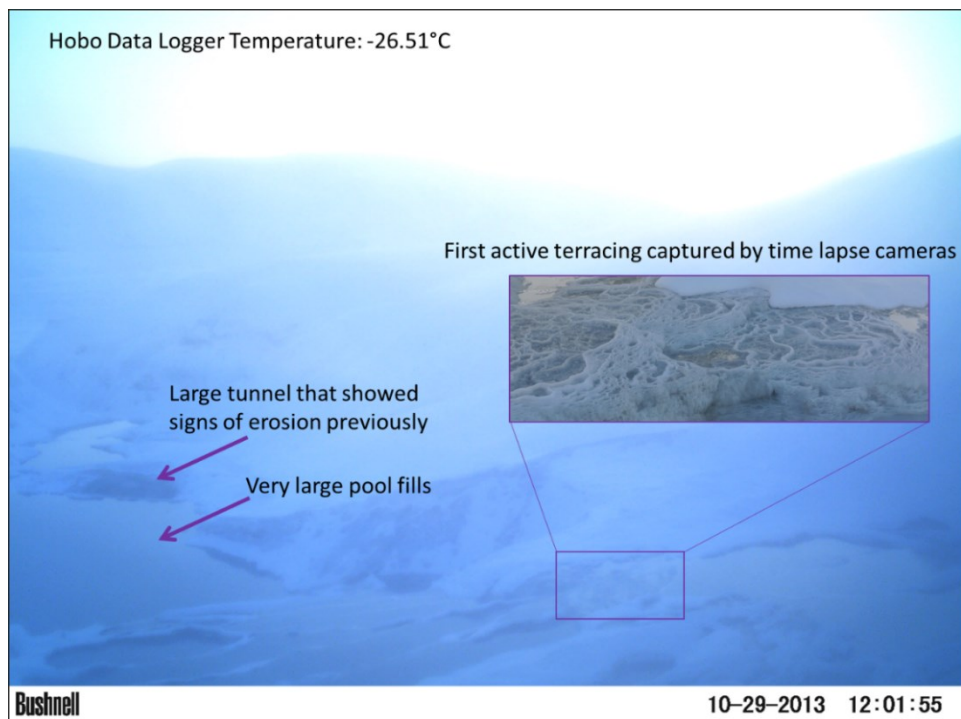


Figure 5.29: Within a day a large amount of water all over the deposit within view of the time lapse camera. This is the first image showing active terracing capture by the time lapse cameras and is highlighted by the dark purple square. An image taken from other terraces near the valley opening is included to give an idea of what the smaller terraces look like.

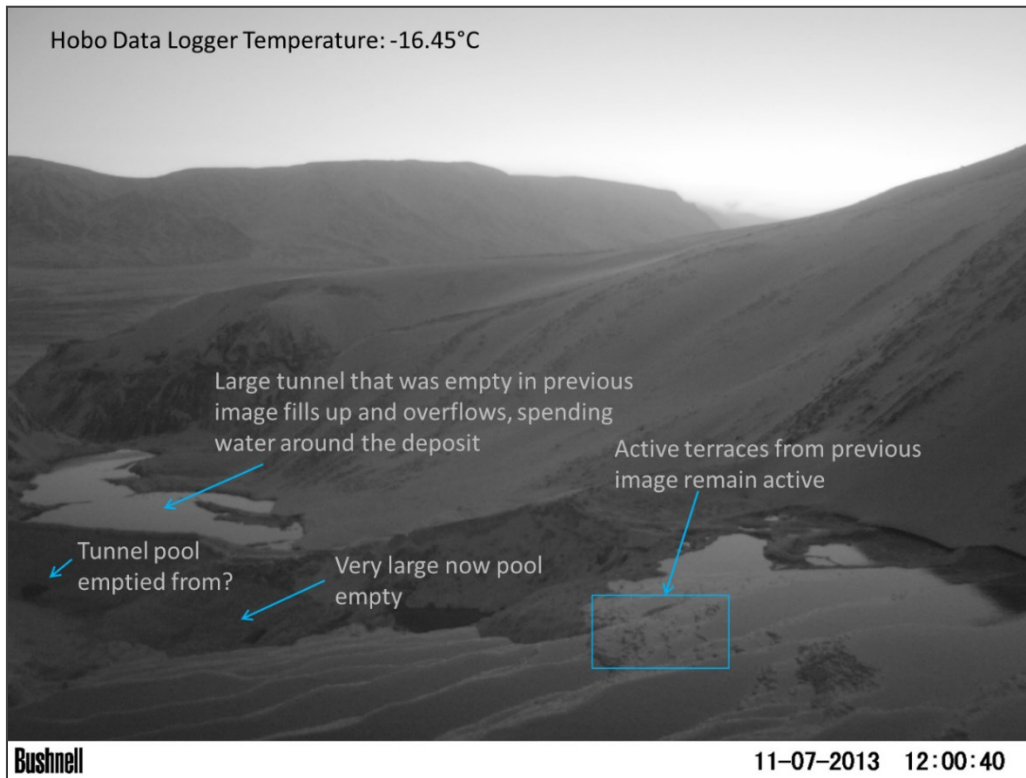


Figure 5.30: After a snowstorm that lasted 8 days (the images taken on those days had no visibility) with temperatures varying between -22.60°C and -30.69°C the upper terraces now appear to be active with many small terraces forming during this time. The very large pool that was in the previous images has emptied, what appears to be a tunnel may be the source the water drained from and the large emptied tunnel has filled with water to create another pool.

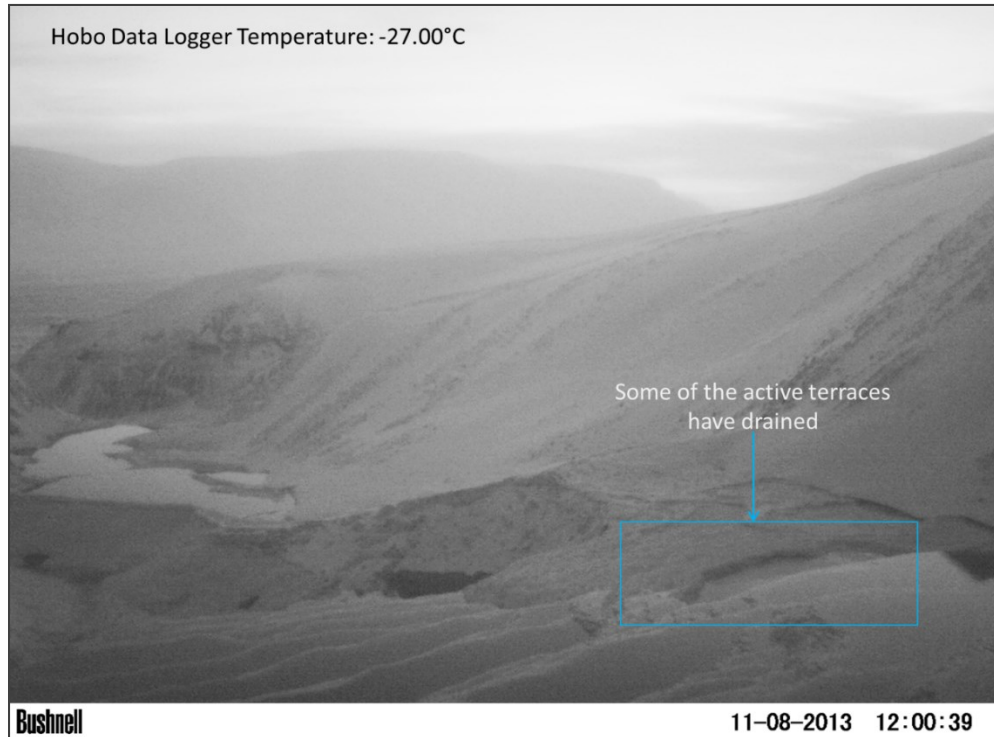


Figure 5.31: Some of the upper terraces have drained and it is unclear how.

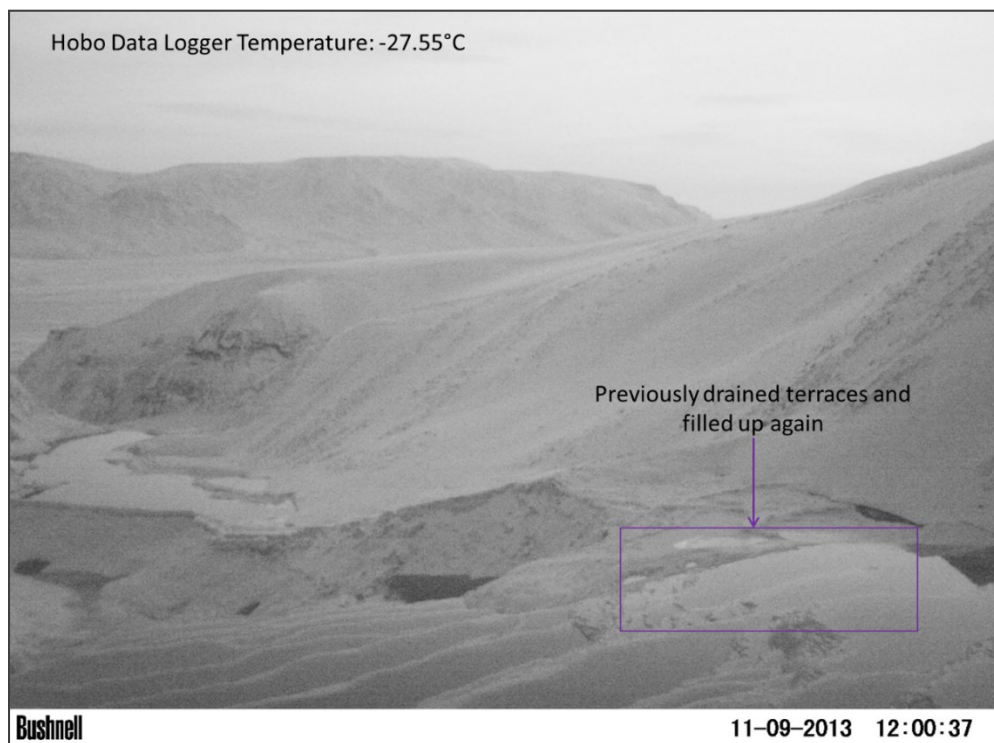


Figure 5.32: Upper pools that previously drained have filled up again.

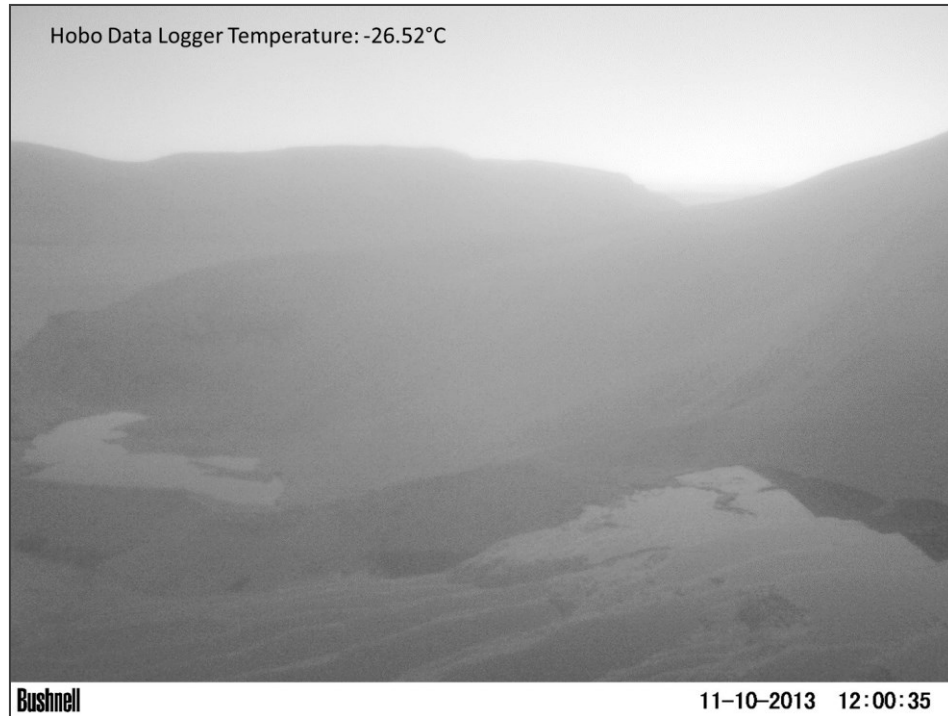


Figure 5.33: Final image that is clear, all images after this date are black (snow covered the lenses) until mid-April.

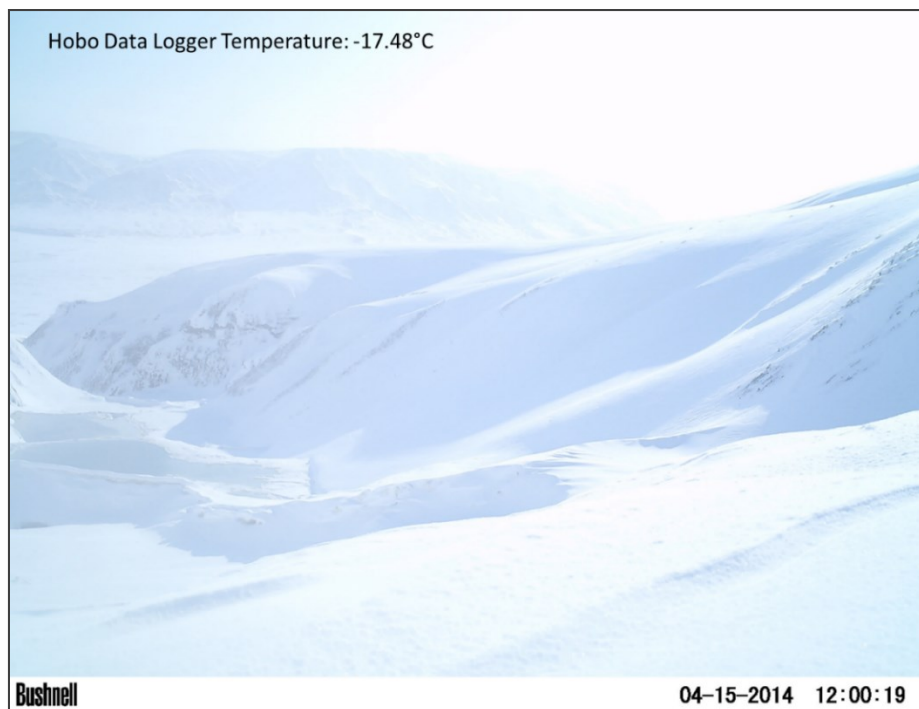


Figure 5.34: First completely clear image after snow blew off the camera lens. One pool (the furthest away) has remained filled since October 13th, 2013 and the other pool (closest) since November 7th, 2013. The upper terraces are no longer active and snow depth on the deposit has increased.

5.1.5.2.2 Lower Valley Time Lapse Camera

The second time lapse camera was located in the lower valley just upstream from the valley mouth. It was mounted on a mast embedded in the salt deposit adjacent to the valley wall (figure 5.35). The (spring fed) stream was not visible at this part of the deposit when the camera was installed, however there was a depression (channel) in the deposit adjacent to the camera.

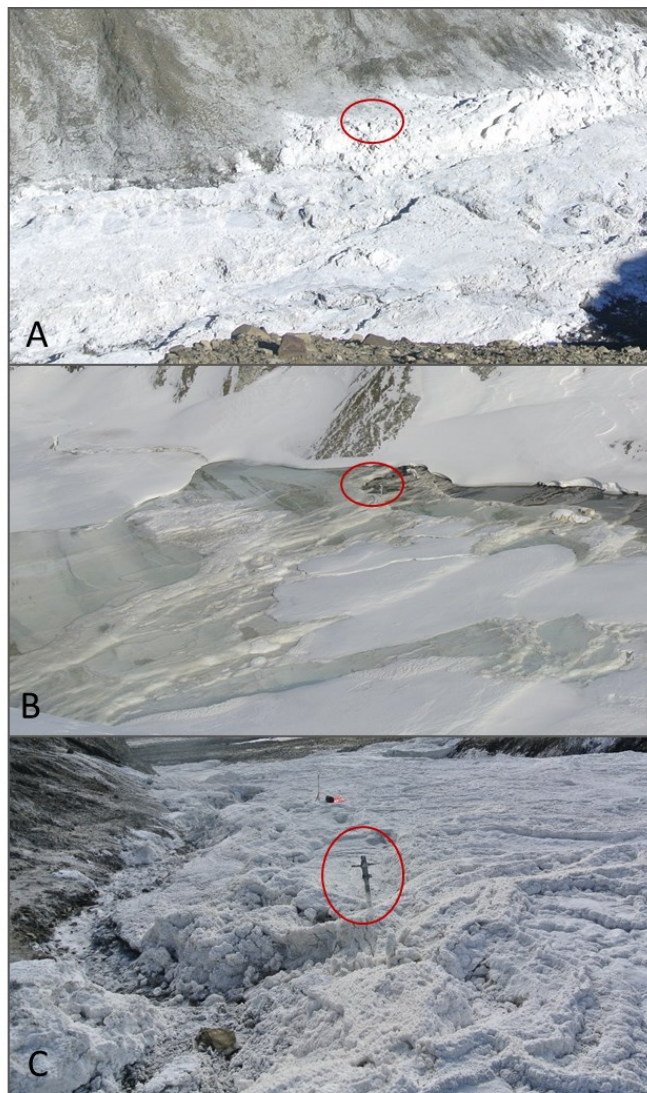


Figure 5.35: Time lapse camera located just upstream of the valley opening the day it was set up (A) in July 2013 and when it was collected (B) in April, 2014 and, (C) it's location in July, 2014 to show the morphology of the deposit where the camera was.

The first image on July 7th shows a research assistant for scale (figure 5.36). Images from this camera are generally not as clear as images taken by the camera located at the outlet. Figure 5.37 is included because it provides the clearest image of the deposit and because it provides a baseline for comparison with subsequent images. August 9th, 2013 (figure 5.38) provides one of first images where the dissolution (erosion) of the deposit by the spring water is visible (it was chosen because it is the clearest image). In this image, part of the stream is visible where the salt deposit has recently collapsed. No stream flow was visible when the camera was installed, only a depression. Over time, this depression dissolved and eroded to form the channel as seen in figures 5.38 to 5.40. Channel formation is gradual and occurring over several days. The deposit continues to dissolve (dissolution is inferred because the part of the deposit that collapses into the stream disappears slowly over time) and erodes. Cobbles on the stream floor become visible on August 14th (figure 5.39). Dissolution appears to occur only when temperatures are above 0°C. Figure 5.40 (taken on September 24th) shows that the stream bed appears to have a layer of recently deposited salt or ice. Figure 5.41 to 5.43 shows rising water levels. When the resulting deposit was examined in July 2014 the stream bed was found to be covered by a thick layer of salt (figure 5.35C).

The image taken on November 7th (Figure 5.44; the day after the snowstorm ended) shows hydrological activity at one of the larger barrage structures upstream, however it is too far away to see significant detail. The last clear image taken by this camera was on November 9th (figure 5.45).



Figure 5.36: Picture 1 from the lower valley time lapse camera. Field Assistant for scale.



Figure 5.37: Clear image taken on August 5th provides the best detail for comparison.



Figure 5.38: Part of the deposit begins to collapse (indicated by red arrow). The spring water was not visible at this location during field work.



Figure 5.39: Further collapse. The deposit where the spring water flows gets completely dissolved and the stream bed becomes visible (as shown by the pebbles that became visible).



Figure 5.40: Stream bed pebbles are no longer visible and bed appears white from precipitating salt minerals.



Figure 5.41: This picture clearly shows the accumulation of recently deposited salt and preliminary pooling.



Figure 5.42: Water level continues to rise

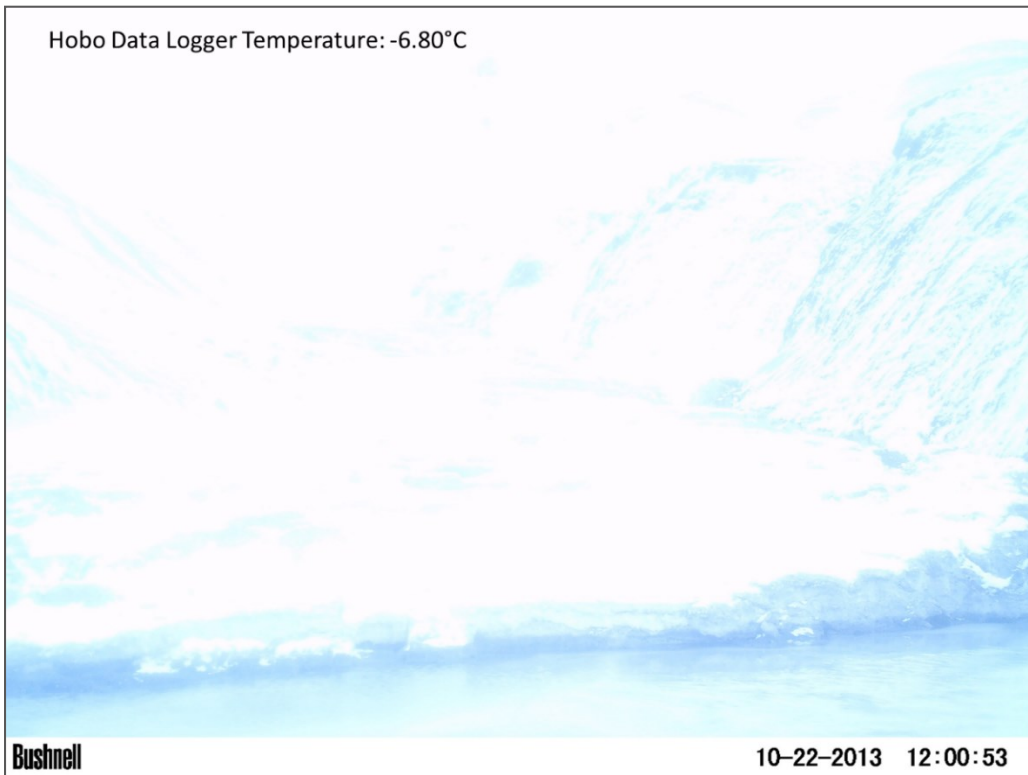


Figure 5.43: Water level continues to rise.

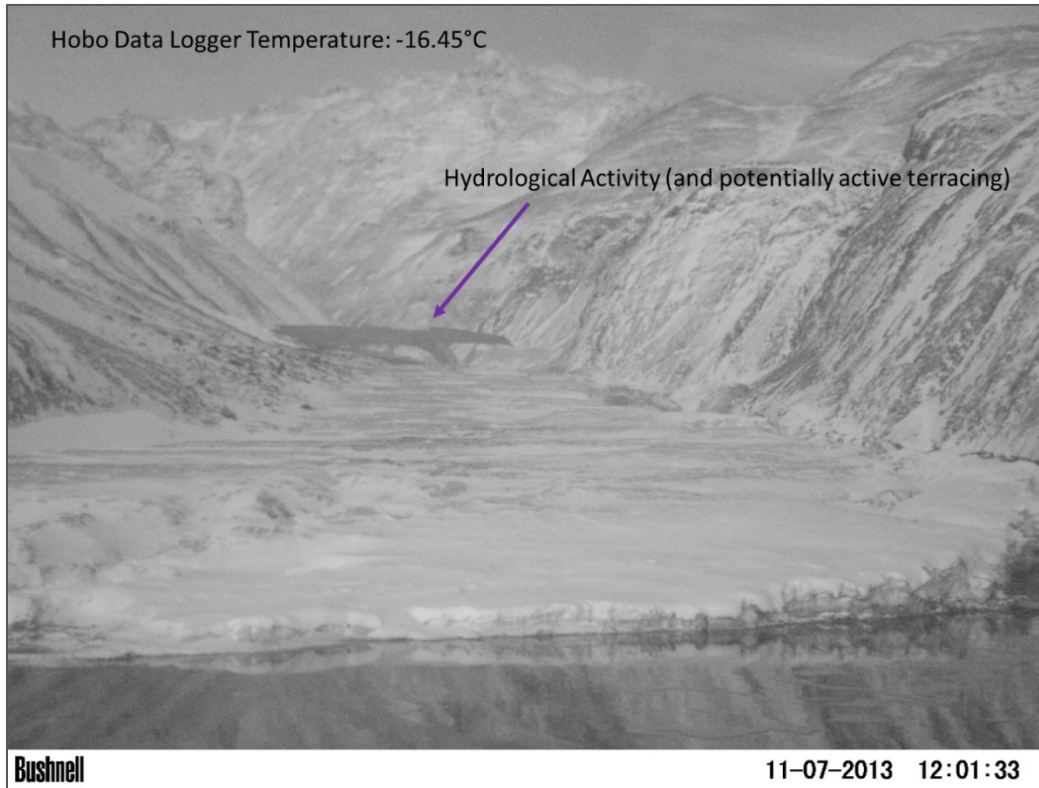


Figure 5.44: First clear image taken after a snowstorm (figure 5.30 shows an image taken on the same day by the other time lapse camera where most of the terraces are actively growing can be seen for the first time). This picture includes the first indication of overflow activity further upstream shown by the purple arrow.

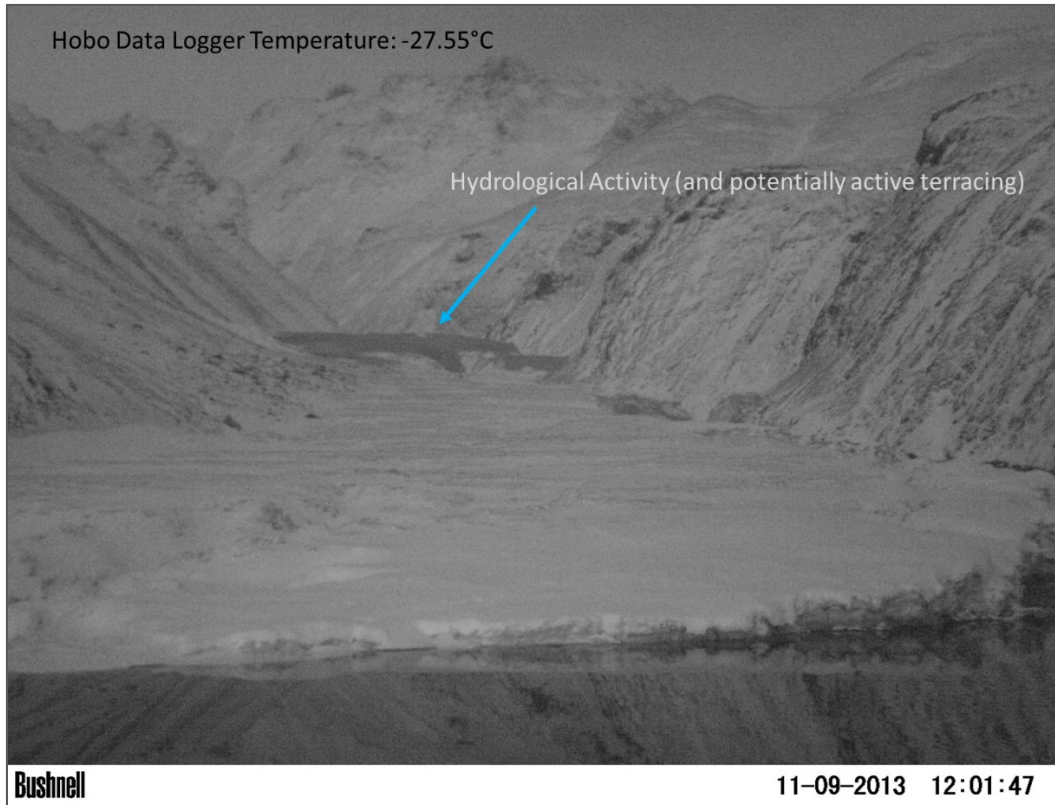


Figure 5.45: Last visible image taken by the lower valley time lapse camera (corresponds to the disappearance of twilight like the other camera). A malfunction stopped the camera at the end of December, 2013. This image show widespread changes in the hydrology and a definite shift to overflow processes.

5.2 Laboratory Results

5.2.1 Water Chemistry

5.2.1.1 Stolz Diapir

Table 5.1 presents the major ion concentrations, pH and temperatures for water samples collected at several locations in the Stolz diapir system in July 2013 and April 2014. Figure 5.46 is a Piper diagram for this water chemistry. The inflow stream reflects the relatively fresh nature of the snow melt runoff. Regardless of the location the samples were collected downstream from the outlet the water chemistry is dominated by high

concentrations of sodium and chloride ions; while calcium, potassium and magnesium are present in relatively low concentrations by comparison. The concentration of sulfate ions varies along the spring channel depending on the season. In the summer, sulfate ions gradually increase with increasing distance downstream from the spring outlet; but in the winter sulfate ions gradually decrease with increasing distance from the outlet. In summer, pH varies little and ranges between 7.06 and 7.13; in winter it ranges between 6.70 and 7.06.

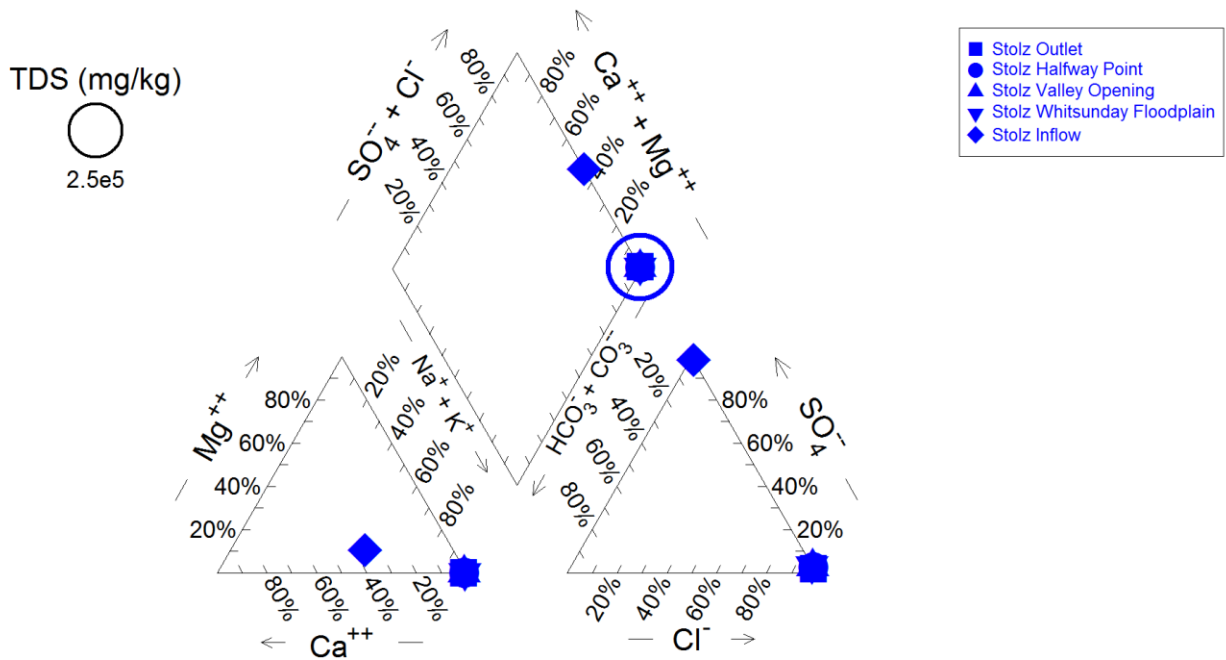


Figure 5.46: Piper diagram of water samples collected at the inflow waters and at various point within the deposit (outflow, stratigraphy site, valley opening and Whitsunday Floodplain)

Table 5.1: Major ion concentrations for water samples taken July 2013 and April 2014. Due to the high concentration of ions, results are presented in g/L rather than mg/L.

	Sample Location	Sample Temp. (°C)	pH	Ca²⁺ (g/L)	K⁺ (g/L)	Mg²⁺ (g/L)	Na⁺ (g/L)	Cl⁻ (g/L)	SO₄²⁻ (g/L)
July 2013	Inflow	--	8.16	0.197	0.005	0.035	0.34	0.006	0.52
	Outlet	-1.30	7.06	1.10	0.39	0.07	132.84	156.37	4.18
	Stratigraphy Site	0.10	7.11	0.94	0.17	0.08	138.87	163.32	5.50
	Valley Opening	1.40	7.17	0.83	0.26	0.07	138.45	144.41	6.00
	Whitsunday Floodplain	6.20	7.13	0.71	0.15	0.09	136.18	155.70	7.07
April 2014	Snow	--	8.97	0.184	0.022	0.036	0.38	0.523	ND
	Outlet	-1.90	6.70	1.44	1.24	0.25	169.51	186.69	5.26
	Pool 1 Surface	-6.20	6.88	1.36	1.34	0.20	172.34	184.52	4.56
	Pool 1 Depth	--	6.80	1.44	1.13	0.22	165.77	184.61	5.15
	Pool 2 Surface	-8.30	6.83	1.41	1.00	0.21	174.39	170.19	4.91
	Pool 2 Depth	--	6.78	1.40	0.82	0.21	165.90	183.24	5.00
	Pool 3 Surface	-9.60	6.93	0.23	0.17	0.04	167.02	176.75	4.51
	Pool 4 Surface (Stratigraphy site)	-13.10	6.92	1.57	1.19	0.23	173.31	186.1	2.72
	Pool 4 Depth	--	6.89	1.57	1.18	0.23	171.22	191.84	3.71
	Valley Opening	-14.90	6.86	1.23	0.83	0.19	158.48	172.83	2.69
	Whitsunday Floodplain	-21.40	7.06	2.06	1.30	0.28	180.30	179.19	1.51

5.2.1.2 Wolf Diapir

The Wolf Diapir data are based on samples taken from the spring outlet and a location downstream. The scale of the system is much smaller than Stolz diapir, in both size and discharge, also the source for this spring is not known hence no inflow values. Like Stolz, the spring waters of Wolf Diapir are highly mineralized, as reflected by the results in table 5.2 and by the Piper diagram in figure 5.47. The water chemistry presented in table 5.2, with the exception of sodium (Na^+) chlorine (Cl^-), are similar to results presented by Niederberger *et al.*, 2010. Sodium and chlorine concentrations for water collected at the outlet is 108.71 g/L and 126.38 g/L where results from Niederberger *et al.*, (2010) are 67.0 g/L and 140 g/L, respectively. The author was not able to measure HS concentrations (only SO_4) so the HS value of 0.05g/L obtained from Niederberger *et al.*, (2010) is presented.

Table 5.2: Water chemistry data for Wolf Diapir Spring. Samples collected in June 2013. Due to the high concentration of ions, results are presented in g/L rather than mg/L.*Data from Niederberger *et al.*, 2010.

	Concentration (g/L)	
	Outlet	Channel (5m from outlet)
K⁺	0.36	0.33
Na⁺	108.71	103.92
Mg²⁺	0.35	0.34
Ca²⁺	1.50	1.36
Cl⁻	126.38	123.92
SO₄²⁻	5.28	5.29
NO₃⁻	ND	ND
PO₄³⁻	ND	ND
Sulfide*	0-50ppm dissolved H ₂ S/sulfide	--
pH	6.87	7.18
Temperature (°C)	-4.3	-2.1

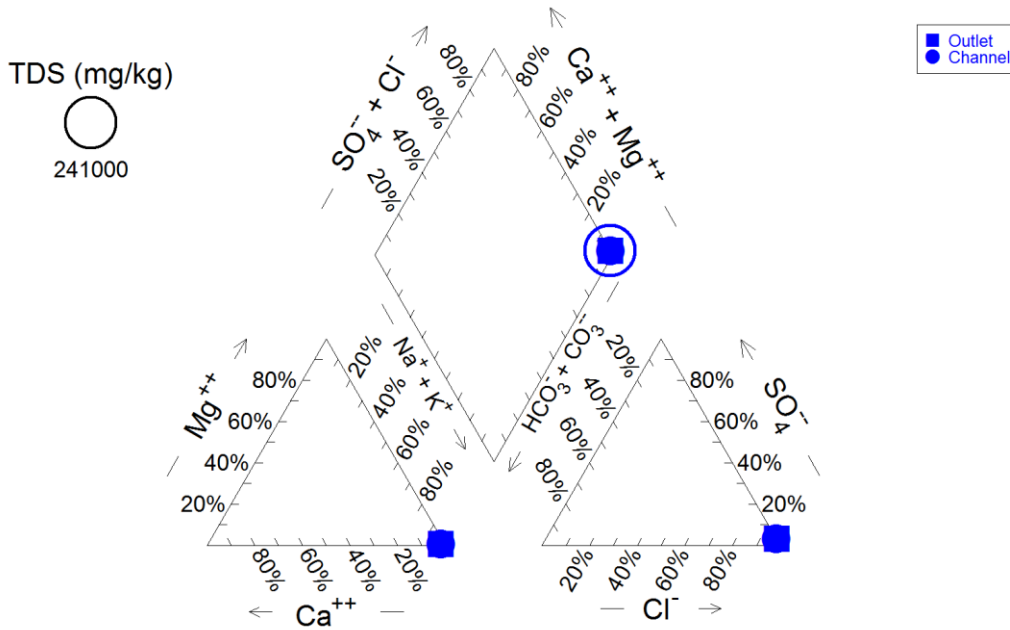


Figure 5.47: Piper diagram of Wolf Diapir spring water chemistry at the outlet and in the channel 5m away from outlet. Both samples were collected in June 2013.

5.2.2 Mineralogy Results

5.2.2.1 Stolz Diapir

The mineralogy of the deposit is dominated by halite (NaCl). Thernadite (Na₂SO₄) is also present but in smaller amounts. Figures 5.48 shows diffraction patterns of halite (NaCl) and thernadite (Na₂SO₄). Figure 5.49 shows x-ray diffraction patterns from collected samples. Individual diffraction patterns of each sample with labelled peaks are presented in appendix A.

The morphology of mineral precipitates gradually changes downstream from the outlet. The upper structures near the outlet are characterized by loosely packed cubic crystals and hexagonal pseudomorphs. These crystals were identified as halite. At the halfway point downstream, a fine white powder (thernadite) forms a light dusting on the

surface of the deposit and is present all the way into the Whitsunday River Floodplain. Below the halfway point, more thernadite is present in the samples and their overall composition is a halite-thernadite mixture.

These deposits are progressively more compact (dense) with increasing distance downstream. At the mouth of the valley a distinct ‘hard’ crust occurs (<1cm thick) that is a mixture of white precipitate and fine grained (silt – fine sand) mineral sediment. The presence of sediment in this part of the salt deposit indicates that sometimes the stream flow is sufficiently strong to transport suspended sediments in areas where the flow is channelized. Based on observations made in both April and July the source of the sediment appears to be a combination of debris that is carried into the open channel from the valley sides (small mudflows and debris slides), windblown dust (often present as a slight discolouring on the salt surface) and channel erosion.

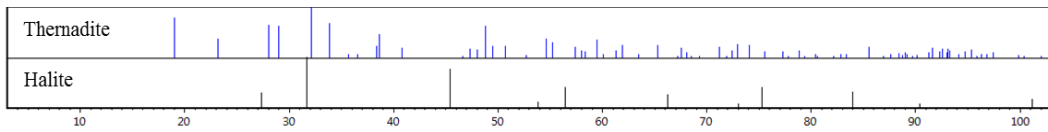


Figure 5.48: X-ray Diffraction peaks for thernadite (Na_2SO_4) and halite (NaCl).

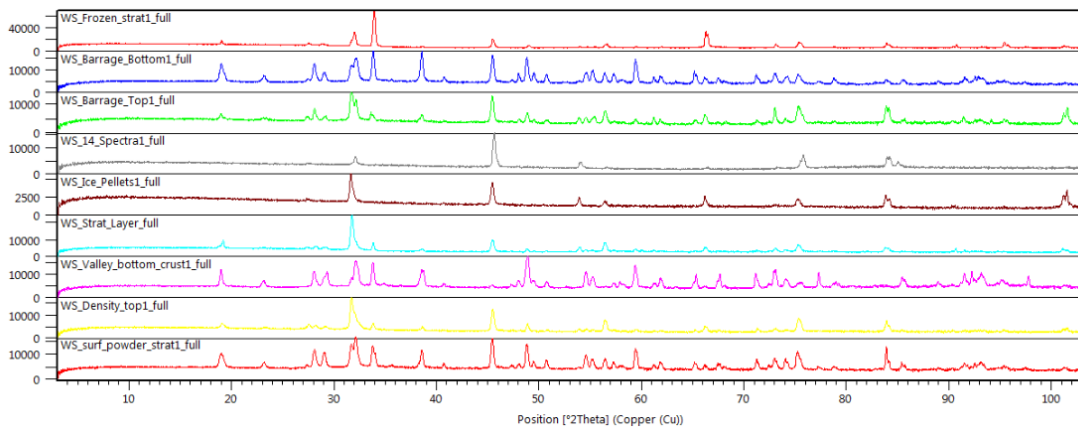


Figure 5.49: X-ray Diffraction patterns for selected samples from the Stolz Diapir site, the primary peaks correspond with halite and thernadite.

5.2.2.2 Wolf Diapir

At Wolf Diapir, the cone-shaped deposit is extremely hard and rigid; and is also covered with a fine white powdery residue, just as with Stolz Diapir the powdery residue is identified as thernadite. An elevated (~50 cm thick) platform formed from accumulated salt occurs along the downstream direction of spring flow (61m x 22m). This platform deposit thins in a downstream direction but also has a hard surface and is highly compact. In the spring channels white crustal layers of a few millimetres to centimeters thick are present covering underlying gravel sediments. These crystals form distinct clusters of individually precipitated crystals resembling a cauliflower-like floret.

Analysis of the samples collected at the Wolf Diaipir deposit indicate the bulk mineralogy is predominantly sodium sulfate minerals (mirabilite in winter and thernadite in summer). Only two samples contained large concentrations of halite (NaCl) which were collected along the stream channel. See figure 5.50 for x-ray diffraction patterns of collected samples. Individual diffraction patterns of each sample with labelled peaks is found in appendix A.

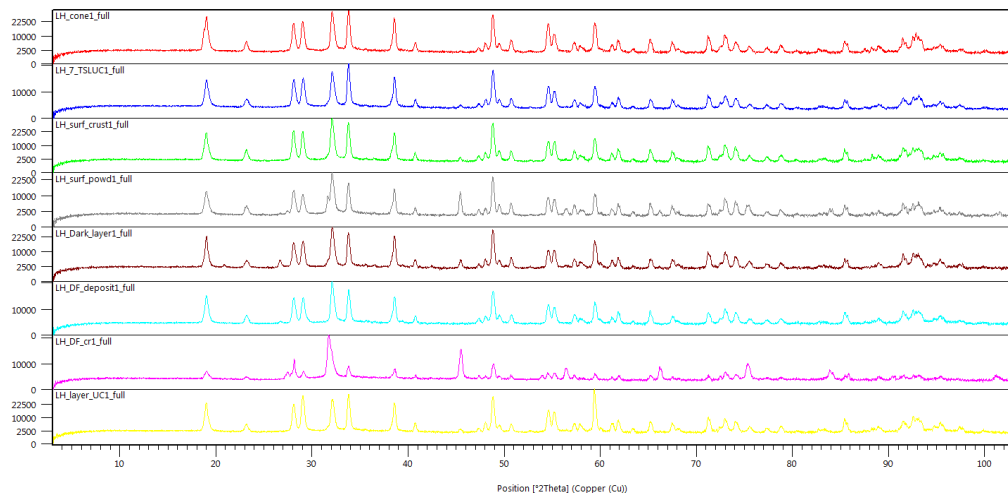


Figure 5.50: X-ray Diffraction patterns from selected samples from the Wolf Diapir site, the primary peaks correspond with halite and thernadite.

5.3 Computer Simulations using Frezchem v. 5.2

Modelling results using Frezchem v. 5.2 are consistent with the mineralogy identified by x-ray diffraction. Using the water chemistry as input Frezchem predicts the dominant mineralogy at both sites to be halite (NaCl, precipitated by both evaporation and by freeze-crystallization at temperatures above 0°C) and hydrohalite (NaCl.2H₂O, by freezing fractionation at temperatures below 0°C with the majority precipitating along with the formation of ice at temperatures below the eutectic point). Other minerals that precipitate are mirabilite (Na₂SO₄*10H₂O), sylvite (KCl), gypsum (CaSO₄*2H₂O); and various hydrated forms of Magnesium Chloride MgCl₂*12H₂O, KMgCl₃*10H₂O, and CaCl₂*6H₂O, that are present in minute amounts and did not precipitate in every Frezchem simulation. The total concentration of minerals precipitating from Frezchem using water samples collected in the field (shown in tables 5.1 for Stolz Diapir and 5.2 for Wolf Diapir) are found in table 5.3.

Table 5.3: Concentrations of mineral precipitates determined by Frezchem v.5.2. Water chemistry shown in table 5.1 was used to obtain results below for Stolz and table 5.2 for Wolf. *Simulations where eutectic point was reached at 228.15K (no liquid remaining so all possible minerals had precipitated. **Simulation where eutectic point was reached at 248.25K.

		Water Sample Location	NaCl	NaCl*	Na ₂ SO ₄ *	CaSO ₄ *	KCl	MgCl ₂ *	KMgCl ₃ *10H ₂ O	CaCl ₂ *	
			(Moles)	2H ₂ O (Moles)	10H ₂ O (Moles)	2H ₂ O (Moles)	(Moles)	12H ₂ O (Moles)	(Moles)	6H ₂ O (Moles)	
Stolz Diapir	Summer 2013 Water Samples	Outlet	7.20	5.97	3.65E-02	4.76E-02	7.69E-03	0.00	0.00	0.00	
		Stratigraphy site	7.13	6.02	5.62E-02	5.15E-02	4.79E-03	3.07E-03	0.00	0.00	
		Valley Opening*	7.10	6.01	7.23E-02	4.71E-02	6.59E-03	0.00	0.00	0.00	
		Whitsunday Floodplain	6.79	5.74	1.45E-01	1.64E-02	2.51E-03	0.00	0.00	0.00	
	Winter 2014 Water Samples	Outlet*	10.73	5.99	2.98E-02	4.49E-02	3.65E-02	0.00	0.00	0.00	
		Pool 1*	13.99	5.92	2.60E-02	8.45E-02	4.65E-02	1.12E-02	3.79E-06	7.50E-03	
		Pool 2	11.19	5.99	2.78E-02	7.26E-02	3.00E-02	6.85E-03	0.00	0.00	
		Pool 3**	9.73	0.18	5.24E-02	5.66E-03	0.00	0.00	0.00	0.00	
		Pool 4 (Stratigraphy site)	14.62	5.95	9.77E-03	6.85E-02	3.93E-02	1.12E-03	0.00	0.00	
		Valley Opening	12.45	5.99	1.27E-02	6.16E-02	2.76E-02	2.58E-03	0.00	0.00	
		Whitsunday Floodplain	16.12	5.91	0.00	4.46E-02	4.21E-02	0.00	0.00	0.00	
	Wolf Diapir	Summer 2013 samples	Outlet	6.96	5.97	3.16E-02	1.00E-01	1.19E-02	1.81E-02	0.00	0.00
			Channel	6.87	5.97	4.07E-02	9.62E-02	1.21E-02	1.87E-02	0.00	0.00

Chapter 6: Discussion

This chapter be is divided into two sections, the first (Section 6.1) discusses the differences between winter and summer processes at both Stolz and Wolf Diapirs. This section answers the following research questions: (1) how do these ‘travertine/tufa-like’ salt structures form? (2) Does the combination of extremely cold winter temperatures and freezing depression of saline groundwater play a role in the formation of these landforms? (3) Do cold winter temperatures lead to eutectic freezing conditions of hyper-saline groundwaters and the formation of hydrohalite? The following specific objectives are also addressed (from Chapter 1): (1) determine the topographic and geomorphic characteristics of both hyper-saline perennial spring systems, (2) characterize the chemistry of hyper-saline discharge, (4) characterize the mineralogy of precipitates forming ‘travertine/tufa-like’ salt structures and (5) using Frezchem (version 5.2), to simulate mineral precipitation and validate hydrochemical analyses.

The second section (section 6.2) presents a conceptual physical model explaining how both spring deposits formed (*per* objective 6) as well as answering the final research question: what are the geomorphic implications of this type of system?

6.1 Winter versus summer processes

There are dramatic seasonal differences in the geomorphic and hydrologic processes occurring in the hyper-saline springs at Stolz and Wolf Diapirs. The winter (cold) season drives mineral precipitation processes that create the travertine/tufa-like salt deposits while summer (warm) processes are responsible for the mechanical and chemical

erosion of both deposits, but it is the dynamic nature of this relationship between both seasons that shapes the overall geomorphology of the deposits. Specifically the salt deposits at the Stolz and Wolf Diapir springs sites results from the interaction of air and water temperatures, water chemistry, mineral precipitation, surface hydrology and specific regional topography.

6.1.1 Winter Processes

6.1.1.1 Temperature Regime and Mineral Precipitation

The Stolz Diapir spring is unique in comparison with the other springs on Axel Heiberg Island in that it is the only spring with a known groundwater source. A seasonal stream flows from the Joy Range directly into the west side of the diapir; it then reappears on the opposite side (figure 6.1; Schwerdtner and Van Kranendonk, 1984). The inflow stream has eroded a deep channel along the west and south-west side of the inner salt core and disappears into a cave midway into the diapir, the cave opening is highly unstable and is prone to collapse. The centre of the diapir displays widespread salt karst with several large sink holes and collapse structures. The water of the inflow is relatively fresh (derived from snowmelt) but becomes highly mineralized through its interaction within the salt core of the diapir emerging at the outflow as a hyper-saline discharge. The high NaCl content relative to other salts confirms its interaction with the salt core of the diapir. It is this highly mineralized groundwater that generates the salt deposits seen at Stolz Diapir. A similar phenomenon occurs at Wolf Diapir except the source water is not known, the discharge rate is quite low and the regional topography differs. Stolz Diapir is also the only diapir on Axel Heiberg Island with an exposed halite core and its water chemistry further confirms

this (table 5.1 and figure 5.42). The subfreezing temperature at the outflow (-1.9°C) also confirms the presence of permafrost within the dome.

The chemistry of the outlet waters and the cold air temperature regime at both study sites are conducive for the formation of various hydrated evaporative minerals. Both sites are conducive for the formation of various hydrated evaporative minerals. Both sites are characterized by hyper-saline waters (see tables 5.1 and 5.2). Outflow temperatures of -1.9°C (Stolz) and -4.3°C (Wolf) are remarkably steady, regardless of the air temperature. In winter, air temperatures cool spring waters and in the summer, air temperatures warm spring waters. Under cold winter conditions as water temperatures cool downstream from the outlet, dissolved mineral concentrations reach supersaturation by freezing fractionation and precipitate.

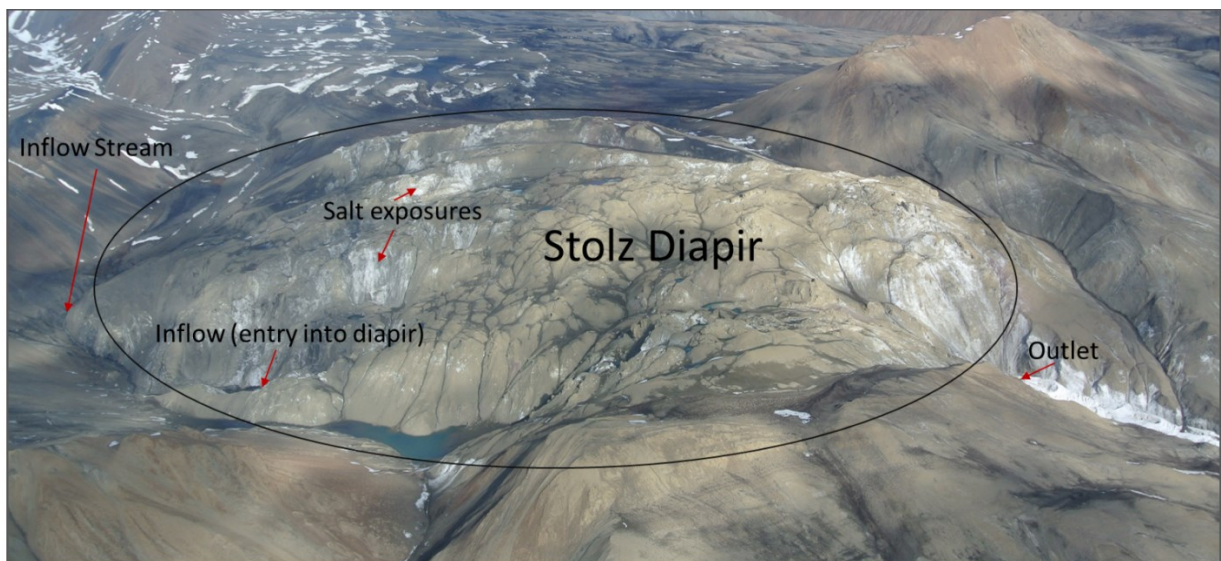


Figure 6.1: Image taken from helicopter that shows the inflow stream flowing into the diapir and the outlet on the other side that is driving the salt deposit. The water of the inflow is fresh whereas the water in the outlet is highly mineralized (dominated by sodium and chloride ions) indicating contact with the evaporites within the diapir (circled in black).

In this part of the Canadian High Arctic, sub-freezing conditions persists for at least ten months of the year. Temperature data collected by the hobo data loggers at the Stolz

Diapir site (see figures 5.14 and 5.15) show that temperatures fall below 0°C in mid-August and remained until late May (despite being shielded these temperatures are probably warmer than ambient due to solar radiation). During the study period average air temperature was -29°C between November and April with a minimum of -45°C. Water temperatures recorded by the logger within a deeper pool (1-3m) during this time averaged -13°C (ranged -11°C to -16°C), however water temperatures at pools' surface and in shallow areas (e.g. flow over barrage rims) would be similar to air temperatures. Unfortunately, since the logger failed at the Wolf Diapir site, temperature readings were not obtained, so this study assumes that air temperatures were approximately similar to those recorded at the Stolz Diapir site.

The dominant minerals precipitating at both sites according to simulations done using Frezchem is hydrohalite during the winter (by freezing fractionation) and halite during the summer (by evaporation). At Stolz, this is supported by mineral samples collected and identified using x-ray diffraction. The dominant 'bulk' mineralogy identified in the majority of samples analyzed was halite, including samples collected in winter that were melted and dried. Upon melting these samples were reduced to a combination of salt crystals and brine water and indirectly confirming the presence of hydrohalite (determining molar ratios of these samples also supports hydrohalite). The eutectic temperature for hydrohalite is -21.1°C for both the Glitterman and Ringer-Nelson-Thompson pathways of seawater freezing (Marion and Kargel, 2008). The next eutectic temperature for mineral precipitation along both pathways for seawater freezing is -36°C ($\text{MgCl}_2 \cdot 12\text{H}_2\text{O}$ for the Glitterman pathway; and sylvite (KCl) and $\text{MgCl}_2 \cdot 12\text{H}_2\text{O}$ for the Ringer-Nelson-Thompson pathway). Having a mean air temperature during the winter of -29°C from

November to April (recorded by the Hobo data logger at Stolz) and a hyper-saline water dominated by sodium (Na) and chloride (Cl) ions favours the deposition of hydrohalite and ice, particularly at barrage rims. Furthermore, all mineral precipitation activity captured by the time lapse cameras at the Stolz site occurs at temperatures below -21.1°C but above -36°C also supporting the large scale deposition of hydrohalite.

It is important to be aware of the difficulty in identifying hydrohalite directly due to its metastable nature. Hydrohalite is only stable at temperatures below $+0.12^{\circ}\text{C}$ (Light *et al.*, 2009), presenting an extremely difficult logistical challenge. At $+0.12^{\circ}\text{C}$ and above, the mineral incongruently melts forming halite and a brine solution. The only study to successfully confirm hydrohalite analytically was by Craig and Light (1975) using x-ray diffraction, however that study used artificial hydrohalite rather than samples collected from the field. This study attempted to identify hydrohalite from samples collected in the field, but without success, so indirect validation was necessary.

At Stolz Diapir, a white powdery residue identified as thernadite (Na_2SO_4) forms a light dusting on the surface of the deposit from the midpoint all the way into the Whitsunday River Floodplain. Thernadite is the dehydrated form of the hydrous mineral mirabilite ($\text{Na}_2\text{SO}_4 \cdot 10\text{H}_2\text{O}$) and as stated by Sonnenfeld (1984), the fine white powder, observed forms from when mirabilite becomes exposed to air and dehydrates, causing it to metamorphose into thernadite. The lack of mirabilite or thernadite within the upper portion of the stream is thought to be due to the kinetic rates of the precipitation of these minerals. According to Marion and Kargel (2008), precipitation rate for sulfate salts tends to be sluggish even at $+25^{\circ}\text{C}$. At Wolf, the spring discharge is so low (1-2L/s) that the time

required for the mound to fill with water (during the winter) is sufficient to allow sodium sulfate minerals to precipitate on the mound walls.

At Wolf Diapir, the mineralogy identified by x-ray diffraction is dominated by thernadite rather than halite, despite Frezchem simulations suggesting that halite should be abundant. Two samples collected in the channels contained a significant amount of halite confirming its presence (albeit limited) in this system. A layer of thernadite also covered the entire deposit at Wolf Diapir. The Battler *et al.*, (2013) mineral survey of the Wolf Diapir spring site found that halite was the most abundant mineral followed by thernadite, validating the Frezchem simulations of this study. It is possible that the sampling at Wolf Diapir in this study was not sufficient to fully assess the bulk mineralogy of this site. The main focus of sampling was on the conical mound and along the stream channel. Battler *et al.*, (2013) also suggests the mound to be composed mostly of thernadite/mirabilite followed by halite. Hard crustal samples from near the channel were composed of halite and thernadite which is consistent with results from this study. Furthermore, sampling from both studies focused mainly on the immediate surface of the deposit at Wolf. This could impact results in two ways: firstly, since mirabilite is less dense than hydrohalite (1.464-1.490 compared with 1.54; Sonnenfeld, 1984) and even though it precipitates in lesser quantities it may be more concentrated at the surface due to density differences. Secondly, mirabilite has a much higher range of temperature stability compared to hydrohalite. Hydrohalite can remain stable only at temperatures below +0.12°C; whereas mirabilite can remain stable up to +32.4°C when it metamorphoses to thernadite (Sonnenfeld, 1984; Herrero *et al.*, 2015). With a mean summer temperature of +7°C it is likely that any

hydrohalite that precipitated along with mirabilite during the winter would destabilize allowing the hydrohalite to dewater leaving only mirabilite behind.

Other evaporite minerals predicted by Frezchem include gypsum ($\text{CaSO}_4 \cdot 2\text{H}_2\text{O}$), sylvite (KCl), $\text{MgCl}_2 \cdot 12\text{H}_2\text{O}$, $\text{KMgCl}_3 \cdot 10\text{H}_2\text{O}$ and antarticite ($\text{CaCl}_2 \cdot 6\text{H}_2\text{O}$), however none of these minerals were identified within collected samples. Their predicted amounts were very minute and therefore were likely not present in sufficient quantities to either be collected and/or be identified using x-ray diffraction.

6.1.1.2 Mineral Deposit Textures and Crusts

The various mineral deposits have a range of textures and morphologies including: extensive surface crusts containing ‘cauliflower’, ‘popcorn’ and smooth ‘spherical’ textures; a floating raft, and halolites. These morphotypes have been identified elsewhere in association with other evaporitic minerals including halite.

Both deposits are characterised by a continuous salt cover except for patches where the spring water dissolves the deposits in summer. Crusts of varying thicknesses are widespread and contain either halite or a mixture of halite and thernadite. De Waele *et al.* (2009) termed similar crusts formed in caves in the Atacama Desert in Chili as “halite floors” (p.100), a term also used in this study. Halite floors form from brine solutions by two mechanisms: either by evaporation or by precipitating subaqueously within a brine (Arthurton, 1973; Sonnenfeld, 1984; De Waele *et al.*, 2009; and Filippi *et al.*, 2011). When water is cold, brines become denser and concentrate along the stream beds, the decrease in temperature also decreases the solubility of evaporitic minerals, helping to drive

precipitation (Arthurton, 1973). In summer, the reverse occurs when increased temperatures cause the brine to rise and concentrate at the surface. This likely allows the bed of the deposit to slowly erode (both chemically and mechanically) over time, as recorded by the time lapse cameras (figures 5.38 and 5.39) long after the spring snowmelt has ended. Halite precipitates as a slush that gradually hardens over time to eventually become rock-salt (Sonnenfeld, 1984). This was observed in the halite floors during April, the same deposits might also harden from evaporation during the summer. Experiments done by Arthurton (1973) showed that several factors might affect halite crustal deposits: shallower bodies of water favour deposition and the texture of the floor affects the size and growth morphology of crystals. Also, once beds are completely coated by precipitating minerals, crusts tend to grow upwards. This would lead to the types of crustal textures observed in this study (i.e. 'smooth spherical', 'popcorn', and 'cauliflower').

Observations of salt crusts in Iran found that euhedral crystals precipitate subaqueously in calmer and more stable environments; whereas globular deposits would form in faster flowing brines (Filippi *et al.*, 2011). The same basic pattern was observed at Stolz Diapir. The smoother spherical textures (figure 5.4B) were produced in the shallower, faster flowing water near the valley mouth (located near the time lapse camera); and the cauliflower textures (figure 5.4A) occurred along the bed of calmer, deeper pools. The descriptive term 'cauliflower' has also been used to describe salt crusts in other studies (i.e. Atacama Desert by Filippi *et al.*, 2011; and Dead Sea, Talbot *et al.*, 1996) without any explanation to indicate how they formed. This texture probably forms as clusters of precipitating crystals that become irregular in shape due to competitive crystal growth. Finally, popcorn-like textures were observed on the walls of pools during the April 2013

(figure 5.3). Filippi *et al.*, (2011) and De Waele and Forti (2010) also describe popcorn textured halite deposits. It is also unclear how they form but De Waele and Forti (2010) attribute it to evaporative processes which is also likely the case at Stolz diapir and results from draining pools during the winter (this texture was not observed during the summer).

A floating (salt) raft occurs as a thin buoyant crust on the surface of oversaturated brines (that are generally shallow and stable) by evaporation (Filippi *et al.*, 2011). Both salt rafts and carbonate rafts have been identified but form differently, carbonate rafts form from the rapid decrease in dissolved CO₂ concentrations in water bodies with high HCO₃⁻. Floating (salt) rafts have been identified in the Dead Sea (Talbot *et al.*, 1996), Iran (Filippi *et al.*, 2011) and at the Mt Sedom Salt Diapir in Israel (Frumkin and Forti, 1997). The Stolz salt raft (figure 5.13B) was a single raft measuring a few meters across, whereas the other rafts reported in the literature were much smaller (measuring only a few centimeters across). Rafts form in brines and grow by multiple rafts coming together. The Stolz raft had a bumpy surface texture possibly suggesting it formed into a single raft by combining multiple smaller rafts. Salt rafts reported in the literature formed at higher air temperatures (above 15°C), but the raft observed at Stolz Diapir occurred in April when air temperatures were ≤ -20°C. Despite the cold temperatures the site experiences 24 hour daylight at this time of the year so the raft might have formed by evaporation (air temperatures were just below the eutectic point for hydrohalite to precipitate so this raft was likely made out of halite and, but it is possible hydrohalite would also be present). Ice is also likely present in the raft, however the hyper-saline nature of the water would make it unlikely for the raft to be composed mainly of ice.

The spherical pellets were limited to pools where water levels were maintained by upwelling water. These pellets were ± 1 cm in diameter and occurred in upwelling pulses. The pellets were collected, isolated and stored in sterile Falcon tubes. This was then dried and x-ray diffraction analysis identified the salt as pure halite, but was likely hydrohalite originally. These pellets identified as halite oolites or “halolites” by Weiler *et al.*, (1974, p. 676) are overgrown halite crystals that have smoothed surfaces and are usually about a centimeter in diameter. Similar crystals are referred to as halopisoids by Tekin *et al.*, (2007). Halolites have been described a few times in the literature (Weiler *et al.*, 1974; Sonnenfeld, 1984; Handford, 1991; Castanier *et al.*, 1992; Perthuisot *et al.*, 1993; Castanier *et al.*, 1999; Tekin *et al.*, 2007;). Weiler *et al.*, (1974) attribute halolite formation to halite crustal precipitation that is subsequently rounded and polished by erosion. However, Castanier *et al.*, (1992; 1999), and Perthuisot *et al.*, (1993) attribute halolite growth to bacterial activity.

6.1.1.3 Travertine/Tufa Morphology

The main forms characterizing these study sites include a large conical mound at Wolf Diapir, micro-barrage structures at both sites and a series of barrage and pool structures at Stolz Diapir. The pools at Stolz vary in size, with the largest being 30m across dammed by a barrage 2-3m high and the smallest only centimeters in scale. The 4-5 large pools occur in the upper part of the system while smaller pools and barrages dominate the lower part. These structures form only during the winter; valley slope, width and distance downstream from the spring outlet (linked to the chemical evolution of stream flow) clearly play a role in the ‘travertine/tufa’ morphology at both sites. The largest features at both

sites, and accordingly, the most rapid rates of precipitate deposition occur in the immediate vicinity of the spring outlet. Whether this is the point where deposition is initiated is unclear given the complex nature of the interaction between changing temperature (progressive cooling) and the changing water chemistry. Once optimal conditions exist (corresponding to the eutectic point for NaCl solutions) the accumulation of halite and hydrohalite will occur. These are self-regulating systems where deposition will logically begin at some distance downstream from the spring outlet and progressively work its way upslope toward the spring outlet. This pattern is confirmed by the sequence of pool infilling observed in the time lapse camera images. Once temperatures remain continuously cold enough to quickly cool the spring flow, deposition will occur at or close to the spring outlet. The formation of either a barrage pool or mound at the spring outlet impounds flow and thus promotes continued deposition. Given that cold temperatures (-20°C to -30°C) prevail for most of the winter, the greatest accumulation of halite and hydrohalite will be in the upper part of the valley at Stolz diapir. The spacing of the 4-5 large pools is a reflection of changing slope. The occurrence of a single mound at Wolf Diapir is a reflection of the low discharge rates and regional topography. With the possible exception of Dzens-Litovskiy (1966, in Russian), no previous study has examined the role of hydrohalite deposition in tufa- and travertine-like deposits. This research will attempt to characterise general mechanisms behind the formation of the deposits at Stolz and Wolf Diapirs using work that has been done on carbonate travertines and tufas, silica deposits around hot springs as well as the formation of ice.

6.1.1.3.1 Barrages

Regardless of mineralogy, two common physical features of all barrages are that they form in shallow bodies of flowing water and waters are supersaturated with the mineral being deposited. Carbonate barrages form from the precipitation and deposition of carbonate minerals at specific points of CO₂ degassing (Hammer *et al.*, 2010); whereas barrages made from silica or ice form where drastic temperature changes occur with deposition in areas of supercooling (Wooding, 1991; Hammer, 2008). In all cases they form due to areas of faster and more turbulent flow caused by slope.

Interestingly, the barrages at Wolf and Stolz share many common morphological features with carbonate barrages, along with some striking differences. As outlined by Hammer *et al.*, (2010), carbonate barrages tend to “display scaling properties” (p. 347) so that the smallest barrages with centimeter dimensions look identical to the largest barrages of tens of meters in dimension. Generally, the higher the slope the smaller the size of pools that form has been observed for carbonate barrages (Hammer *et al.*, 2007). In regions of small slope, small barrages formed with shallow but large pools forming behind. This trend was not observed at Stolz. In areas of very high slopes (such as mounds) tend to produce micro-barrages (centimeters in height and length) with very small pools (or ridges with no pools) that cover the slopes. These micro-barrages were observed on the mound at Wolf (figure 5.9D) and covering the outer barrage wall that curved concavely of empty pools at Stolz (figure 5.3A). Hammer *et al.*, (2010; using data given by Pentecost, 2005) found only the smallest barrages (as just described) experienced ‘bags of water’ would hang over rims due to surface tension. This would allow free flow of water from an upstream pool over the barrage by a meniscus created by surface tension. These are the only carbonate barrages

where height could be affected by temperature as a result of temperature impact on surface tension. Remarkably, similar meniscus caused by surface tension was observed at the barrages at Stolz, however this was observed for all barrages, regardless of size (figure 6.2). Carbonate barrage walls usually form 'convex outwards' (pointing downstream, Hammer *et al.*, 2010, p. 345). The walls of the barrages at Stolz also form in this direction however a potential distinguishing feature of the Stolz barrages is the formation of a 'lip' at the top of the barrages that forms upstream to flow rather than downstream (a common observation in other barrages; figure 5.1). The Stolz barrages also appear to be slowly migrating downstream, as has been observed in carbonate barrages. In addition, like carbonate barrages, it was observed at Stolz that if a dam downstream grows faster than a dam upstream, the growing downstream dam will fill up with water as it is growing, inundating the upstream dam resulting in two pools coalescing (Versey II and Goldenfeld, 2008). The largest pools at Stolz form in this way regardless of slope. Finally, the barrages (specifically) that form at Stolz are extremely hard and rigid (enough to walk on without causing any damage). It is unclear how this compares to the hardness produced by carbonate barrages, however the carbonate terraces at Colour Peak on Axel Heiberg Island (composed of Ikaite [$\text{CaCO}_3 \cdot 6\text{H}_2\text{O}$]; Omelon *et al.*, 2001, 2006) were very weak and easily damaged. The difference in hardness observed between Stolz Diapir and Colour Peak may be a reflection of the mechanism of mineral precipitation. Turbulent flow can cause both CO_2 degassing and supercooling (Wooding, 1991). Barrages formed by supercooling may simply form a harder mineral deposit and also form more slowly due to the low rate of discharge.



Figure 6.2: Example of meniscus caused by surface tensions of flow over small barrages (a few centimeters in height) at Stolz. Image taken by Prof. Pollard in 2008.

The physical similarities between the salt barrages at Stolz Diapir and carbonate barrages in the literature exist despite differences in mineralogy and environmental factors (like temperature), but suggest that similar controlling factors may be present within each system (like water turbulence) ultimately causing the deposition of each mineral type. Carbonate barrages may involve both abiotic and biotic processes, although many models have shown pattern formation due only to abiotic processes (Goldenfeld *et al.*, 2006; Chan and Goldenfeld, 2007; Hammer *et al.*, 2007; Veysey II and Goldenfeld, 2008). Of particular interest to this research is the experimental work by Kerr and Turner (1996). They conducted dome (similar to the mound formed at Wolf) and barrage forming experiments by cooling heated NaCO_3 and KNO_3 solutions to drive precipitation. Their experiments were done on a mesh that was either laid flat or on an angle and had the solution run on it to simulate stream flow. The domes and barrages formed during the experiments are morphologically identical to those observed in nature. Kerr and Turner's

(1996) work suggests that landform morphology (e.g. terrace and dome (or mound) deposits) can be independent of mineralogy; but it is more likely the case that a range of minerals can precipitate and create these deposits as long as they are able to reach saturation by supercooling or by the loss of CO₂ (in the case of carbonate deposits). Many of these deposits form in arid and semi-arid environments and it is unclear to which extent evaporation plays a role.

Numerical simulations of abiotic dome and barrage formation have been done for carbonate minerals. Hammer *et al* (2007) were able to simulate the formation and growth of carbonate travertines on an inclined surface using a 2D precipitation model that coupled flow rates with surface-normal growth rates. Veysey II and Goldenfeld (2008) used discrete lattice of cells to simulate the formation of travertine dams using precipitation driven terrace growth paired with turbulent fluid flow. The role of microbiology in travertine/tufa formation remains unclear but based on the findings of Niederberger *et al* (2010) it remains possible that biotic processes could play a role in the formation of the deposit at Wolf. However the success of simulating terrace morphology using only abiotic processes indicate that organisms may not have a large impact on barrage formation as was previously hypothesized. To the knowledge of the author, no computer simulations have been conducted for barrage formation produced by cooling.

6.1.1.3.2 Mounds

Mounds and barrages form by similar processes in the precipitation and build-up of depositing minerals. Again this is achieved by CO₂ degassing for carbonate mounds and supercooling for other mound types. The main factor controlling the morphology of the deposit is the topographic setting. Mounds form on flat surfaces with a fixed point source

of spring flow or resurgent point with a standing body of water, whereas barrages form on sloping surfaces. For carbonate mounds these point sources would correspond with CO₂ degassing and generally linked to hydrothermal systems. These mounds continue to grow until artesian pressure is no longer sufficient to lift water over the growing mound (Kerr and Tuner, 1996). Mounds formed by supercooling such as the mound at Wolf Diapir and the mounds reported by Dzents-Litovskiy (1966) in Eastern Siberia form similarly to icing deposits. Upwelling water would supercool and freeze soon after it reaches the surface and precipitate hydrated salts. Subsequent and continuous upwelling would create a mound structure.

6.1.2 Summer Processes

6.1.2.1 Stolz diapir

The deposits at Wolf and Stolz Diapirs are unique in comparison to other travertine/tufa or salt deposits, not only because of their scale and mineralogy but also because each deposit undergoes an annual cycle driven by the seasonal conditions. During the winter, minerals precipitates cause the deposits form and accumulate year after year. During the summer the deposits erode and are partially destroyed through dissolution and mechanical erosion by melt and spring water (that is above the temperature for mineral precipitation). The pattern of summer erosion involving channels troughs and large tunnels under the salt mass cause localized collapse of pool, and barrage structures. This further influences how accumulation rebuilds the system in the following winter. It is this dynamic that shapes the deposits and forces the deposits to be in a constant state of change.

Air temperatures finally increase above 0°C generally at the end of the month of May, although based on field observations it appears the accumulation phase ends and pools drain by early May. At Stolz Diapir, annual observations and results from the time lapse cameras (figures 5.21 to 5.34) show that pools can fill and drain at various times during the winter season. If water is still within a pool and water temperatures increase enough for the water to begin dissolving the deposits, the barrage may either break completely (figure 6.3A) potentially causing additional damage downstream (a wash out event) or the water may drain at a specific location, such locations have been identified at Stolz (figure 6.3B).

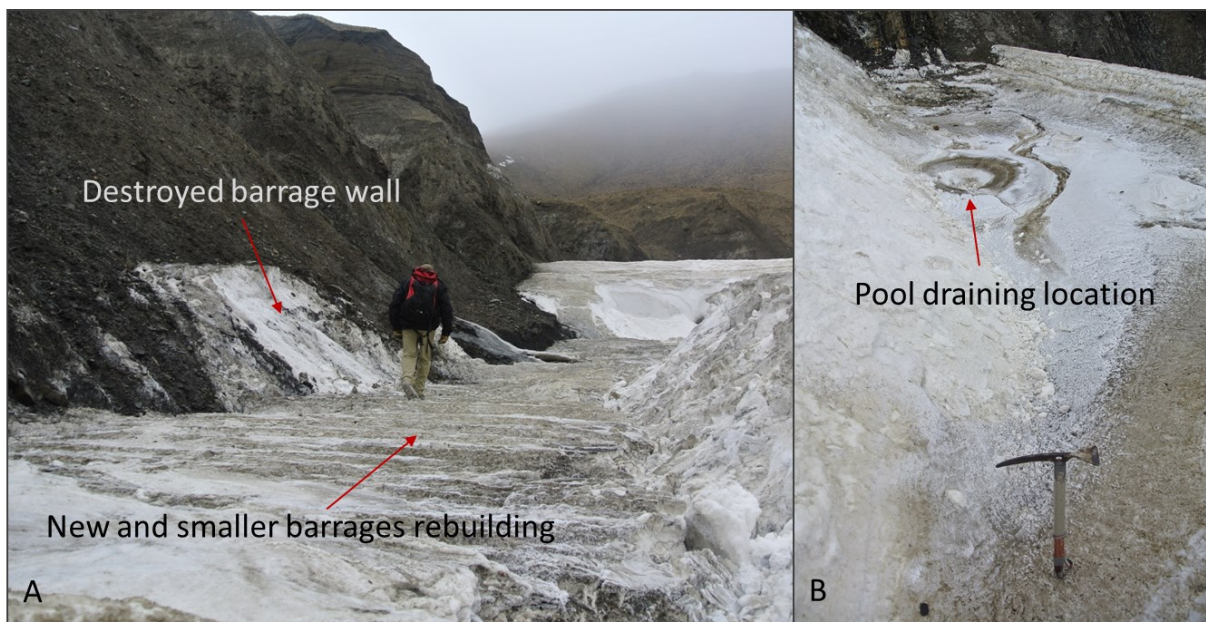


Figure 6.3: (A) a barrage wall broke, unleashing the water within its pool was destroyed parts of the deposit downstream, known as a washout event; (B) pool drained an emptied from a specific location.

Summer observations at Stolz Dipair show that stream flow dissolves mechanically erodes a path through the deposit (the stream dissolves the deposit right down to the valley floor) and is only visible at a few locations. Annual observations since 2005 have shown

that the location of the summer stream channel varies considerably. During the spring surface runoff from snowmelt enters the valley at several points as a function of valley topography (figure 6.4). This input of freshwater dissolves and washes out the deposit at these locations (if freshwater enters in higher volumes, structures immediately downstream can be destroyed also), destroying some structures that were created during the winter. Snow fall directly on the deposit during winter can also partially dissolve the deposit when it melts in spring.

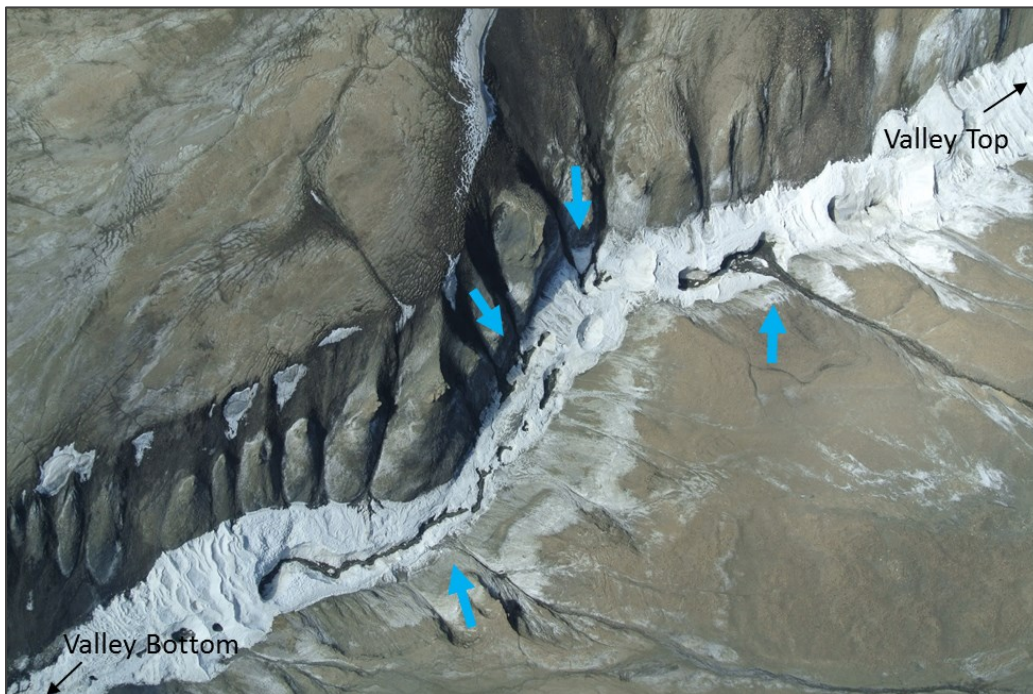


Figure 6.4: Image taken from helicopter at the end of June, 2014 at Stolz. Blue arrows point to entry points of freshwater from snowmelt.

6.1.2.2 Wolf diapir

To increase in size, the mound at Wolf diapir, must fill completely with water and overflow. As it overflows the saline spring water rapidly cools and drives mineral precipitation along the upper lip of the mound and down its sides. In this way the mound

tends to grow (both in height and width) uniformly although the growth of the salt platform downstream tends to be irregular. During the summer the mound empties when spring water dissolves at the base of the mound to continue flowing downstream. The location of the channel changes annually. In summer 2013, the spring channel flowed downstream from the left side of the mound and in 2014 it flowed downstream from the right side.

6.1.2.3 Legacy features

An interesting observation made at both sites is dissolution and mechanical erosion patterns produced during the summer can have a lasting impact on the morphology of the deposit. A good example of this is shown in figure 6.5 at Wolf Diapir. In 2004, higher river flows carved channels into the deposit that are still clearly seen today (images in figure 6.5 were taken in 2004 and 2013). This dissolution event appears to have carved out the platform feature in front of the deposit. The discharge of the Wolf Diapir spring is most likely too low to deposit enough minerals during winter to cause significant change to the deposit. Whatever precipitates during the winter largely gets dissolved in summer so the net built up of the deposit is extremely small. It is likely that at some points the ephemeral channel could shift and completely remove the Wolf Diapir mound structure.

As shown in figure 6.4, valley topography at Stolz tends to concentrate snow melt to erode the deposit in specific areas, the dissolution patterns appear to vary year to year depending on snow fall patterns during the winter. The Stolz Diapir spring has a larger discharge than Wolf and so is able to deposit more minerals during the winter. Stolz differs from Wolf because of its topography it experiences more change due to snowmelt however like Wolf there are still patterns of legacies that can be identified.

Figure 6.6 illustrates the evolution of the Stolz Diapir deposit through time between 2005 and 2013. The figure include both summer and winter photos. A barrage wall (that has changed slightly over time) is identified in each photo to demonstrate that despite the changes, certain features appear to be consistent. Legacy features are particularly important at Stolz Diapir because it is probably responsible for creating tunnels (pipes) within the deposit. The time lapse photos show that while various pools upstream are filled and then drain (while others remain filled), the photos taken at the valley mouth downstream also show that spring flow stays consistent. This can be attributed to the tunnels within the deposit allowing water to flow in more than one route through the deposit. Photos taken by Prof. Pollard and Dale Andersen over the last decade shows that the stream path in summer migrates from one year to the next. These tunnels would be relict stream paths carved from summer channels and then then potentially covered from the surface by winter mineral deposition. Finally, results from the time-lapse camera shows that barrage formation resumed in barrages that were still present from previous seasons. The water had simply filled existing pools and continued to build up the pre-existing barrage walls (figures 5.30 to 5.32).

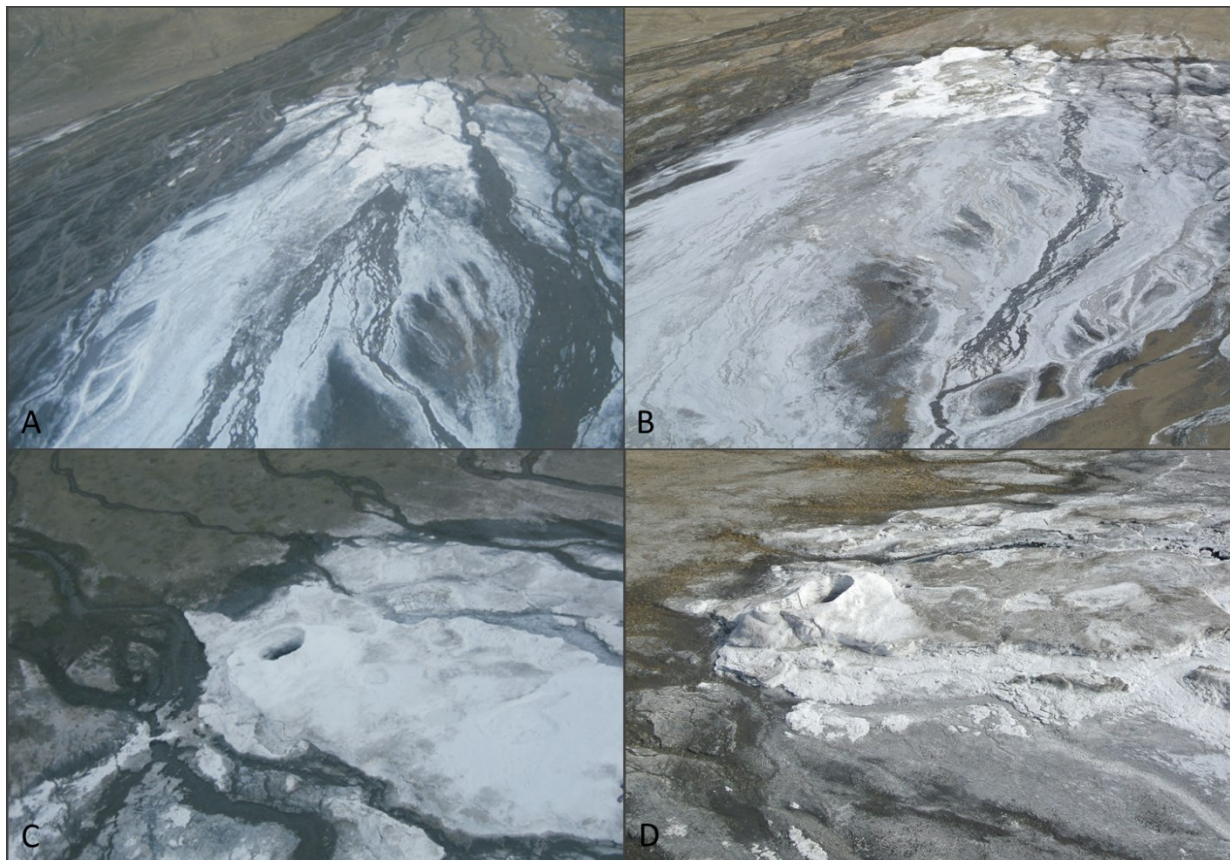


Figure 6.5: (A) and (C) are images from Harrison and Jackson (2008). Higher river flows carved part of the deposit in 2004 and these dissolved parts of the deposit are still easily seen in 2013 (B and D are comparable angles of the images by Harrison and Jackson (2008) of the deposit and images were taken in June 2013).

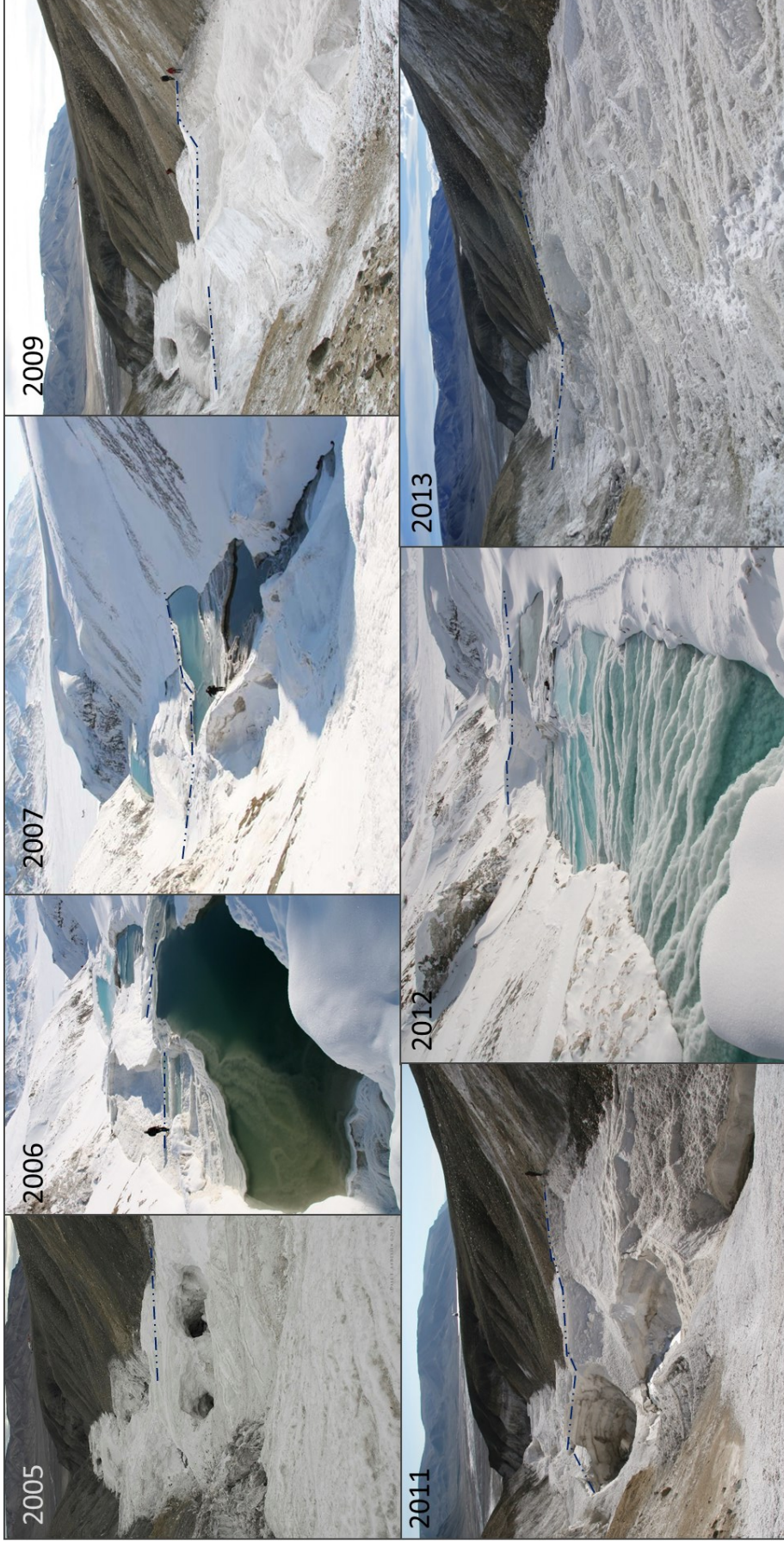


Figure 6.6: Images showing the evolution of the Stolz deposit over time between 2005 and 2013. The year the image was taken is shown on the image itself. A legacy feature identified as a barrage wall can be recognized within each image and has been traced with a dashed dark blue line. Note that this feature does change slightly over time. The image taken in 2005 was taken by Dale Andersen, the images between 2006 and 2012 were taken by Wayne Pollard. The image from 2013 was taken by the author.

6.2 Conceptual Model

This section proposes a model for the formation and evolution Stolz and Wolf Diapir deposits. There are still many unknowns about these two systems however it is still possible to conceptualize the general processes behind the formation of the deposits.

6.2.1 Stolz Diapir

The Stolz Diapir deposit is located within a narrow V-shaped valley. It is unclear if the valley formed before the deposit or while the deposit itself was forming. The valley probably formed by fluvial erosion following deglaciation. The presence of salt deposits perched along the side of the upper valley several meters above the current travertine/tufa deposit is curious. It is unclear if these perched deposits are linked to an earlier stage in diapiric uplift or maybe relict accumulations of the halite at an early stage when the stream bed was higher up. Figure 6.7A shows the possibilities highlighted above. Figure 6.7B shows cobbles within the valley mouth, adjacent to the deposit, suggesting they were placed by stream activity at an earlier time when discharge was greater. Given the topographic setting of the valley, the most probable explanation for the formation is downcutting by a stream fed by the spring.

Regardless of how the valley formed, mineralized groundwater discharges from a spring outlet at the head of the valley and supports a stream that flows the entire length of the present v-shaped valley. In the winter, when conditions were conducive for the precipitation of hydrated salts (outlined in section 6.1.1.1), the deposit would have begun to accumulate. Due to stream flow the accumulation zone of salt would travel downstream, elongating the deposit every year. Hugon and Schwerdtner (1982) reported the length of the deposit to be 500m long; in 2013 it was 800m long. This pattern of growth might

explain why the deposit is thickest at the outlet and gradually thins out into a salt pan on the Whitsunday River Floodplain; and why barrages in the upper half of the valley are generally larger than the lower half of the deposit. As seen in the results from the time lapse cameras, when barrages are active they tend to continue building the existing barrage walls rather than build completely new barrages, so established barrages slowly grow every year. Experimental work done by Kerr and Turner (1996) showed that barrage walls would grow as long as a supersaturated solution flows over the rim. New barrages will form when existing structures are destroyed by either snowmelt or a wash out event (figure 6.3A). If only part of the barrages gets destroyed, the part that remained intact continues to grow and the side that was removed gets replaced by a series of smaller barrages; so that barrages of different sizes grow adjacent to each other (figure 6.8B). It is likely that the group of new smaller barrages will evolve into a single large pool as one barrage structure preferentially develops.

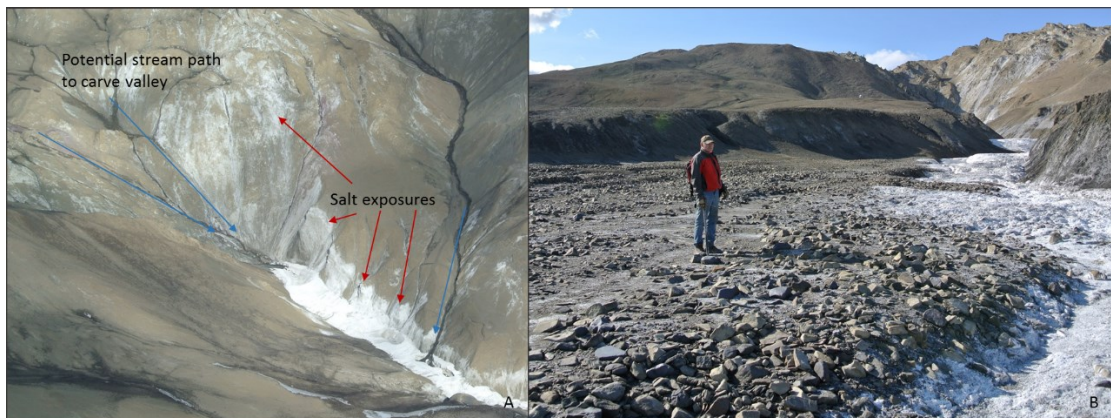


Figure 6.7: (A) Spring outlet of Stolz Diapir. The red arrows point to some of the salt located on the upper reaches of the valley. Blue arrows show flow direction of annual snow melt streams that may have carved the valley over time. (B) Cobbles within the valley mouth, adjacent to the deposit, suggesting they were placed by stream activity at an earlier time when discharge was greater.

Kerr and Turner (1966) demonstrated that on a uniform slope barrages will eventually form from supersaturated flowing water. In the case of cold evaporate minerals forming, a layer of single crystals precipitate along the stream bed due to convective heat loss. As the crystals grow, minute irregularities between the growing crystals begin to form, and eventually barrages will form. Combining images of active barrage formation from the time lapse camera located at the outlet, with air temperature data from the hobo temperature data logger strongly suggests hydrohalite is the main mineral precipitating during barrage formation. Barrage formation occurs between -22.9°C to -35°C , which is an ideal temperature window for hydrohalite formation based on salt water freezing sequences (Marion and Kargel, 2008). Other minerals present, like mirabilite (identified as thernadite), could also be contributing to barrage formation however, other minerals are not sufficiently abundant to have a significant impact on the morphology of the deposit. Ice is also likely present but in small quantities due to the highly mineralized groundwater feeding the spring.

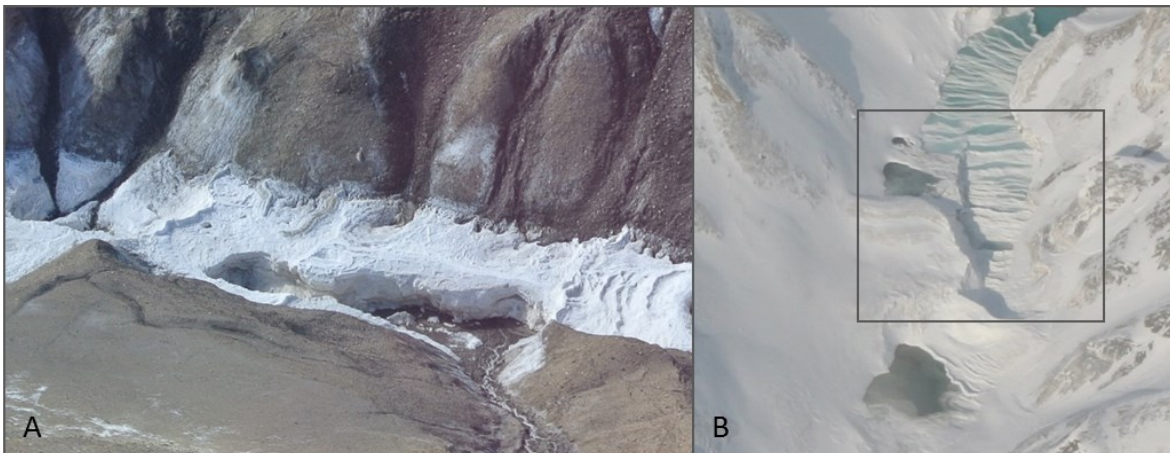


Figure 6.8: (A) example of snowmelt only dissolving part of the deposit, image taken in July 2014; (B) example of new terrace formation on the side that was dissolved and larger terraces on the side that remained intact (highlighted within box), image taken in April 2012 by Prof. Pollard.

Stratigraphic analysis (figure 5.11), results from the time lapse camera located at the valley opening (figures 5.21 to 5.34) and general observations show that the deposit does not accumulate uniformly and that accumulation appears to be a function of winter stream flow. Winter accumulation can be as low as a few millimetres in some parts of the deposit and over half a meter in others. Stratigraphic analyses show that accumulation in a single season can infill pools sufficient to bury a smaller barrage when it becomes inundated within a pool. Note that in summer, dissolution and consolidation due to dewatering of hydrated salts, melting ice and snow, the upper layers of the deposit would be transformed to NaCl and be partially destroyed or compressed so winter accumulation rates based on measured sections are most likely an underestimation.

It is likely that when the deposit was thinner, the dominant hydrological regime of the deposit differed slightly. The deposit was likely be too thin for tunnels to form within the deposit and all water would flow at the surface. In winter the spring would flow filling pools until they overflowed (causing the barrages walls to get larger) and continue downstream until all the pools were filled. In the summer the spring flow and draining pools would erode to the valley floor as is seen today. As the deposit becomes thicker and longer the hydrology changes to reflect the seasonal differences. Subsurface flow would begin to flow through the thicker parts of the deposit reflecting the summer flow path. The geometry of these subsurface conduits lead to complex patterns of flow that allow some pools to fill during winter while others remain empty (as captured by the time lapse cameras). For part of the winter season the presence of subsurface flow affected the erratic way pools filled and drained. Rather than a system where pools fill sequentially from overflow from the pool immediately upstream, this systems allows for subsurface flow to

fill pools downstream first, probably where the salt deposit is thinner. As documented in 2013, some pools are connected to subsurface conduits directly allowing water to fill a pool by upwelling (as was seen with the upwelling halolites).

In recent years the discharge at the Stolz diapir spring appears to be decreasing. Pollard (personal communication) reported a discharge of 30.5L/s in June 2008. Discharge in 2013 was 11.33L/s, however this value may be an underestimate because the outlet was covered by salt, so discharge had to be measured downstream. Any change in discharge will have an impact on the deposit (less salt accumulation occurring during the winter) and maybe likely the reason for the decreased number of active pools during the 2012 and 2013 April field seasons. The decrease in active pools during the winter may also be attributed to the thickness of the deposit, causing the hydrological regime to shift from a surface to a subsurface flow. It is unclear if the discharge will continue to decrease until the spring is no longer active or if discharge rates will increase in the future.

6.2.2 Wolf Diapir

Unlike the Stolz deposit, the source of spring water at Wolf is unknown, however the highly mineralized nature of spring water reflects a groundwater source in contact with the evaporate beds associated with diapiric processes. Its proximity to Wolf Diapir has led to the conclusion that its occurrence is linked specifically to local geologic processes. Due to its topographic setting in the middle of a wide valley, the morphology of the deposit is very different from the deposit at Stolz Diapir. The Wolf deposit forms in the middle of a wide U-shape valley on a flat, unconstrained surface with a very gentle slope (rough

estimation is 4-5%) that is too low to form a terrace deposit. Spring flow is in a southwest direction and the deposit itself also follows this direction.

The deposit would have formed much like an icing mound during the winter by the gradual built-up of salt over a point source of discharge (figure 6.9A). Discharge at this site is extremely low (approximate 1-2L/s), and so once the spring water discharged from the outlet, it will supercool fairly rapidly and deposit salt as thin sheets. Because of the topography, the first layer of mineral deposition would have occurred in a southwest direction, following the direction of slope. These first sheets of salt minerals probably would have changed the immediate topography at the outlet causing flow to shift position in a self leveling manner. At some point, probably during a period of extreme cold, the salt precipitates would have enclosed the spring outlet initiating the development of a mound. The mound would grow incrementally each winter, and once the mound got larger, its structure became a driving factor in the pattern of winter discharge. For example, spring water would have to first fill the mound and once it overflowed it, would slowly grow the sides of the mound. Each summer, when mineral deposition is replaced by dissolution, the insides of the mound would get carved out, hollowing it over time (especially if the mound was still full of water when air temperatures increased). The spring water then dissolves part of the mound and flows into the floodplain.

Large scale disturbances (as seen in 2004) will obviously cause significant changes to the mound and salt platform morphology and size, it is likely that in various times in the past, the mound, platform and saltpan may have been one continuous structure that would gradually thin out with increasing distance from the outlet. The most recent disturbance in 2004 documented by Harrison and Jackson (2008) involves flooding of the area by

meltwater streams and dissolving and carving the deposit and leaving it as it is today (Figure 6.5). No images are available prior to 2004 so any earlier comparison is not possible. However it is possible that the stream water is regularly reshaping the mound or even destroying it completely. The part of the mound that was destroyed in 2004 has been rebuilt (winter flow would have concentrated in this part of the mound, causing it to self-repair itself, figure 6.10). It formed outwards, changing the overall morphology of the mound because its shape appears to have evolved from a circular to an elliptical shaped mound. Also as the mound was repairing itself, it formed a series of micro-barrages in this part of the mound specifically because of the change in slope (increased) and spring flow was concentrated there to repair the mound. In the 10 years since the disturbance, the morphology of the deposit has changed little (with the exception of the mound itself), due to the low discharge of the spring. It is likely the morphology will remain so until another large scale disturbance happens.

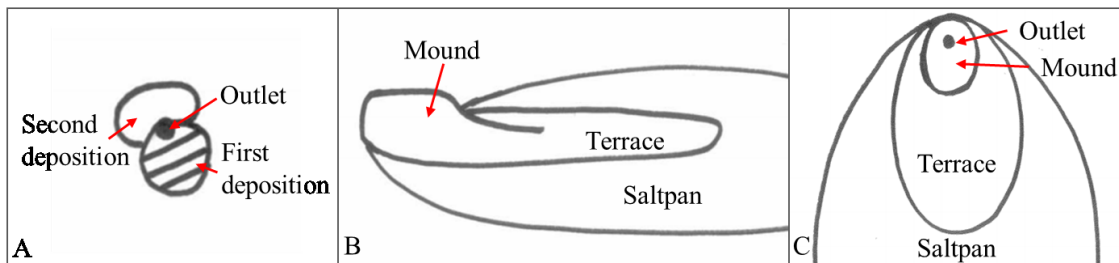


Figure 6.9: Sketch of various points in the formation of the Wolf deposit. (A) the deposit would have initially formed by an icing-like process; (B) side view of the deposit, the terrace and saltpan would likely have been a continuous deposit before large scale disturbances from dissolution by other fresh water springs; and (C) aerial view of the deposit before large scale disturbances.

Finally this site determined the bulk mineralogy using x-ray diffraction to be mirabilite (thernadite in summer), whereas computer simulations using Frezchem and the study by Battler *et al* (2013) suggests hydrohalite (halite in summer) is the dominant

mineral. Experimental work done by Kerr and Turner (1996) showed mounds and terraces could form regardless of mineralogy so both minerals are likely forming the mound.

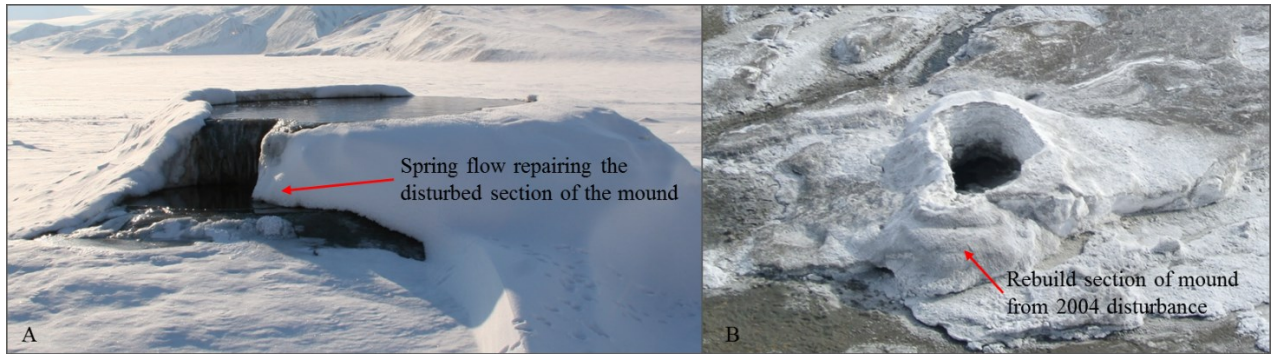


Figure 6.10: Image of Wolf Diapir deposit highlighting the section of the mound that has rebuilt after it was dissolved in 2004. (A) the section as it is being rebuild. Image taken in 2008 by Prof. Pollard; and (B) the section is done being rebuilt as the rim of the whole mound is at the same height.

Chapter 7: Conclusions

This research documents the geomorphic and geochemical characteristics of travertine/tufa-like salt deposits at Stolz Diapir (Whitsunday Bay) and Wolf Diapir (Strand Fiord), two hyper-saline springs on Axel Heiberg Island. This research was predicated on four hypothesis: (1) the hyper-saline nature of groundwater linked to the evaporite geology of salt diapirs on Axel Heiberg Island exhibit depressed freezing conditions as part of an eutectic system; (2) hydrohalite is one of the dominant minerals precipitating in winter at both springs; (3) salt minerals (primarily hydrohalite) create travertine/tufa-like structures under extreme cold conditions; and (4) surface hydrological patterns change seasonally with the precipitation and dissolution of hydrated evaporative minerals (mainly hydrohalite). To test these hypotheses this research asked the following research questions:

- (1) How do salt travertine/tufa-like structures form?
- (2) How does the combination of extremely cold winter temperatures and freezing depression of saline groundwater play a role in the formation of these landforms?
- (3) Do cold winter temperatures lead to eutectic freezing conditions of saline groundwaters and the formation of hydrohalite?
- (4) What are the geomorphic implications of this type of system?

Based on fieldwork undertaken on Axel Heiberg Island, laboratory analysis of mineral and water chemistry, and computer simulation of brine freezing the following conclusions can be drawn:

- (1) The highly mineralized groundwater and extreme air temperatures rapidly cool water temperatures leading to eutectic freezing conditions driving the precipitation of hydrated salt minerals.
- (2) The precipitation of hydrated salt minerals by supercooling, and other factors like discharge and local topography produce the travertine/tufa-like deposits at both study sites.
- (3) The precipitation and dissolution of hydrated minerals, as controlled by air temperature, does change surface hydrological patterns seasonally.
- (4) The dominant mineral precipitating at Stolz is hydrohalite in winter (however this has been validated indirectly), halite in summer and the second most abundant mineral is mirabilite in winter (that metamorphoses to thernadite in summer).
- (5) This study found that the dominant mineral precipitating at Wolf is mirabilite in winter (that would metamorphose into thernadite in summer), hydrohalite in winter and halite in summer.

7.1 Significance of this research

Saline water systems (brines) are the most common form of water on Earth and have unique properties that allow them to operate outside the normal range of conditions of fresh water systems, which dominate terrestrial hydrologic systems. Freezing and freezing fractionation brines lead to the sequential precipitation of the minerals dissolved in the brine solution. The range of environments in which these systems occur suggest an impressive range of conditions that define the limits of water on Earth, in particular its

ability to remain in a liquid phase under extreme cold conditions. These deposits are one of few large scale salt landforms that resemble travertines and tufas, and in particular are the most extensive surface deposits of hydrohalite in the world (based on published sources). These salt deposits further our understanding of geomorphic systems responsible for travertines and tufas, landforms previously thought limited to carbonate-rich groundwater discharge. These landforms not only provide an example of morphologically similar features with a very different mineralogy but also furthering the understanding of physical processes generating these morphologies.

Traditional travertine and tufa landforms are associated with carbonate groundwater systems that tend to occur under relatively warm geologic conditions, and sometimes superheated geothermal systems (hot springs). However, understanding these deposits can help explain similar geomorphic processes occurring beyond Earth. An interesting application of this research pertains to the search of liquid water and life on Mars. The spring systems at Stolz and Wolf Diapirs offer a potentially unique indication of groundwater activity in areas of cold permafrost and thus offer a valuable analogue in the search for liquid water and life-supporting environments under the range of cold temperatures that currently exist on Mars. Furthermore, the nature of these analogues may have the immediate benefit of a geomorphic target for future Mars missions. Numerous features on the surface of Mars indicate the past presence and action of liquid water; e.g. gullies were observed within a small number of impact craters that suggest these have been formed in the recent past. It is believed liquid water could only exist currently in a briny form that would allow it to remain stable on the surface for short periods of time. Results from NASA's Phoenix Mars mission have provided the first physical evidence of the

presence of liquid saline water (Rennó *et al.*, 2009). In addition, features identified that are thought to have formed by ancient springs at Vernal Crater, Arabia Terra on Mars show remarkable morphological similarities to the deposits documented at Stolz and Wolf Diapirs (figure 8.1; Allen and Oehler, 2008). The mineralogy of these deposits on Mars is impossible to accurately identify using satellites because the original deposits have been covered by wind-blown sediments, however this research adds strong geomorphic evidence that similar deposits can form under extreme cold conditions and by hyper-saline waters, both of which could easily occur on Mars today and in the past. Therefore, the morphological similarities and the processes of generating the deposits on Axel Heiberg Island by hyper-saline-springs offer a unique perspective of these deposits on Mars.

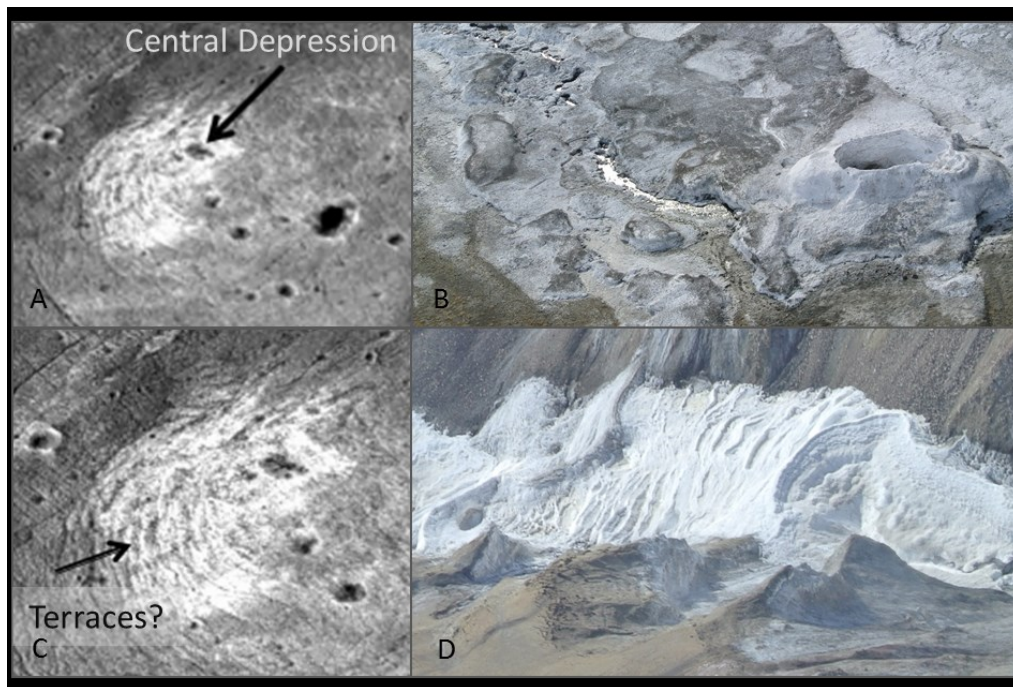


Figure 7.1: Comparison of a features identified on Mars (A and C; Allen and Oehler, 2008) to the deposits on Axel Heiberg Island (B and D). (A) A feature with a central like depression (10m diameter) looks similar to the mound at Wolf Diapir (B) and (C) features (>100m) thought to be terraces would form similarly to the terraces at Stolz Diapir (D).

Chapter 8: References

- Allen, C. C., & Oehler, D. Z. (2008). A case for ancient springs in Arabia Terra, Mars. *Astrobiology*, 8(6), 1093-1112.
- Andersen, D., Pollard, W., & McKay, C. (2008). The perennial springs of Axel Heiberg Island as an analogue for groundwater discharge on Mars. Paper presented at the Proceedings of the Ninth International Conference on Permafrost, University of Alaska Fairbanks.
- Andersen, D., Pollard, W., McKay, C., Heldmann, J., Toon, O., & Jakosky, B. (2000). Cold springs in permafrost on Earth and Mars. Paper presented at the Bulletin of the American Astronomical Society.
- Arthurton, R. S. (1973). Experimentally produced halite compared with Triassic layered halite-rock from Cheshire, England. *Sedimentology*, 20(1), 145-160.
- Battler, M. M., Osinski, G. R., & Banerjee, N. R. (2013). Mineralogy of saline perennial cold springs on Axel Heiberg Island, Nunavut, Canada and implications for spring deposits on Mars. *Icarus*, 224(2), 364-381.
- Braitsch, O. (1971). Salt deposits: their origin and composition. *Minerals, rocks and inorganic materials* (4): Springer-Verlag.
- Capezzuoli, E., Gandin, A., & Pedley, M. (2014). Decoding tufa and travertine (fresh water carbonates) in the sedimentary record: The state of the art. *Sedimentology*, 61(1), 1-21.
- Castanier, S., Perthuisot, J.-P., Matrat, M., & Morvan, J.-Y. (1999). The salt ooids of Berre salt works (Bouches du Rhône, France): the role of bacteria in salt crystallisation. *Sedimentary Geology*, 125(1), 9-21.
- Castanier, S., Perthuisot, J.-P., Rouchy, J.-M., Maurin, A., & Guelorget, O. (1992). Halite ooids in Lake Asal, Djibouti: biocrystalline build-ups. *Geobios*, 25(6), 811-821.
- Chan, P. Y., & Goldenfeld, N. (2007). Steady states and linear stability analysis of precipitation pattern formation at geothermal hot springs. *Physical Review E*, 76(4), 046104.
- Craig, J., Light, J., Parker, B., & Mudrey, M. (1975). Identification of hydrohalite. *Antarctic Journal of the United States*, 10(4), 178-179.
- Craig, J. R., Fortner, R. D., & Weand, B. L. (1974). Halite and hydrohalite from Lake Bonney, Taylor Valley, Antarctica. *Geology*, 2(8), 389-390.

- Davies, G. R., & Nassichuk, W. (1975). Subaqueous evaporites of the carboniferous Otto fiord formation, Canadian Arctic Archipelago: a summary. *Geology*, 3(5), 273-278.
- De Waele, J., & Forti, P. (2010). Salt rims and blisters: peculiar and ephemeral formations in the Atacama Desert (Chile). *Zeitschrift für Geomorphologie, Supplementary Issues*, 54(2), 51-67.
- De Waele, J., Picotti, V., Forti, P., Brook, G., Cucchi, F., & Zini, L. (2009). Age of caves in the Cordillera de la Sal (Atacama, Chili). Paper presented at the 15th International Congress on Speleology, Kerrville, Texas, USA. National Speleological Society.
- Dzens-Litovskii, A. I. (1966). *Sodianoi karst SSSR*. Leningrad: Nedra.
- Dzens-Litovskiy, A. (1968). Salt lakes of the USSR and their mineral resources. Nedra, Leningrad, Russia, 1-119.
- Filippi, M., Bruthans, J., Palatinus, L., Zare, M., & Asadi, N. (2011). Secondary halite deposits in the Iranian salt karst: general description and origin. *International Journal of Speleology*, 40(2), 8.
- Fomenko, K. Y. (1976). The problem of formation of salt domes in the Caspian basin. *International Geology Review*, 18(3), 345-350.
- Ford, T., & Pedley, H. (1996). A review of tufa and travertine deposits of the world. *Earth-Science Reviews*, 41(3), 117-175.
- Freeze, R. A., & Cherry, J. A. (1979). *Groundwater*, 1979. Englewood Cliffs, NJ: Prentice-Hall Inc, 604p.
- Frumkin, A., & Forti, P. (1997). Liquid crystal cave, Israel. *Cave Minerals of the World*. National Speleological Society, Huntsville, 319-322.
- Garrett, D. E. (2001). *Sodium Sulfate: Handbook of Deposits, Processing, & Use*: Academic press.
- Gitterman, K. (1937). Thermal analysis of seawater. *CRREL TL*, 287.
- Goldenfeld, N., Chan, P. Y., & Veysey, J. (2006). Dynamics of precipitation pattern formation at geothermal hot springs. *Physical review letters*, 96(25), 254501.
- Grasby, S. E., Allen, C. C., Longazo, T. G., Lisle, J. T., Griffin, D. W., & Beauchamp, B. (2003). Supraglacial sulfur springs and associated biological activity in the Canadian high arctic-signs of life beneath the ice. *Astrobiology*, 3(3), 583-596.

- Grasby, S. E., Chen, Z., & Dewing, K. (2012). Formation water geochemistry of the Sverdrup Basin: Implications for hydrocarbon development in the High Arctic. *Applied Geochemistry*, 27(8), 1623-1632.
- Grasby, S. E., Proemse, B. C., & Beauchamp, B. (2014). Deep groundwater circulation through the High Arctic cryosphere forms Mars-like gullies. *Geology*, 42(8), 651-654.
- Hammer, Ø. (2008). Pattern formation: Watch your step. *Nature Physics*, 4(4), 265-266.
- Hammer, Ø., Dysthe, D., & Jamtveit, B. (2007). The dynamics of travertine dams. *Earth and Planetary Science Letters*, 256(1), 258-263.
- Hammer, Ø., Dysthe, D. K., & Jamtveit, B. (2010). Travertine terracing: patterns and mechanisms. Geological Society, London, Special Publications, 336(1), 345-355.
- Handford, C. R. (1991). Marginal marine halite: sabkhas and salinas. *Evaporites, petroleum and mineral resources*, 1-66.
- Harrison, J., & Jackson, M. (2008). Bedrock geology, Strand Fiord-Expedition Fiord area, western Axel Heiberg Island, northern Nunavut (parts of NTS 59E, F, G, and H). Geological Survey of Canada, Ottawa. Open File, 5590.
- Harrison, J., & Jackson, M. (2014). Exposed evaporite diapirs and minibasins above a canopy in central Sverdrup Basin, Axel Heiberg Island, Arctic Canada. *Basin Research*, 26(4), 567-596.
- Heldmann, J. L., Pollard, W. H., McKay, C. P., Andersen, D. T., & Toon, O. B. (2005). Annual development cycle of an icing deposit and associated perennial spring activity on Axel Heiberg Island, Canadian High Arctic. *Arctic, Antarctic, and Alpine Research*, 37(1), 127-135.
- Herrero Fernández, M. J., Escavy Fernández, J. I., & Schreiber, B. (2015). Thenardite after mirabilite deposits as a cool climate indicator in the geological record: lower Miocene of central Spain. *Climate of the Past*, 11(1), 1-13.
- Herut, B., Starinsky, A., Katz, A., & Bein, A. (1990). The role of seawater freezing in the formation of subsurface brines. *Geochimica et Cosmochimica Acta*, 54(1), 13-21.
- Hu, X., & Pollard, W. H. (1997). Ground icing formation: experimental and statistical analyses of the overflow process. *Permafrost and Periglacial Processes*, 8(2), 217-235.
- Hudec, M. R., & Jackson, M. P. (2012). De Re Salica: Fundamental principles of salt tectonics. *Regional Geology and Tectonics: Phanerozoic Passive Margins, Cratonic Basins and Global Tectonic Maps: Phanerozoic Passive Margins, Cratonic Basins and Global Tectonic Maps*, 19.

- Hugon, H., & Schwerdtner, W. (1982). Discovery of Halite in a Small Evaporite Diapir on Southeastern Axel Heiberg Island, Canadian Arctic Archipelago: GEOLOGICAL NOTE. *Bulletin of Canadian Petroleum Geology*, 30(4), 303-305.
- Jackson, M., & Harrison, J. (2006). An allochthonous salt canopy on Axel Heiberg Island, Sverdrup Basin, Arctic Canada. *Geology*, 34(12), 1045-1048.
- Jackson, M., & Talbot, C. J. (1991). A glossary of salt tectonics: Bureau of Economic Geology, University of Texas at Austin.
- Kerr, R. C., & Turner, J. S. (1996). Crystallization and gravitationally controlled ponding during the formation of mound springs, terraces, and “black smoker” flanges. *Journal of Geophysical Research: Solid Earth (1978–2012)*, 101(B11), 25125-25137.
- Last, W. M. (1984). Sedimentology of playa lakes of the northern Great Plains. *Canadian Journal of Earth Sciences*, 21(1), 107-125.
- Last, W. M. (1989). Continental brines and evaporites of the northern Great Plains of Canada. *Sedimentary Geology*, 64(4), 207-221.
- Lay, C.-Y., Mykytczuk, N. C., Niederberger, T. D., Martineau, C., Greer, C. W., & Whyte, L. G. (2012). Microbial diversity and activity in hyper-saline high Arctic spring channels. *Extremophiles*, 16(2), 177-191.
- Light, B., Brandt, R. E., & Warren, S. G. (2009). Hydrohalite in cold sea ice: Laboratory observations of single crystals, surface accumulations, and migration rates under a temperature gradient, with application to “Snowball Earth”. *Journal of Geophysical Research: Oceans (1978–2012)*, 114(C7).
- Marion, G. (1997). A theoretical evaluation of mineral stability in Don Juan Pond, Wright Valley, Victoria Land. *Antarctic Science*, 9(01), 92-99.
- Marion, G., Farren, R., & Komrowski, A. (1999). Alternative pathways for seawater freezing. *Cold Regions Science and Technology*, 29(3), 259-266.
- Marion, G. M., & Grant, S. A. (1994). FREZCHEM: A chemical-thermodynamic model for aqueous solutions at subzero temperatures: DTIC Document.
- Marion, G. M., & Kargel, J. S. (2008). Cold aqueous planetary geochemistry with FREZCHEM from modeling to the search for life at the limits.
- Matsubaya, O., Sakai, H., Torii, T., Burton, H., & Kerry, K. (1979). Antarctic saline lakes—stable isotopic ratios, chemical compositions and evolution. *Geochimica et Cosmochimica Acta*, 43(1), 7-25.

Nelson, K. H., & Thompson, T. G. (1954). Deposition of salts from sea water by frigid concentration: DTIC Document.

Niederberger, T. D., Perreault, N. N., Tille, S., Lollar, B. S., Lacrampe-Couloume, G., Andersen, D., . . . Whyte, L. G. (2010). Microbial characterization of a subzero, hyper-saline methane seep in the Canadian High Arctic. *The ISME journal*, 4(10), 1326-1339.

Omelson, C. R., Pollard, W. H., & Andersen, D. T. (2006). A geochemical evaluation of perennial spring activity and associated mineral precipitates at Expedition Fjord, Axel Heiberg Island, Canadian High Arctic. *Applied Geochemistry*, 21(1), 1-15.

Omelson, C. R., Pollard, W. H., & Marion, G. M. (2001). Seasonal formation of ikaite ($\text{CaCO}_3 \cdot 6\text{H}_2\text{O}$) in saline spring discharge at Expedition Fiord, Canadian High Arctic: Assessing conditional constraints for natural crystal growth. *Geochimica et Cosmochimica Acta*, 65(9), 1429-1437.

Pentecost, A. (2005). *Travertine*: Springer Science & Business Media.

Pentecost, A., & Viles, H. (1994). A review and reassessment of travertine classification. *Geographie physique et Quaternaire*, 48(3), 305-314.

Perreault, N. N., Andersen, D. T., Pollard, W. H., Greer, C. W., & Whyte, L. G. (2007). Characterization of the prokaryotic diversity in cold saline perennial springs of the Canadian high Arctic. *Applied and environmental microbiology*, 73(5), 1532-1543.

Perreault, N. N., Greer, C. W., Andersen, D. T., Tille, S., Lacrampe-Couloume, G., Lollar, B. S., & Whyte, L. G. (2008). Heterotrophic and autotrophic microbial populations in cold perennial springs of the high Arctic. *Applied and environmental microbiology*, 74(22), 6898-6907.

Perthuisot, J., Castanier, S., Rouchy, J., & Maurin, A. et Guelorget, O. (1993). Le rôle des bactéries dans la précipitation du sel. Exemple du Lac Asal (Djibouti). *Actes Coll. Int. du Sel, Salies de Béarn*, 119-144.

Pollard, W. (2005b). Axel Heiberg Island. In M. Nuttall (Ed.), *Encyclopaedia of the Arctic* (pp. 181-182). London: Fitzroy Dearborn Publishing Company.

Pollard, W., & Bell, T. (1998). Massive ice formation in the Eureka Sound lowlands: a landscape model. Paper presented at the Proceedings, Seventh International Permafrost Conference.

- Pollard, W., Haltigin, T., Whyte, L., Niederberger, T., Andersen, D., Omelon, C., . . . Lebeuf, M. (2009). Overview of analogue science activities at the McGill Arctic Research Station, Axel Heiberg Island, Canadian High Arctic. *Planetary and Space Science*, 57(5), 646-659.
- Pollard, W., Omelon, C., Andersen, D., & McKay, C. (1999). Perennial spring occurrence in the Expedition Fiord area of western Axel Heiberg Island, Canadian high Arctic. *Canadian Journal of Earth Sciences*, 36(1), 105-120.
- Pollard, W. H. (2005). Icing processes associated with high arctic perennial springs, Axel Heiberg Island, Nunavut, Canada. *Permafrost and Periglacial Processes*, 16(1), 51-68.
- Pollard, W. H., & van Everdingen, R. O. (1992). Formation of seasonal ice bodies. Paper presented at the The Binghampton Symposia in Geomorphology: International Series.
- Prowse, T. D., & Ommanney, C. S. L. (1990). Northern hydrology: Canadian perspectives. NHRI science report.
- Rennó, N. O., Bos, B. J., Catling, D., Clark, B. C., Drube, L., Fisher, D., . . . Kok, J. F. (2009). Possible physical and thermodynamical evidence for liquid water at the Phoenix landing site. *Journal of Geophysical Research: Planets* (1991–2012), 114(E1).
- Richardson, C. (1976). Phase relationships in sea ice as a function of temperature. *Journal of Glaciology*, 17, 507-519.
- Ringer, W. (1906). Ueber die Veränderungen in der Zusammensetzung des Meereswassersalzes beim Ausfrieren. *Verhandelingen uit het Rijksinstituut voor het Onderzoek der Zee*, 1, 1-55.
- Schwerdtner, W., & Van Kranendonk, M. (1984). Structure of Stolz Diapir--A Well-Exposed Salt Dome on Axel Heiberg Island, Canadian Arctic Archipelago. *Bulletin of Canadian Petroleum Geology*, 32(2), 237-241.
- Sonnenfeld, P. (1984). Brines and evaporites: Academic Pr.
- Sonnenfeld, P., Perthuisot, J. P., & International Geological, C. (1989). Brines and evaporites. Washington, D.C.: American Geophysical Union.
- Talbot, C., Stanley, W., Soub, R., & AL-SADOUN, N. (1996). Epitaxial salt reefs and mushrooms in the southern Dead Sea. *Sedimentology*, 43(6), 1025-1047.
- Tekin, E., Ayyildiz, T., Gündoğan, İ., & Orti, F. (2007). Modern halolites (halite oolites) in the Tuz Gölü, Turkey. *Sedimentary Geology*, 195(3), 101-112.

Thorsteinsson, R. (1974). Carboniferous and Permian stratigraphy of Axel Heiberg Island and western Ellesmere Island, Canadian Arctic Archipelago: Department of Energy, Mines and Resources.

Van Everdingen, R. (1990). Ground-water hydrology. *Northern Hydrology: Canadian Perspectives*, 77-101.

Van Everdingen, R. O. (1991). Physical, chemical, and distributional aspects of Canadian springs. *Memoirs of the Entomological Society of Canada*, 123(S155), 7-28.

Van Everdingen, R. O. (1998). Multi-language glossary of permafrost and related ground-ice terms in Chinese, English, French, German, Icelandic, Italian, Norwegian, Polish, Romanian, Russian, Spanish, and Swedish: International Permafrost Association, Terminology Working Group.

Veysey II, J., & Goldenfeld, N. (2008). Watching rocks grow. *Nature Physics*, 4(4), 310-313.

Weiler, Y., Sass, E., & Zak, I. (1974). Halite oolites and ripples in the Dead Sea, Israel. *Sedimentology*, 21(4), 623-632.

Woo, M.-k. (2012). *Permafrost hydrology*: Springer Science & Business Media.

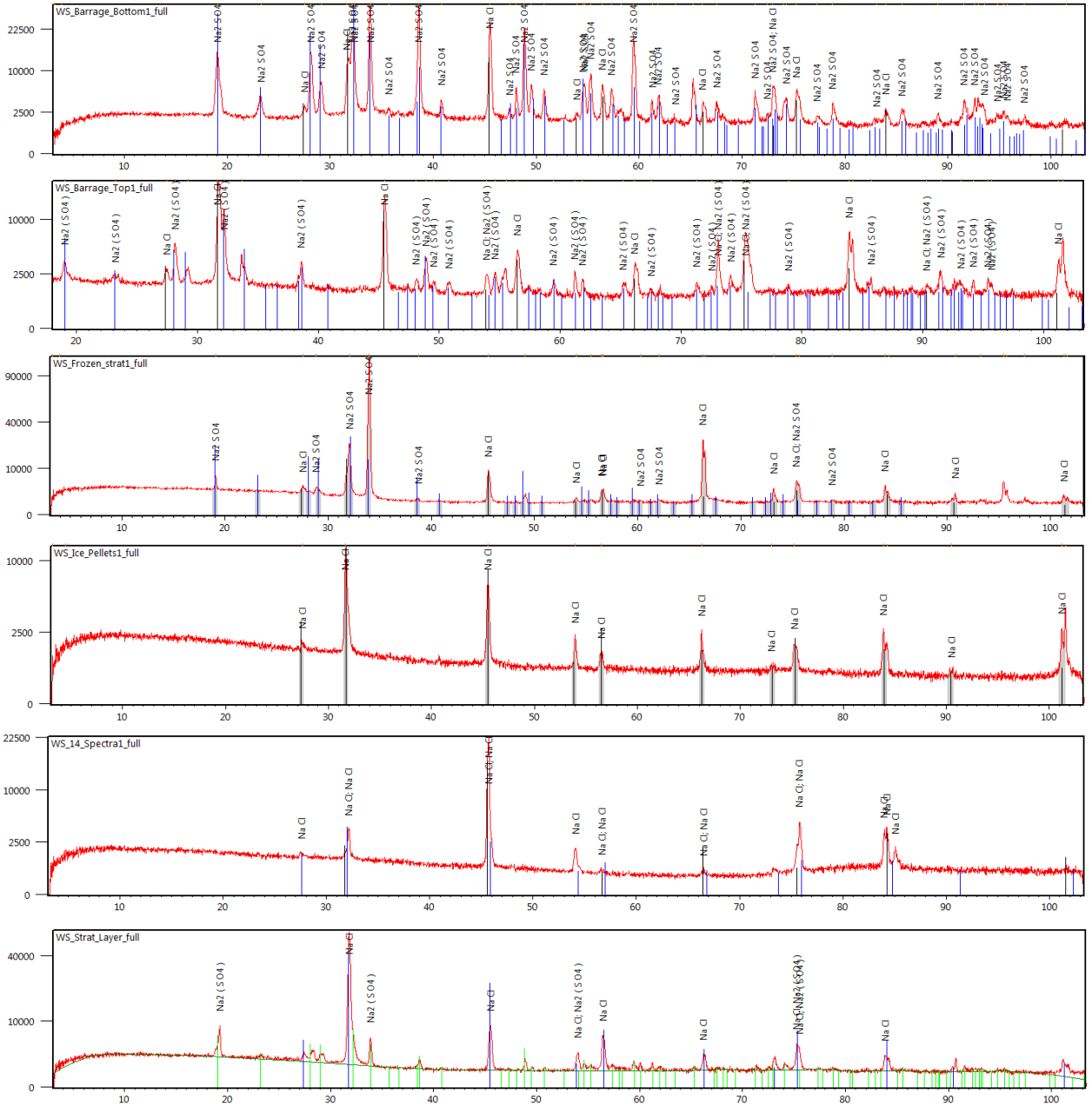
Wooding, R. A. (1991). Growth of natural dams by deposition from steady supersaturated shallow flow. *Journal of Geophysical Research: Solid Earth* (1978–2012), 96(B1), 667-682.

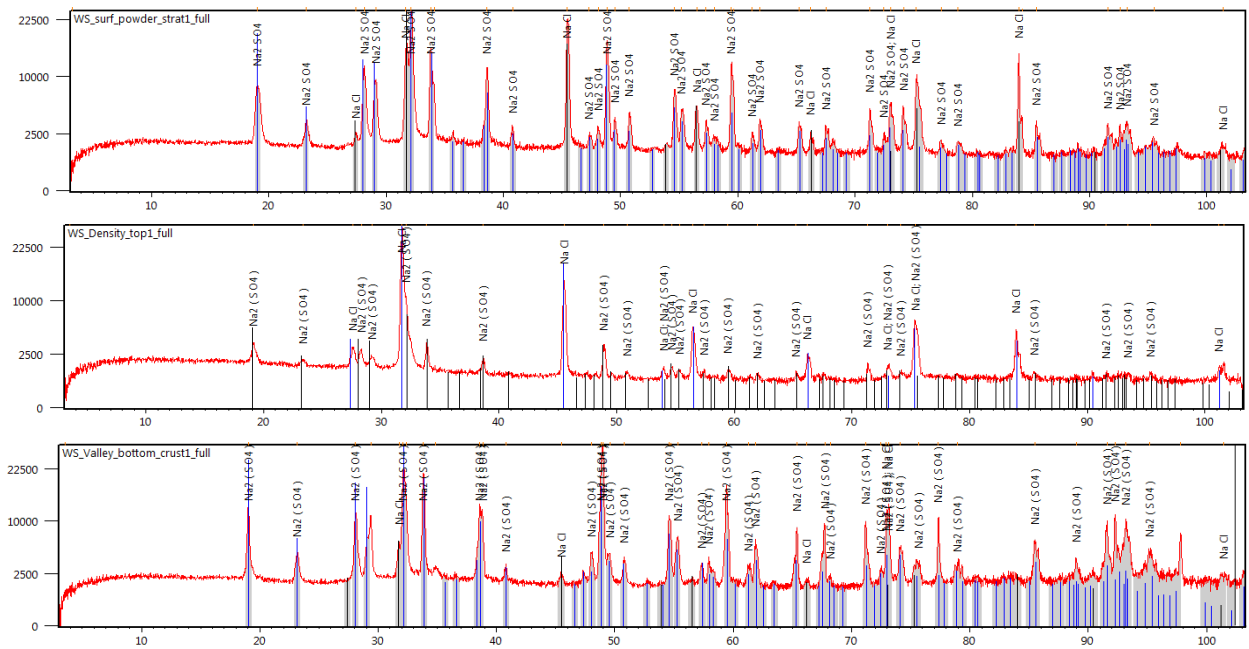
Chapter 9: Appendices

The following appendices are composed of individual x-ray diffraction patterns and output data from modelling simulations using Frezchem (v.5.2). Appendix A contain x-ray diffraction patterns for a portion of samples collected at Stolz. Appendix B contains samples analysed by x-ray diffraction at Wolf Diapir. Appendix C provides a few examples of outputs for mineral precipitation simulations for Stolz Diapir and appendix D provides examples simulations for Wolf Diapir (each example consists of outlet water samples). Each sample inputted into the model was simulated twice for each mechanism type to precipitate evaporative minerals. The first simulation was done to simulate mineral precipitation by evaporation at 7°C (mean summer temperature recorded by the Hobo data logger). The second simulation simulated mineral precipitation by freezing fractionation over a +15°C to -45°C temperature range (as recorded by the Hobo temperature data logger).

Appendix A

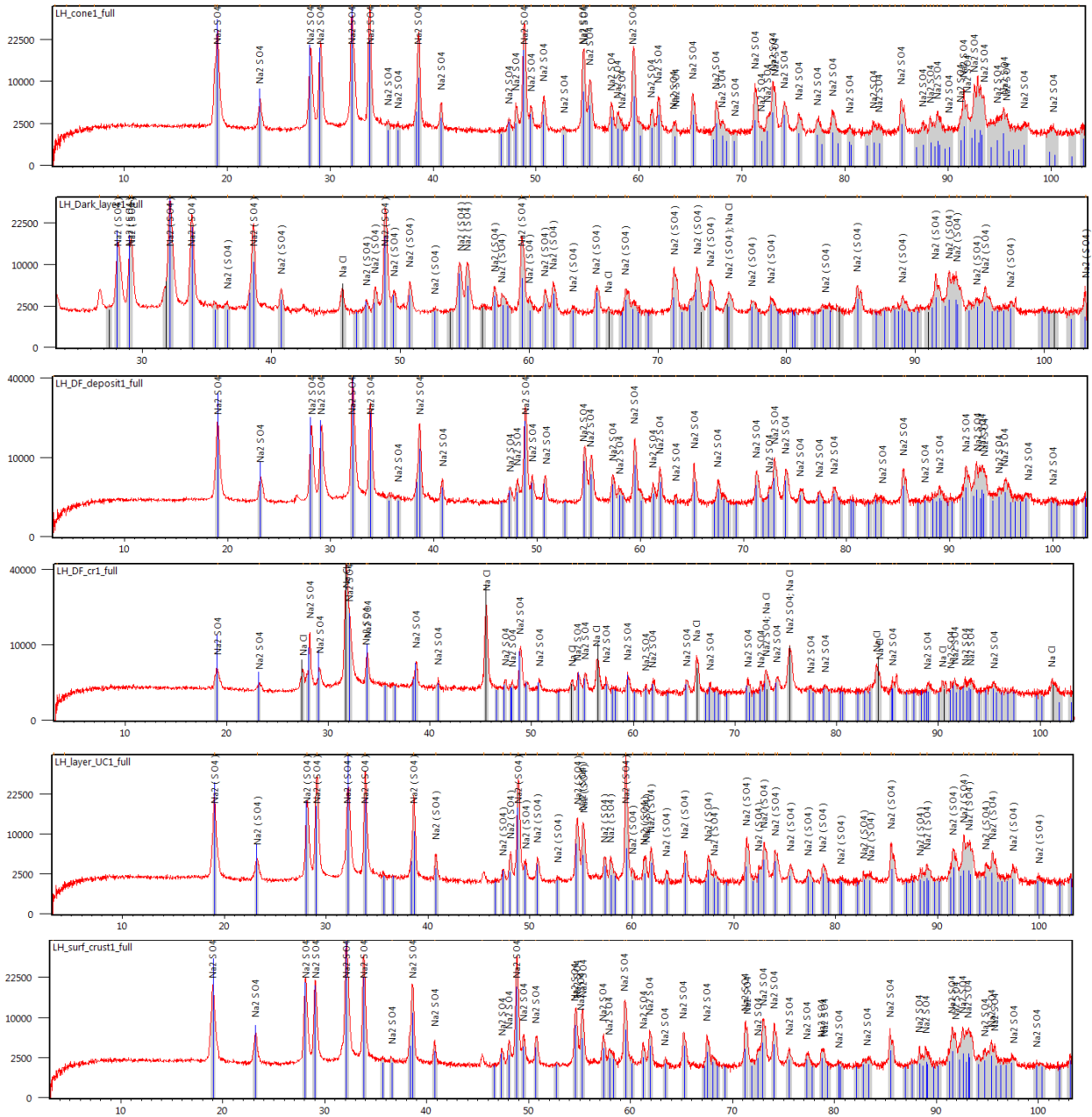
X-ray diffraction patterns for individual samples at Stolz Diapir. Main peaks were labelled with the chemical formula of the corresponding mineral (halite, NaCl or thernadite, Na₂SO₄).

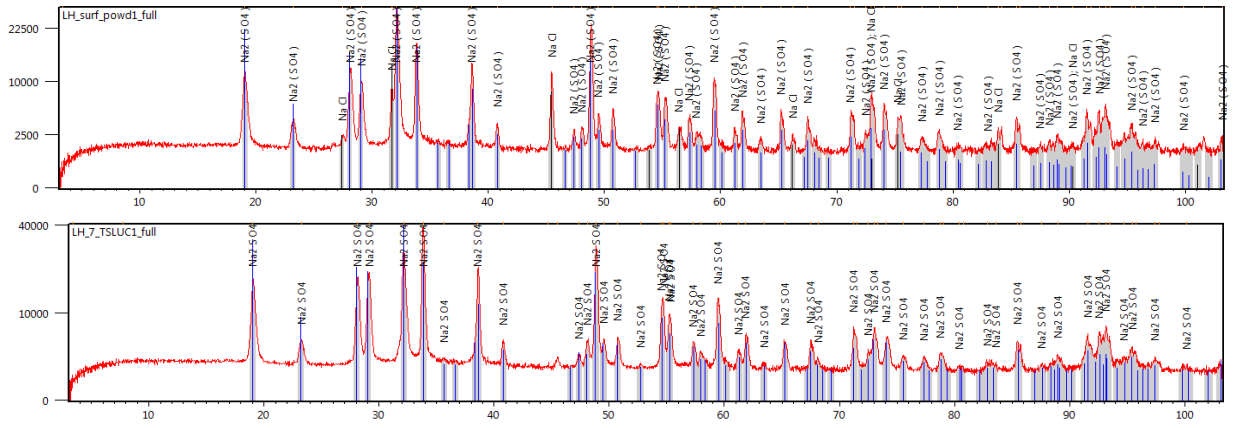




Appendix B

X-ray diffraction patterns for individual samples at Wolf Diapir. Main peaks were labelled with the chemical formula of the corresponding mineral (halite, NaCl, or thernadite, Na_2SO_4).





Appendix C

Stolz Diapir Frezchem v.5.2 mineral precipitation simulation by evaporation of outlet water sample. Units for water samples had to be converted from g/L to mol/Kg to be inputted into the model.

Input Water Chemistry for Outlet Water Summer Sample

Sample Temp. (°C)	pH	Ca ²⁺ (mol/Kg)	K ⁺ (mol/Kg)	Mg ²⁺ (mol/Kg)	Na ⁺ (mol/Kg)	Cl ⁻ (mol/Kg)	SO ₄ ²⁻ (mol/Kg)
-1.30	7.06	0.0329	0.0120	0.0035	6.9225	6.9341	0.0521

Output for Mineral Precipitation by Evaporation

Stolz Summer Outlet Evap

Temp(K)	Ion.Str.	AH2O	Phi	H2O(g)	Ice(g)	
280.15	6.6188	0.75223	1.2650	98.847	0.00000	
Solution	Initial	Final				Mass
SPECIES	Conc.	Conc.	Act.Coeff.	Activity	Moles	Balance
NA	6.9225	6.0033	0.95164	5.7130	0.59341	6.9225
K	0.12000E-01	0.12140	0.48768	0.59204E-01	0.12000E-01	0.12000E-01
CA	0.32900E-01	0.92042E-02	1.4802	0.13624E-01	0.90981E-03	0.32900E-01
MG	0.35000E-02	0.35408E-01	3.1089	0.11008	0.35000E-02	0.35000E-02
CL	6.9341	6.1207	0.95634	5.8535	0.60501	6.9341
S04	0.52100E-01	0.20344	0.15065E-01	0.30648E-02	0.20110E-01	0.52100E-01
H2O(G)					49.958	
H2O(L)	55.508			.75223	5.4869	55.508
Solid		Equil.	Accum.			
SPECIES	Moles	Constant	Moles			
ICE	0.00000	1.0726	0.00000			
NACL.2H2O	0.00000	22.263	0.00000			
NACL	0.60708	33.439	6.3291			
KCL	0.00000	4.7708	0.00000			
CACL2.6H2O	0.00000	2536.2	0.00000			
MGCL2.6H2O	0.00000	53827.	0.00000			
MGCL2.8H2O	0.00000	8991.2	0.00000			
MGCL2.12H2O	0.00000	2001.3	0.00000			
KMGCL3.6H2O	0.00000	10739.	0.00000			
CACL2.2MGCL2.12H2O	0.00000	0.10455E+19	0.00000			
NA2S04.10H2O	0.00000	0.71968E-02	0.00000			
NA2S04	0.00000	0.49763	0.00000			
MGS04.6H2O	0.00000	0.20893E-01	0.00000			
MGS04.7H2O	0.00000	0.77174E-02	0.00000			
K2S04	0.00000	0.84801E-02	0.00000			
MGS04.K2S04.6H2O	0.00000	0.15466E-04	0.00000			
NA2S04.MGS04.4H2O	0.00000	0.36640E-02	0.00000			
CAS04.2H2O	0.25101E-02	0.23628E-04	0.31990E-01			
CAS04	0.00000	0.61142E-04	0.00000			
MGS04.12H2O	0.00000	0.83820E-04	0.00000			
NA2S04.3K2S04	0.00000	0.14767E-11	0.00000			
CAC03(CALCITE)	0.00000	0.38118E-08	0.00000			
MGC03	0.00000	0.22762E-06	0.00000			
MGC03.3H2O	0.00000	0.32059E-03	0.00000			
MGC03.5H2O	0.00000	0.30800E-01	0.00000			
CAC03.6H2O	0.00000	0.22131E-08	0.00000			
NAHCO3	0.00000	0.13426	0.00000			
NA2CO3.10H2O	0.00000	0.58121E-03	0.00000			
NAHCO3.NA2CO3.2H2O	0.00000	0.15963E-01	0.00000			
3MGC03.MG(OH)2.3H2O	0.00000	0.95118E-31	0.00000			
CAMG(CO3)2	0.00000	0.10951E-14	0.00000			

Output for Mineral Precipitation by Freezing Fractionation

Stolz Summer Outlet

Temp(K)	Ion.Str.	AH2O	Phi	H2O(g)	Ice(g)	
228.15	10.231	0.65196	1.7725	8.8456	0.85346	
Solution	Initial	Final				Mass
SPECIES	Conc.	Conc.	Act.Coef.	Activity	Moles	Balance
NA	6.9225	0.92570	0.46238	0.42802	0.81884E-02	6.9225
K	0.12000E-01	0.48764	0.55816E-01	0.27218E-01	0.43135E-02	0.12000E-01
CA	0.32900E-01	1.9594	4.8418	9.4868	0.17332E-01	0.32900E-01
MG	0.35000E-02	0.39568	3.5297	1.3966	0.35000E-02	0.35000E-02
CL	6.9341	9.6276	1.7144	16.505	0.85162E-01	6.9341
S04	0.52100E-01	0.21565E-03	0.54027E-02	0.11651E-05	0.19075E-05	0.52100E-01
H2O(L)	55.508			.65196	0.49101	55.508
Solid			Equil.	Accum.		
SPECIES	Moles		Constant	Moles		
ICE	0.47374E-01		0.65195	42.682		
NACL.2H2O	0.24662E-02		3.0028	5.9693		
NACL	0.00000		11.584	0.87196		
KCL	0.66308E-03		0.44924	0.76865E-02		
CACL2.6H2O	0.00000		462.91	0.00000		
MGCL2.6H2O	0.00000		22891.	0.00000		
MGCL2.8H2O	0.00000		343.17	0.00000		
MGCL2.12H2O	0.00000		3.4433	0.00000		
KMGCL3.6H2O	0.00000		246.46	0.00000		
CACL2.2MGCL2.12H2O	0.00000		0.14258E+22	0.00000		
NA2S04.10H2O	0.00000		0.10607E-04	0.36530E-01		
NA2S04	0.00000		0.45011	0.00000		
MGS04.6H2O	0.00000		0.14632E-01	0.00000		
MGS04.7H2O	0.00000		0.10337E-02	0.00000		
K2S04	0.00000		0.64989E-03	0.00000		
MGS04.K2S04.6H2O	0.00000		0.63572E-07	0.00000		
NA2S04.MGS04.4H2O	0.00000		0.23895E-02	0.00000		
CAS04.2H2O	0.10300E-05		0.46979E-05	0.15568E-01		
CAS04	0.00000		0.61142E-04	0.00000		
MGS04.12H2O	0.00000		0.83820E-04	0.00000		
NA2S04.3K2S04	0.00000		0.14767E-11	0.00000		
CAC03(CALCITE)	0.00000		0.38118E-08	0.00000		
MGC03	0.00000		0.22762E-06	0.00000		
MGC03.3H2O	0.00000		0.32059E-03	0.00000		
MGC03.5H2O	0.00000		0.30800E-01	0.00000		
CAC03.6H2O	0.00000		0.22131E-08	0.00000		
NAHCO3	0.00000		0.13426	0.00000		
NA2CO3.10H2O	0.00000		0.58121E-03	0.00000		
NAHCO3.NA2CO3.2H2O	0.00000		0.15963E-01	0.00000		
3MGC03.MG(OH)2.3H2O	0.00000		0.95118E-31	0.00000		
CAMG(CO3)2	0.00000		0.10951E-14	0.00000		

Appendix D

Wolf Diapir Frezchem v.5.2 mineral precipitation simulation by evaporation of outlet water sample. Units for water samples had to be converted from g/L to mol/Kg to be inputted into the model.

Input Water Chemistry for Outlet Water Summer Sample

Sample Temp. (°C)	pH	Ca ²⁺ (mol/Kg)	K ⁺ (mol/Kg)	Mg ²⁺ (mol/Kg)	Na ⁺ (mol/Kg)	Cl ⁻ (mol/Kg)	SO ₄ ²⁻ (mol/Kg)
-4.30	6.87	0.0537	0.0132	0.0207	6.7813	6.7922	0.0788

Output for Mineral Precipitation by Evaporation

Wolf evap

Temp(K)	Ion.Str.	AH2O	Phi	H2O(g)	Ice(g)	
280.15	6.9201	0.74892	1.2950	98.093	0.00000	
Solution	Initial	Final				Mass
SPECIES	Conc.	Conc.	Act.Coeff.	Activity	Moles	Balance
NA	6.7813	5.8324	0.90586	5.2833	0.57211	6.7813
K	0.13200E-01	0.13457	0.46103	0.62039E-01	0.13200E-01	0.13200E-01
CA	0.53700E-01	0.77777E-02	1.2521	0.97382E-02	0.76294E-03	0.53700E-01
MG	0.20700E-01	0.21102	2.5706	0.54247	0.20700E-01	0.20700E-01
CL	6.7922	5.9435	1.0650	6.3297	0.58301	6.7922
SO4	0.78800E-01	0.26366	0.16407E-01	0.43259E-02	0.25863E-01	0.78800E-01
H2O(G)					49.958	
H2O(L)	55.508			.74892	5.4450	55.508
Solid			Equil.	Accum.		
SPECIES	Moles		Constant	Moles		
ICE	0.00000		1.0726	0.00000		
NACL.2H2O	0.00000		22.263	0.00000		
NACL	0.60723		33.439	6.2092		
KCL	0.00000		4.7708	0.00000		
CACL2.6H2O	0.00000		2536.2	0.00000		
MGCL2.6H2O	0.00000		53827.	0.00000		
MGCL2.8H2O	0.00000		8991.2	0.00000		
MGCL2.12H2O	0.00000		2001.3	0.00000		
KMGCL3.6H2O	0.00000		10739.	0.00000		
CACL2.2MGCL2.12H2O	0.00000		0.10455E+19	0.00000		
NA2SO4.10H2O	0.00000		0.71968E-02	0.00000		
NA2SO4	0.00000		0.49763	0.00000		
MGSO4.6H2O	0.00000		0.20893E-01	0.00000		
MGSO4.7H2O	0.00000		0.77174E-02	0.00000		
K2SO4	0.00000		0.84801E-02	0.00000		
MGSO4.K2SO4.6H2O	0.00000		0.15466E-04	0.00000		
NA2SO4.MGSO4.4H2O	0.00000		0.36640E-02	0.00000		
CASO4.2H2O	0.21084E-02		0.23628E-04	0.52937E-01		
CASO4	0.00000		0.78744E-04	0.00000		
MGSO4.12H2O	0.00000		0.83625E-02	0.00000		
NA2SO4.3K2SO4	0.00000		0.41473E-08	0.00000		
CAC03(CALCITE)	0.00000		0.39778E-08	0.00000		
MGC03	0.00000		0.18213E-07	0.00000		
MGC03.3H2O	0.00000		0.68909E-05	0.00000		
MGC03.5H2O	0.00000		0.62805E-05	0.00000		
CAC03.6H2O	0.00000		0.95754E-07	0.00000		
NAHCO3	0.00000		0.23545	0.00000		
NA2CO3.10H2O	0.00000		0.29119E-01	0.00000		
3MGC03.MG(OH)2.3H2O	0.00000		0.95118E-31	0.00000		
CAMG(CO3)2	0.00000		0.10951E-14	0.00000		

Output for Mineral Precipitation by Freezing Fractionation

Wolf Freeze Outlet

Temp(K)	Ion.Str.	AH2O	Phi	H2O(g)	Ice(g)
228.15	10.437	0.65196	1.8852	3.3004	4.1869

Solution SPECIES	Initial Conc.	Final Conc.	Act.Coeff.	Activity	Moles	Mass Balance
NA	6.7813	0.78320	0.43340	0.33944	0.25849E-02	6.7813
K	0.13200E-01	0.39096	0.55210E-01	0.21585E-01	0.12903E-02	0.13200E-01
CA	0.53700E-01	1.9582	1.9494	3.8174	0.64628E-02	0.53700E-01
MG	0.20700E-01	0.80113	1.6827	1.3480	0.26440E-02	0.20700E-01
CL	6.7922	8.6614	2.4030	20.813	0.28586E-01	6.7922
S04	0.78800E-01	0.44188E-03	0.65531E-02	0.28957E-05	0.14584E-05	0.78800E-01
H2O(L)	55.508			.65196	0.18320	55.508

Solid SPECIES	Moles	Equil. Constant	Accum. Moles
ICE	0.23241	0.65195	42.765
NACL.2H2O	0.11437E-01	3.0028	5.9667
NACL	0.00000	11.584	0.74893
KCL	0.35266E-02	0.44924	0.11910E-01
CACL2.6H2O	0.00000	462.91	0.00000
MGCL2.6H2O	0.00000	22891.	0.00000
MGCL2.8H2O	0.00000	343.17	0.00000
MGCL2.12H2O	0.18056E-01	3.4433	0.18056E-01
KMGCL3.6H2O	0.00000	246.46	0.00000
CACL2.2MGCL2.12H2O	0.00000	0.14258E+22	0.00000
NA2S04.10H2O	0.00000	0.10607E-04	0.31561E-01
NA2S04	0.00000	0.45011	0.00000
MGS04.6H2O	0.00000	0.14632E-01	0.00000
MGS04.7H2O	0.00000	0.10337E-02	0.00000
K2S04	0.00000	0.64989E-03	0.00000
MGS04.K2S04.6H2O	0.00000	0.63572E-07	0.00000
NA2S04.MGS04.4H2O	0.00000	0.23895E-02	0.00000
CAS04.2H2O	0.21716E-04	0.46979E-05	0.47237E-01
CAS04	0.00000	0.61142E-04	0.00000
MGS04.12H2O	0.00000	0.83820E-04	0.00000
NA2S04.3K2S04	0.00000	0.14767E-11	0.00000
CAC03(CALCITE)	0.00000	0.38118E-08	0.00000
MGC03	0.00000	0.22762E-06	0.00000
MGC03.3H2O	0.00000	0.32059E-03	0.00000
MGC03.5H2O	0.00000	0.30800E-01	0.00000
CAC03.6H2O	0.00000	0.22131E-08	0.00000
NAHC03	0.00000	0.13426	0.00000
NA2C03.10H2O	0.00000	0.58121E-03	0.00000
NAHC03.NA2C03.2H2O	0.00000	0.15963E-01	0.00000
3MGC03.MG(OH)2.3H2O	0.00000	0.95118E-31	0.00000
CAMG(CO3)2	0.00000	0.10951E-14	0.00000